Radio Science Bulletin

ISSN 1024-4530

INTERNATIONAL
UNION OF
RADIO SCIENCE

UNION
RADIO-SCIENTIFIQUE
INTERNATIONALE

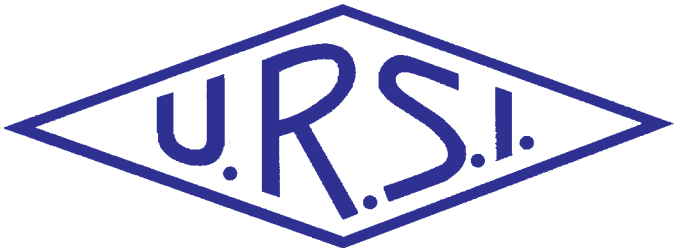

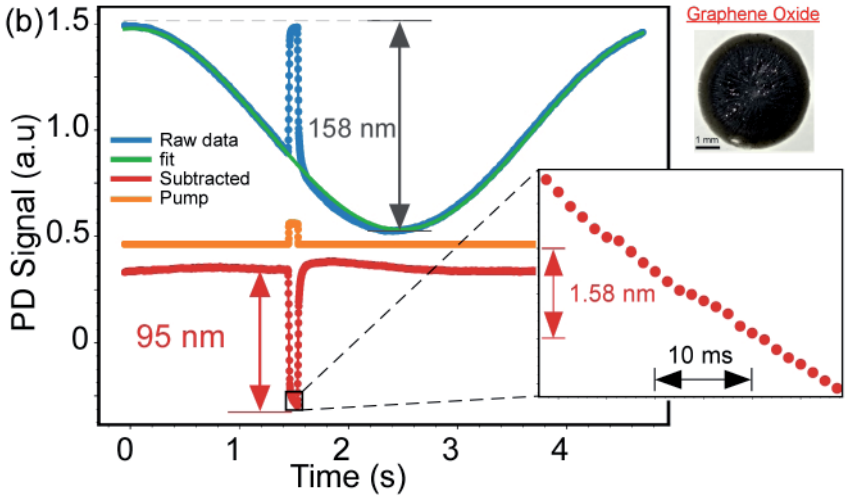

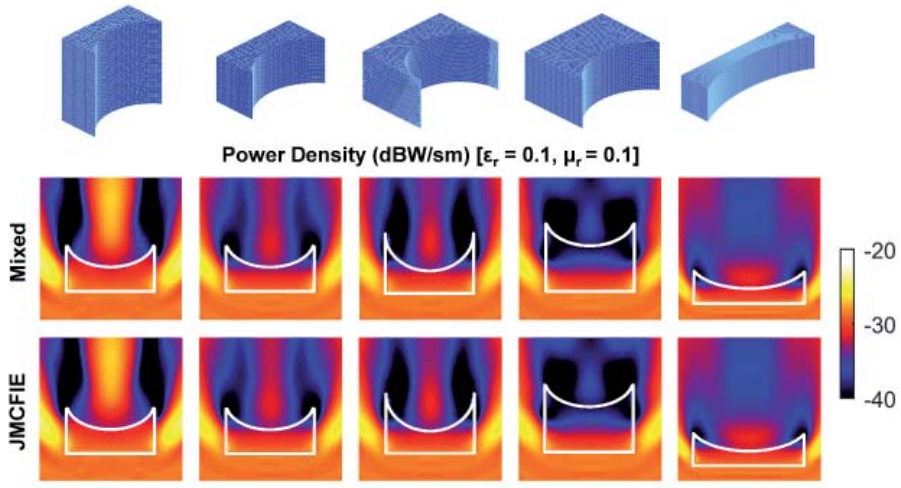

Vol. 2019, No. 370
September 2019

URSI, c/o Ghent University (INTEC)
Technologiepark - Zwijnaarde 126, B-9052 Gent (Belgium)

Contents

Cover: (top) The time-resolved laser-induced deformation of a rough sample: the deformation of a graphene oxide film for an incident power of $P = 4.7$ mW and a pulse duration of 80 ms. The upper-right inset shows a picture of a graphene-oxide film drop cast onto a glass slide. See the paper by Pooja Munjal and Kamal P. Singh. (bottom) The computed results (power density) for Geometries 1-5 of SOLBOX-17 when both the relative permittivity and relative permeability of the structures were 0.1. See the SOLBOX column by Hande İbili and Özgür Ergül.

The International Union of Radio Science (URSI) is a foundation Union (1919) of the International Council of Scientific Unions as direct and immediate successor of the Commission Internationale de Télégraphie Sans Fil which dates from 1914.

Radio Science Bulletin Staff

Editor

W. R. Stone
Stoneware Limited
840 Armada Terrace
San Diego, CA 92106, USA
Tel: +1-619 222 1915, Fax: +1-619 222 1606
E-mail: r.stone@ieee.org

Editor-in-Chief

P. Van Daele
URSI Secretariat
Ghent University - INTEC
Technologiepark - Zwijnaarde 126
B-9052 Gent, BELGIUM
Tel: +32 9-264 33 20, Fax: +32 9-264 42 88
E-mail: Pet.VanDaele@UGent.be

Production Editor

I. Lievens
URSI Secretariat / Ghent University - INTEC
Technologiepark - Zwijnaarde 126
B-9052 Gent, BELGIUM
Tel: +32 9-264.33.20, Fax: +32 9-264.42.88
E-mail: ingeursi@ugent.be, info@ursi.org

Senior Associate Editors

A. Pellinen-Wannberg
Department of Physics
Umea University
BOX 812
SE-90187 Umea, SWEDEN
Tel: +46 90 786 74 92, Fax: +46 90 786 66 76
E-mail: asta.pellinen-wannberg@umu.se

O. Santolik
Institute of Atmospheric Physics
Academy of Sciences of the Czech Republic
Bocni II
1401, 141 31 Prague 4, CZECH REPUBLIC
Tel: +420 267 103 083, Fax +420 272 762 528
E-mail os@ufa.cas.cz, santolik@gmail.com

Associate Editors, Commissions

Commission A

Nuno Borges Carvalho
Instituto de Telecomunicaçoes
Universidade de Aveiro, Campus Universitario
3810-193 Aveiro, Portugal
Tel: +351 234377900, Fax: +351 234377901
E-mail: nbcarvalho@ua.pt

Pedro Miguel Cruz
Rua Sao Sebastiao
n34 Hab 33
4520-250 Santa Maria da Feira, Aveiro, PORTUGAL
Tel: +351 225898410
E-mail: pedro.cruz@controlar.pt

Tian Hong Loh
National Physical Laboratory
Hampton Road
Teddington TW11 0LW, United Kingdom
Tel: +44 020 8943 6508
E-mail: tian.loh@npl.co.uk

Nosherwan Shoaib
School of Electrical Engineering and Computer Science (SEECS)
National University of Sciences and Technology (NUST)
NUST Campus H-12, Islamabad, Pakistan
Tel: 051 90852561
E-mail: nosherwan.shoaib@seccs.edu.pk

Commission B

Andrea Michel
Department of Information Engineering
Università di Pisa
Pisa, Italy
E-mail: andrea.michel@iet.unipi.it

John Volakis
College of Engineering and Computing
Florida International University
10555 W. Flagler Street, EC2477
Miami, FL 33174, USA
Tel: +1 305 348 2807
E-mail: jvolakis@fiu.edu

Commission C

Yves Louet
CS 47601, SUPELEC
Avenue de Boulaie
F-35576 Cesson-Sévigné, France
Tel: +33 2 99 84 45 34, Fax: +33 2 99 84 45 99
E-mail: yves.louet@supelec.fr

Commission D

Naoki Shinohara
RISH
Kyoto University
Uji 611-0011, Japan
Tel: +81 774 38 3807 Fax: +81 774 31 8463
E-mail: shino@rish.kyoto-u.ac.jp

Commission E

Virginie Deniau
IFSTTAR
20. rue Elisée Reclus BP 70317
F-59666 Villeneuve d'Ascq Cedex, France
Tel: +33 03 20438991
E-mail: virginie.deniau@ifsttar.fr

Commission F

Haonan Chen
Earth System Research lab, Physical Sciences Division
NOAA
325 Broadway, Boulder, CO 80305, USA
Tel: +1 303 497 4616
E-mail: haonan.chen@noaa.gov

Tullio Tanzi
Télécom ParisTech - LabSoC, c/o EURECOM
Campus SophiaTech Les Templiers
450 route des Chappes 06410 Biot, FRANCE
Tel: +33 0 4 93008411, Fax: 33 0 493008200
E-mail: tullio.tanzi@telecom-paristech.fr

Commission G

Giorgiana De Franceschi
Dept. Arenonomy, Istituto Nazionale di Geofi sica e Vulcanology
Via di Vigna, Murata 605
00 143 Roma, Italy
Tel: +39 06 51860307, Fax: +39 06 51860397
E-mail: giorgiana.defranceschi@ingv.it

Commission H

Jyrki Manninen
Sodankylä Geophysical Observatory
Tähteläntie 62
FIN-99600 Sodanskylä, Finland
Tel: +358 400 151503, Fax +358 16 610248
E-mail: Jyrki.Manninen@oulo.fi

Commission J

Jacob W. Baars
Max Planck Institute for Radio Astronomy
Auf dem Hügel 69
53121 Bonn, Germany
Tel: +49 228 525303
E-mail: jacobbaars@arcor.de

Commission K

Kensuke Sasaki
Applied EM Research Institute
NICT
Koganei, Tokyo, Japan
E-mail: k_sasaki@nict.go.jp

Associate Editors, Columns

Book Reviews

G. Trichopoulos
Electrical, Computer & Energy Engineering ISTB4 555D
Arizona State University
781 E Terrace Road, Tempe, AZ, 85287 USA
Tel: +1 (614) 364-2090
E-mail: gtrichop@asu.edu

Historical Papers

J. D. Mathews
Communications and Space Sciences Lab (CSSL)
The Pennsylvania State University
323A, EE East
University Park, PA 16802-2707, USA
Tel: +1(814) 777-5875, Fax: +1 814 863 8457
E-mail: JDMathews@psu.edu

Et Cetera

T. Akgül
Dept. of Electronics and Communications Engineering
Telecommunications Division
Istanbul Technical University
80626 Maslak Istanbul, TURKEY
Tel: +90 212 285 3605, Fax: +90 212 285 3565
E-mail: tayfunakgul@itu.edu.tr.

Women in Radio Science

A. Pellinen-Wannberg
Department of Physics and Swedish Institute of Space Physics
Umeå University
S-90187 Umeå, Sweden
Tel: +46 90 786 7492
E-mail: asta.pellinen-wannberg@umu.se

Ethically Speaking

R. L. Haupt
Colorado School of Mines
Brown Building 249
1510 Illinois Street, Golden, CO 80401 USA
Tel: +1 (303) 273 3721
E-mail: rhaupt@mines.edu

A. J. Shockley
E-mail: aj4317@gmail.com

Solution Box

Ö. Ergül
Department of Electrical and Electronics Engineering
Middle East Technical University
TR-06800, Ankara, Turkey
E-mail: ozgur.ergul@eee.metu.edu.tr

Telecommunications Health & Safety

J. C. Lin
University of Illinois at Chicago
851 South Morgan Street, M/C 154
Chicago, IL 60607-7053 USA
Tel: +1 312 413 1052, Fax: +1 312 996 6465
E-mail: lin@uic.edu

Historical Column

G. Pelosi
Department of Information Engineering
University of Florence
Via di S. Marta, 3, 50139 Florence, Italy
E-mail: giuseppe.pelosi@unifi.it

Early Career Representative Column

S. J. Wijnholds
Netherlands Institute for Radio Astronomy
Oude Hoogeveensedijk 4
7991 PD Dwingeloo, The Netherlands
E-mail: wijnholds@astron.nl

Education Column

Madhu Chandra
Microwave Engineering and Electromagnetic Theory
Technische Universität Chemnitz
Reichenhainerstrasse 70
09126 Germany
E-mail: madhu.chandra@etit.tu-chemnitz.de

URSI Officers and Secretariat

Current Officers triennium 2017-2020

President

M. Ando
Senior Executive Director
National Institute of Technology
701-2, Higashi Asakawa, Hachioji,
Tokyo 193-0834, Japan
Tel:+81-42-662-3123,
Fax: +81-42-662-3131
E-mail: ando@kosen-k.go.jp,
mando@antenna.ee.titech.ac.jp

Vice President

O. Santolik
Institute of Atmospheric Physics
Electrical Eng. Dept
Academy of Sciences of the Czech Republic
Bocni II, 1401
141 31 Prague 4, CZECH REPUBLIC
Tel: +420 267 103 083
Fax: 420 272 762 528
E-mail: os@ufa.cas.cz, santolik@gmail.com

Past President

P. S. Cannon
Gisbert Kapp Building
University of Birmingham
Edgbaston , Birmingham, B15 2TT,
UNITED KINGDOM
Tel: +44 (0) 7990 564772
Fax: +44 (0)121 414 4323
E-mail: p.cannon@bham.ac.uk

Vice President

A. Sihvola
Electronic Science Department
Aalto University
School of Electrical Engineering
PO Box 13000
FI-00076 AALTO
FINLAND
Tel: +358 50 5871286
E-mail: Ari.Sihvola@aalto.fi

Secretary General

P. Van Daele
URSI Secretariat
Ghent University - INTEC
Technologiepark - Zwijnaarde 126
B-9052 Gent
BELGIUM
Tel: +32 9-264 33 20
Fax: +32 9-264 42 88
E-mail: Pet.VanDaele@UGent.be

Vice President

P. L. E. Uslenghi
Dept. of ECE (MC 154)
University of Illinois at Chicago 851
S. Morgan Street
Chicago, IL 60607-7053
USA
Tel: +1 312 996-6059
Fax: +1 312 996 8664
E-mail: uslenghi@uic.edu

Vice President

W. Baan
Astron
Asserweg 45
9411 LP Beilen
THE NETHERLANDS
Tel: +31 521-595 773/100
Fax: +31 521-595 101
E-mail: baan@astron.nl

URSI Secretariat

Secretary General

P. Van Daele
URSI Secretariat
Ghent University - INTEC
Technologiepark - Zwijnaarde 126
B-9052 Gent
BELGIUM
Tel: +32 9-264 33 20
Fax: +32 9-264 42 88
E-mail: Pet.VanDaele@UGent.be

Assistant Secretary General AP-RASC

K. Kobayashi
Dept. of Electr and Commun. Eng,
Chuo University
1-13-27 Kasuga, Bunkyo-ku
Tokyo, 112-8551, JAPAN
Tel: +81 3 3817 1846/69
Fax: +81 3 3817 1847
E-mail: kazuya@tamacc.chuo-u.ac.jp

Assistant Secretary General

Stefan J. Wijnholds
Netherlands Institute for
Radio Astronomy
Oude Hoogeveensedijk 4
7991 PD Dwingeloo
The Netherlands
E-mail: wijnholds@astron.nl

Executive Secretary

I. Heleu
URSI Secretariat
Ghent University - INTEC
Technologiepark - Zwijnaarde 126
B-9052 Gent
BELGIUM
Tel. +32 9-264.33.20
Fax +32 9-264.42.88
E-mail info@ursi.org

Assistant Secretary General Publications & GASS

W. R. Stone
840 Armada Terrace
San Diego, CA 92106
USA
Tel: +1-619 222 1915
Fax: +1-619 222 1606
E-mail: r.stone@ieee.org

Administrative Secretary

I. Lievens
URSI Secretariat
Ghent University - INTEC
Technologiepark - Zwijnaarde 126
B-9052 Gent
BELGIUM
Tel: +32 9-264.33.20
Fax: +32 9-264.42.88
E-mail: ingeursi@ugent.be

Editor's Comments

W. Ross Stone
Stoneware Limited
840 Armada Terrace
San Diego, CA 92106, USA
Tel: +1-619 222 1915, Fax: +1-619 222 1606
E-mail: r.stone@ieee.org

Special Issue on URSI AP-RASC 2019

This issue is the first of two special issues of the *Radio Science Bulletin* with papers based on presentations from the 2019 URSI Asia-Pacific Radio Science Conference (AP-RASC 2019), held March 10-14, 2019, at the India Habitat Centre, New Delhi, India. This issue contains three papers based on Student Paper Competition papers and the keynote presentation from Commission B. The December issue will contain additional papers based on Student Paper Competition papers, more of the Commission keynote presentations, and a paper based on one of the General Lectures.

We are grateful to Amitava Sen Gupta, Subra Ananthakrishnan, and Kazuya Kobayashi, the guest editors of this special issue, for all of their excellent efforts in bringing these papers to us. They have provided a separate introduction to the special issue.

While all of these papers are based on presentations at AP-RASC 2019, they all were invited on the basis of being significantly extended beyond the conference papers.

The paper by Pooja Munjal and Kamal Singh looks at the challenging effort to optically probe the laser-induced deformation of a solid surface with picometer resolution. They demonstrated the deformation and relaxation of both smooth and rough surfaces using low-power laser pulses. They then showed how to measure this deformation as a function of time using a simple, single-lens interferometer. The results should find application in laser heating and cooling experiments.

Understanding the theoretical generation of kinetic Alfvén waves in the Earth's magnetosphere is the topic of the paper by K. C. Barik, S. V. Singh, and G. S. Lakhina. They considered a three-component plasma model consisting of cold background ions, hot electrons, and hot ion beams. They showed that the ion beam alone can excite kinetic Alfvén waves. However, the presence of an anti-parallel ion beam and positive shear results in much larger wave growth. They applied the model to polar cusp and auroral regions of the Earth's magnetosphere. Their results were able to explain several properties of the observed ultra-low-frequency waves observed in those regions.

The topic of the paper by Mia Filić and Renato Filjar is a method for providing an early warning for potential GNSS (Global Navigation Satellite System) position-performance deterioration. This is based on GPS-derived observations of total electron content (TEC). The authors used a case study involving measurements made during the 2015 St. Patrick large ionospheric storm. Measurements were taken of sudden ionospheric disturbance (SID) monitoring using reception of VLF signal strength. These measurements were correlated with the GPS-derived TEC observations. The results indicated that the technique could be used for the proposed early-warning system. Such results might also aid in understanding the lower-ionospheric contribution to the overall TEC.

The paper based on the Commission B keynote talk by Ari Sihvola and Ismo Lindell should be fascinating reading for anyone interested in basic electromagnetics. It deals with what happens when electromagnetic fields interact with a surface on which given boundary conditions are enforced, with a particular focus on waves matched at the surface. The boundary conditions discussed go substantially beyond the classical perfect-electric-conductor and perfect-magnetic-conductor cases. However, they are conditions that are experimentally encountered, and have particular importance for interfaces with graphene and metamaterial structures. The authors also identify and explain a very interesting phenomenon associated with a resonant structure in the scattering spectrum of sub-wavelength impedance-boundary scatterers.

Our Other Contributions

In his Book Review column, George Trichopoulos has brought a review of an unusual biography of Jan Hendrik Oort. What is unusual about the biography is that it is at least as much about the science that Oort studied as it is about Oort. The review was provided by Jacob Baars.

You will get a laugh out of Tayfun Akgul's perspective on artificial intelligence in his Et Cetera column.

We have several important and interesting reports in this issue. There is a summary of the URSI Commission B triennial Electromagnetic Theory Symposium. The 2018 annual report on the Scientific Committee on Frequency Allocations for Radio Astronomy and Space Science (IUCAF) is included.

Amy Shockley and Randy Haupt look at the concept of personal bandwidth in their Ethically Speaking column. They discuss the Planning Fallacy, which I had not previously heard of but I had certainly experienced. I think you'll find this column thought provoking.

The 2020 EurAAP Felsen Award is announced in this issue. The deadline for nominations is **January 31, 2020**.

Giuseppe Pelosi's Historical Corner has a very nice account of a recent tour by Giuseppe and Stefano Selleri, visiting the houses of James Clerk Maxwell. The history associated with the houses is also described and, as usual, the article is illustrated with some very interesting photos.

Sadly, we have In Memoriam pieces for three very respected radio scientists in this issue: Yakov S. Shifrin, Edward J. Smith, and Richard M. Thorne.

Özgür Ergül's Solution Box column presents an interesting study of cylindrical lens structures by Hande İbili and Özgür Ergül. These are made of near-zero-index materials, and the dimensions and wavelengths are such that the computations of the fields in the vicinities of the lens structures are quite challenging. The results provide fascinating insights both into the way of doing such computations, and into how such lens structures behave.

If you have any interest at all in the possible relationship between cell-phone electromagnetic radiation and cancer in animals, you need to read Jim Lin's Telecommunications Health and Safety column. He takes a critical look at the US National Toxicology Program's recent final report on an important study, and notes one significant aspect that should not be overlooked.

Asta Pellinen Wannberg has brought us many very interesting contributions from women radio scientists around the world in her Women in Radio Science column. In this issue, she introduces Rowayda Sadek. Prof. Sadek has held important positions in both academia and industry in Egypt, other parts of the Middle East, and Canada. Prof. Sadek provides a unique perspective on the challenges and opportunities for women in radio science in those geographic and cultural areas as part of the narrative of her own story. She also shares her own particular views on the potential roles of women.

Submit Your Papers Now!

The triennial URSI General Assembly and Scientific Symposium (GASS) will be held August 29 to September 5, 2020, at the Sapienza University campus, Rome, Italy. The paper-submission Web site is now open: https://www.ursi2020.org/author-info-abstract-submission/. The deadline for submission is **January 31, 2020**. The preliminary scientific program is available on the Web site. Contributed papers are welcome. I urge you to submit!

Best Wishes for the New Year!

This issue was delayed, so it may reach you at the end of 2019. It comes with best wishes for most joyous holidays, and for a very happy, healthy, safe, and prosperous New Year!

Introduction to the Special Issue on the 2019 URSI AP-RASC Student Paper Competition

The 2019 URSI Asia-Pacific Radio Science Conference (URSI AP-RASC 2019) was held at the India Habitat Centre, New Delhi, India, during March 10-14, 2019 [1, 2]. This special issue of the *Radio Science Bulletin* provides a collection of invited papers authored by the recipients of the awards from the URSI AP-RASC 2019 Student Paper Competition.

According to the tradition of the AP-RASC conferences, the Student Paper Competition (SPC) was organized at the URSI AP-RASC 2019 jointly by URSI and the Indian National Committee of URSI (INCURSI). In order to review the Student Paper Competition applications and select the recipients, the URSI AP-RASC 2019 Young Scientist Program Committee was formed: Prof. Willem Baan (Chair), URSI Vice President; Prof. Makoto Ando (Co-Chair), URSI President; Prof. Subra Ananthakrishnan (Co-Chair), URSI past Vice-President; Prof. Stefan Wijnholds (Co-Chair), URSI Assistant Secretary-General.

Members of the committee included the following (the first person listed for each Commission is the Chair of the corresponding URSI Commission; the second person listed chairs the INCURSI Commission):

Commission A: Dr. Yashuhiro Koyama, Dr. Amitava Sen Gupta

Commission B: Prof. Kazuya Kobayashi, Prof. Debatosh Guha

Commission C: Dr. Amir Zaghloul, Dr. M. V. S. N. Prasad

Commission D: Dr. Apostolos Georgiadis, Prof. Anantha Ramakrishna

Commission E: Prof. Frank Gronwald, Prof. Subra Ananthakrishnan

Commission F: Prof. V. Chandrasekhar, Prof. Animesh Maitra

Commission G: Prof. Patricia Doherty, Dr. Amit Patra

Commission H: Janos Lichtenberger, Prof. Gurubax Lakhina

Commission J: Dr. Richard Bradley, Prof. Janardhan Padmanabhan

Commission K: Prof. Joe Wiart, Prof. Rajamani Paulraj

The Young Scientist Program Committee (YSPC) selected seven finalists from among 34 Student Paper Competition applicants before the conference. All the Student Paper Competition finalists were given free registration for the conference, free accommodations, and free tickets for the banquet. The Student Paper Competition special session was organized on March 11, 2019, where all the finalists made oral presentations. The Young Scientist Program Committee further carefully evaluated the presentations by the finalists, and selected the three winners of the first, second, and third prizes. Three more were presented with honorable mention. One person did not respond.

The results of the selection were the following:

First Prize: Pooja Munjal

Second Prize: Shuto Takahashi

Third Prize: Krushna Chandra Barik

Honorable Mention: Shuang Liu, Mia-Filic, Sreenath Reddy Thummaluru

The award ceremony was held during the banquet on March 13, where the prize winners received certificates and prizes of US$1,000, US$750, and US$500, respectively. The two non-winning finalists each received a certificate. Figure 1 shows a group photo of the five Student Paper Competition recipients.

The following three invited papers, based on the entries of the Student Paper Competition award recipients, appear in this special issue of the *Radio Science Bulletin*:

Pooja Munjal and Kamal P. Singh, "Optically Probing Picometer-Resolved Photo-Dynamics of Solid Surfaces"

K. C. Barik, S. V. Singh, and G. S. Lakhina, "A Theoretical Model for the Generation of Kinetic Alfvén Waves in the Earth's Magnetosphere by Ion Beam and Velocity Shear"

Mia Filić and Renato Filjar, "A Considerable Level of Correlation Between SID-Monitoring Time Series and GPS-Derived TEC Observations Taken During Development of a Massive Ionospheric Storm"

Figure 1. A group photo of the five Student Paper Competition recipients, along with the 2019 AP-RASC organizers.

In addition, a paper based on the 2019 AP-RASC Commission B keynote lecture is also included in this issue:

Ari Sihvola and Ismo V. Lindell, "Matched Waves and Unexpected Resonances: Variety of Boundary Conditions"

Additional papers based on papers from the 2019 AP-RASC Student Paper Competition, as well as papers based on the Commission keynote lectures and General Lectures, will appear in the December 2019 issue of the *Radio Science Bulletin*.

We were happy that the URSI AP-RASC 2019 Student Paper Competition was a great success. This success was due to the constant efforts by the Indian National Committee of URSI during the course of preparations of the conference. We were particularly thankful to the URSI AP-RASC 2019 Young Scientist Program Committee for their hard work. In addition, the team from JNU did an outstanding job as the Conference Secretariat. Finally, we would like to express our appreciation to the Student Paper Competition recipients who contributed to this special issue.

References

1. URSI AP-RASC 2019 Web site, http://aprasc2019.org/.

2. URSI AP-RASC 2019 final program, http://www.ursi.org/content/AP-RASC/AP-RASC2019/URSI_APRASC_2019_Program.pdf

Guest Editors:
Amitava Sen Gupta
LOC Chair, URSI AP-RASC 2019
NorthCap University, India
E-mail: sengupta53@yahoo.com

Subra Ananthakrishnan
General Chair, URSI AP-RASC 2019
S. P. Pune University, India
E-mail: subra.anan@gmail.com

Kazuya Kobayashi
General Co-Chair, URSI AP-RASC 2019
Chuo University, Japan
E-mail: kazuya@tamacc.chuo-u.ac.jp

Optically Probing Picometer-Resolved Photo-Dynamics of Solid Surfaces

Pooja Munjal and Kamal P. Singh

Department of Physical Sciences
Indian Institute of Science Education and Research
Mohali
Sector-81, Manauli 140306, India
E-mail: poojamunjal4@gmail.com

Abstract

Optical probes for precisely studying laser-solid interactions are of utmost importance in various fields. Here we demonstrate a simple, single-lens interferometer for measuring time-resolved deformation of solid surfaces induced by optical excitation with about 150 pm ($\lambda/4000$) precision by analyzing the local intensity of the interference fringes in a self-referencing manner. We first show picometer-resolved deformation and relaxation of a smooth acrylic surface due to absorption of a sub-mW low-power laser pulse. We demonstrate the applicability of our approach to samples producing non-specular reflections, such as a dried drop of blood and a black rough surface of graphene oxide, prepared by drop-casting on a glass slide. We suggest that the thermo-mechanical deformation from our interferometer can be used to measure thermal effects (such as the local change in temperature) of different solid materials with high precision, which is needed in many applications such as in laser heating or cooling experiments. It will be interesting to extend our approach to study real-time thermal and non-thermal deformation in solids due to nanosecond or picosecond laser pulses.

1. Introduction

Precise mechanical characterization of various materials and devices has always been a basic necessity for revolutionizing technology. A sample exposed to electromagnetic radiation exhibits thermal effects through non-radiative processes, causing the sample to expand or contract or to form a local bulge or dimple. Various physical quantities, such as the optical density, the photo-thermal and photo-elastic response of materials, the thermal expansion coefficient, etc., rely on the measurement of such mechanical effects caused by external fields. Many techniques exist for surface-deformation analysis of materials, such as scanning electron microscopy (SEM) [1], X-ray diffraction [2], photo-thermal deflection spectroscopy (PDS) [3], atomic-force microscopy (AFM) [4], and Raman microscopy [5]. Optical techniques based on Michelson [6] and Mirau [7] interferometers have also been demonstrated, with the advantages of being contactless, noninvasive, and free of sample preparation, yet offering precision in the nanometer range or below.

Interferometry is widely used in industry [8], for example, to measure crystal growth [9], metrology [10], and for surface topography and surface temperature measurements [11, 12]. Most existing precision interferometers require optical-quality components (beam splitters, mirrors, samples, etc.), which limit their applications to smooth sample surfaces. A multi-component interferometer requires careful alignment and stabilization of each component against various sources of noise. It is important and necessary to develop a minimal-component interferometric technique that is compact and highly-precise to quantitatively measure deformations of smooth as well as rough surfaces in real time.

Here we used a robust single-lens interferometer, and demonstrate its application in measuring local deformation of three samples with about 100 pm precision, without any need for an external calibration standard. We measured the time-resolved photo-thermal mechanics of solid surfaces illuminated by a focused low-power pump laser by measuring the interference intensity through a photodiode and iris system. We demonstrated the application of our setup to measure deformation dynamics of two representative rough samples (graphene oxide and dried blood) by obtaining an interference pattern from their non-specular reflection. Such deformation dynamics may enable the measurement of the real-time change in local temperature of solid samples, provided one has a prior knowledge of the coefficient of absorption and thermal expansion coefficient. Our setup will find application in studying laser cooling of solids as well [13-15], on sub-ns time scales.

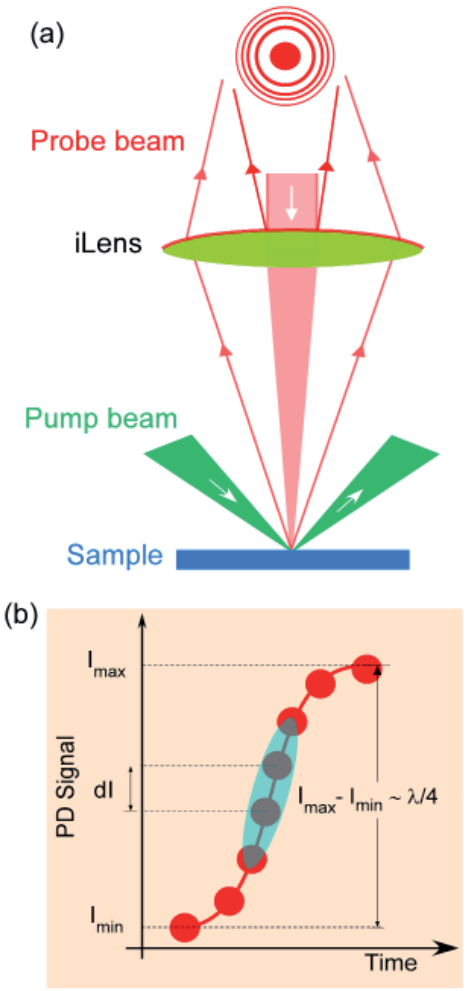

Figure 1. The experimental setup and an illustration of self-calibration. (a) A schematic of the single-lens interferometer for probing solid samples. A low-power He-Ne laser (10 mW, $\lambda = 632$ nm) was used as a probe to produce interference fringes from the sample, while another low-power green laser ($\lambda = 532$ nm) induced local deformation. (b) An illustration of a self-calibrated picometer measurement using a single-point interference intensity. The shaded blue region shows the linear-response regime.

2. Experimental Setup

The schematics of our setup are shown in Figure 1a. We used a collimated Gaussian beam of a He-Ne laser (10 mW, $\lambda = 632$ nm, $1/e^2$ full waist $2\omega_0 = 1.0$ mm) to obtain high-contrast interference fringes from the sample surface using our versatile single-lens interferometer [16]. Our interferometer consisted of a single partially-silver-coated convex lens (hereafter referred to as iLens) that integrated the functions of a beam splitter, a reference mirror, and a light collector, which are generally derived from three or more optical components of any interferometer. Briefly, the incoming probe beam was divided into two beams, a reference beam and the object beam, at the front surface of the iLens. The iLens then collected the back-scattered light from the sample and projected it towards the screen, where it combined with the reference beam to produce high-contrast fringes.

We measured pico-mechanical dynamics on three different sample surfaces: a smooth red-acrylic surface, and two rough surfaces (producing non-specular reflection), namely, a dried blood drop and a graphene-oxide thin film prepared by drop-casting a corresponding solution onto a glass slide. We generated a reference modulation in the fringe intensity by vertically displacing the sample by a known amount using a piezo stage (with a calibration of 7.5V ≈ 2 μm). A half-fringe collapse in the signal corresponded to a sample displacement of $\lambda/4$, which equaled 158 nm in our case. We further resolved intensity using the PD with a resolution of dI, giving

$$dI = \frac{I_{max} - I_{min}}{N},$$

where N denotes the number of data points, as shown in Figure 1b. The displacement resolution is then given by $\lambda/4N$, as shown in the schematic illustration of Figure 1b.

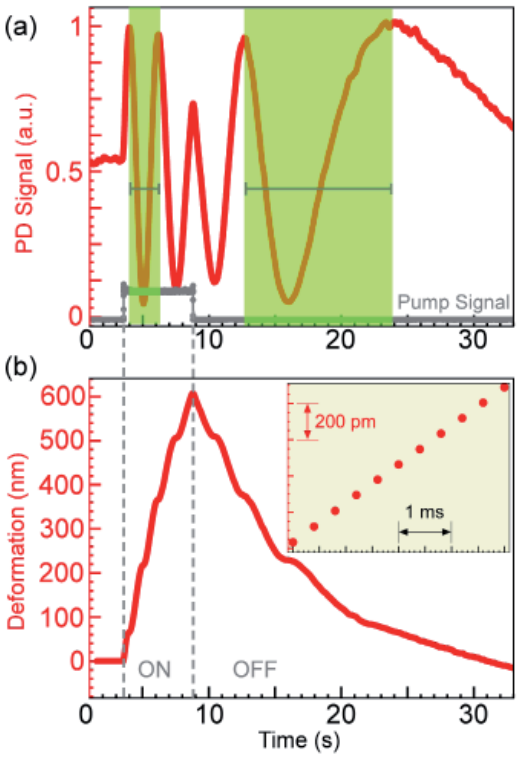

Figure 2. The measurement of time-resolved deformation of the acrylic surface induced by a pump laser. (a) The interference intensity and corresponding pump signal (shown in grey). A shutter was used to control the pump exposure. Note that the time interval between fringe maxima varied. (b) The deformation of the sample surface with 150 pm precision.

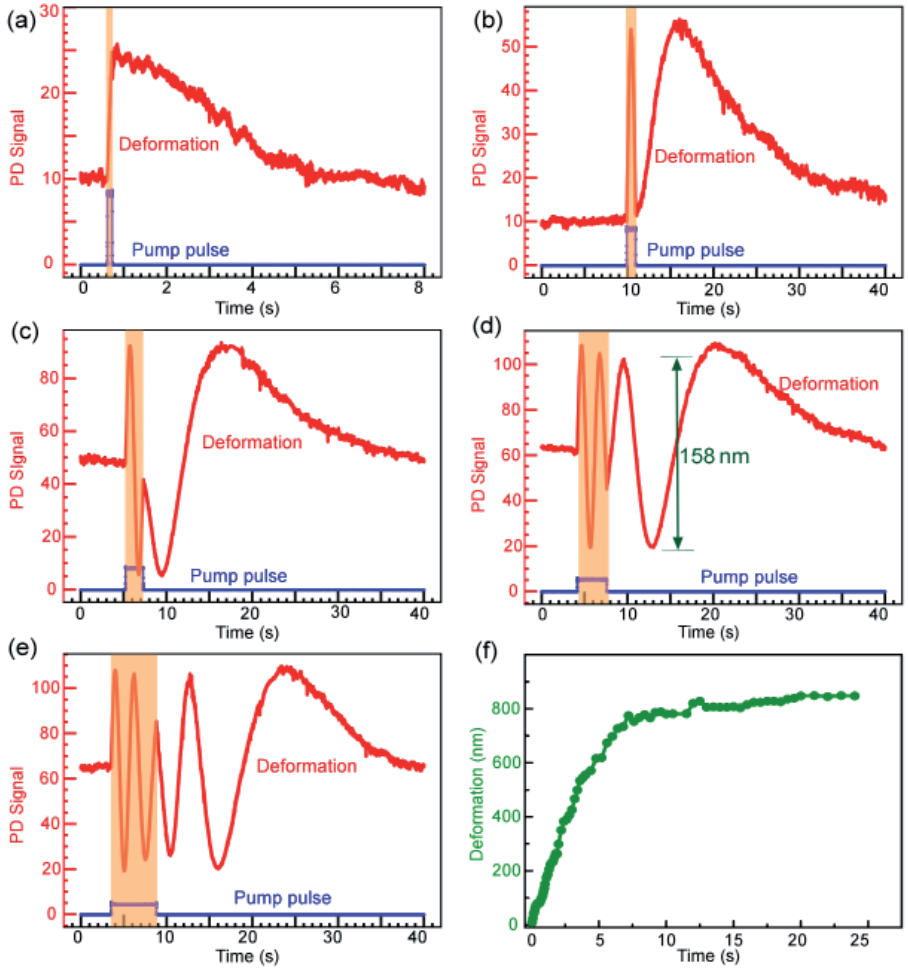

Figure 3. The deformation dynamics of acrylic for fixed $P = 6$ mW at different exposure times: (a) 100 ms, (b) 1 s, (c) 2 s, (d) 3.4 s, (e) 5.2 s. (f) Maximum deformation at the end of the pulse showed a saturation for a pulse exposure greater than 7.5 s.

For our case, $N \sim 1000$, leading to a precision of ~ 150 pm. The intensity at the center of the fringes obtained was recorded on an oscilloscope using a photodiode and a pinhole iris, the dimensions of which were chosen to obtain high contrast in the interference oscillations.

To determine the direction of deformation, the piezo stage was electronically displaced such that the length of the interferometric cavity was increasing relating to a corresponding change in the interference-fringe intensity.

The sample was locally deformed by focusing a low-power CW pump laser ($\lambda = 532$ nm, $P = 6$ mW) for varying exposure times. The pump laser was spatially overlapped on the probe beam on the sample, and was made to be obliquely incident, as shown in Figure 1a. The spot size of both the pump and the probe beam on the sample were around 300 µm and 400 µm, respectively (measured with a CCD beam profiler from Thorlabs). Since the spot size for the probe was larger than the spot size of the pump beam, the maximum deformation at the center of the pump was recorded. We used a 650 nm ± 40 nm bandpass filter to block the unwanted stray reflection of the pump laser.

3. Results

3.1 Pico-Mechanical Dynamics of a Smooth Surface

To measure photo-induced deformation by a mW-level pump beam, we biased the piezo stage to be at the center of the linear regime, i.e., of the interference intensity (the shaded region in Figure 1b). The direction of deformation (i.e., the formation of a bump or a dimple on the sample) was a priori determined by relating the change in the interference intensity (increase or decrease) by displacing the sample in the known direction. With no pump exposure, a constant interference intensity was observed. The pump exposure and the interference intensity were simultaneously recorded on the oscilloscope.

Figure 2a shows the deformation dynamics of an acrylic surface for a $P = 6$ mW pump beam exposed for 5 s duration. We clearly observed a bulge induced by local heating, followed by relaxation when the pump pulse was switched off. During the heating period, the rate of collapse of fringes tended to reduce and the sample deformation reached a maximum value at the end of the pump pulse (corresponding to maximum temperature) as shown in Figure 2b. After the pump exposure, the sample relaxed back to its original state (corresponding to cooling back to the initial temperature). Note that for such a low-power laser, the deformation was fully reversible, without any permanent physical-state change. The magnitude of deformation in Figure 2b was calculated by extracting the phase corresponding to the recorded intensity variation. The deformation in the sample was successively added after every half-fringe collapse corresponding to $\lambda/4 \approx 158$ nm. The displacement resolution in our measurement was sub-200 pm as shown in the inset of Figure 2b.

The deformation dynamics of acrylic for different exposure times from 40 ms to 25 s is shown in Figure 3f. We observed that for a fixed pump power, a longer exposure time produced a larger deformation, as shown in Figures 3a-3e. The deformation in the sample attained a maximum value (for ≈ 7.5 s exposure) and then remained at this value for longer exposure times as shown in Figure 3f. We attributed this behavior to the fact that the sample had attained its maximum temperature and reached thermal equilibrium. If a higher power laser was used, permanent damage to the sample could be observed.

3.2 Displacement of Rough Surfaces

To measure the displacement of a rough sample, we prepared two samples: a dried blood drop and a graphene-oxide film on a glass slide by the drop-casting method (see Figures 4a and 4b for actual pictures of the samples). Remarkably, our single-lens interferometer was able to collect non-specular reflections from these samples and fringes were obtained. Using the above-described approach of fringe analysis, we observed displacements of 60 nm and 95 nm, respectively, with a real-time resolution of 200 pm for the two samples, as shown in Figures 4a and 4b.

With these photo-induced mechanical deformations of various samples, our technique can also be used to estimate the change in the local temperature of the sample. At mW-level laser power, the solid sample mostly locally expands due to the absorption of heat. The magnitude of the radiation-pressure force is expected to be in the pico-Newton range (of the order of P/c, where c is the speed of light), and the resulting mechanical deformation of solids is beyond the detection sensitivity of our technique. In our experiments, the absorption of the laser radiation causes the sample to locally heat and the induced thermal stress is balanced by the elasticity of the material. Knowing the thermal-expansion coefficient and the elasticity modulus of the material, the geometry of sample, and its optical-absorption coefficient, one can quantitatively estimate the local temperature change in the sample [17, 18]. While a detailed modeling will be of interest, our approach may help to isolate competing effects of radiation-pressure and heating towards developing a better understanding of light-matter interaction in rough samples.

4. Summary

In conclusion, we have reported a simple and versatile optical technique for measuring time-resolved optical deformation with picometer resolution using high-contrast fringes produced by a compact single-lens interferometer. The dynamic fringes produced by the modulating sample were recorded using a photodiode with a pinhole. Application of our technique to observe the time-resolved fast dynamics of solid surfaces and to measure reversible deformation (heating and cooling) of substrates at picometer scales was demonstrated with a precision of 150 pm for the acrylic sample. We also extended our approach to probe

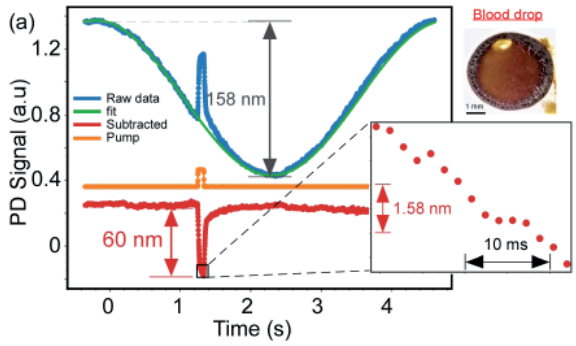

Figure 4a. The time-resolved laser-induced deformation of rough samples. The deformation dynamics of a blood sample for $P = 500$ µW and 80 ms. The upper-right inset shows the image of a dried blood drop on a glass slide.

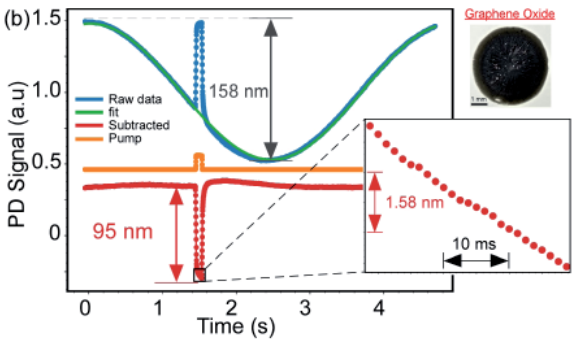

Figure 4b. The time-resolved laser-induced deformation of rough samples. The deformation of a graphene oxide film for $P = 4.7$ mW and 80 ms. The upper-right inset shows a picture of a graphene-oxide film drop cast onto a glass slide.

the nano-mechanical dynamics of two rough surfaces, a dried drop of blood and a graphene-oxide surface. These measurement properties may allow determination of various thermo-mechanical properties, such as the thermal diffusivity and surface temperature of the materials.

We envision that our single-lens interferometer may allow probing the ultra-fast dynamics of solid surfaces exposed to nanosecond or picosecond laser pulses. Furthermore, the technique can also be adapted to measure sub-nm deformations of liquids and semi-solids subjected to external fields.

5. Acknowledgements

We thank DST and the Max-Plank Society for financial support.

6. References

1. J. I. Goldstein, D. E. Newbury, J. R. Michael, N. W. Ritchie, J. H. J. Scott, and D. C. Joy, *Scanning Electron Microscopy and X-Ray Microanalysis*, Berlin, Springer, 2017.

2. B. E. Warren, *X-Ray Diffraction*, Courier Corporation, 1990.

3. S. Chen, C. P. Grigoropoulos, H. K. Park, P. Kerstens, and A. C. Tam, "Photothermal Displacement Measurement of Transient Melting and Surface Deformation During Pulsed Laser Heating," *Applied Physics Letters*, **73**, 15, October 1998, pp. 2093-2095.

4. C. R. Blanchard, "Atomic Force Microscopy," *The Chemical Educator*, **1**, 5, December 1996, pp. 1-8.

5. A. Hartschuh, E. J. Sánchez, X. S. Xie, and L. Novotny, "High-Resolution Near-Field Raman Microscopy of Single-Walled Carbon Nanotubes," *Physical Review Letters*, **90**, 9, March 2003, pp. 095503.

6. A. A. Michelson and E. W. Morley, "LVIII. On the Relative Motion of the Earth and the Luminiferous Æther," *The London, Edinburgh, and Dublin Philosophical Magazine and Journal of Science*, **24,** 151, December 1887, pp. 449-463.

7. M. A. Henri, "Interferometer," US Patent 2,612,074, September 1952.

8. A. Wada, M. Kato, and Y. Ishii, "Multiple-Wavelength Digital Holographic Interferometry Using Tunable Laser Diodes," *Applied Optics*, **47**, 12, April 2008, pp. 2053-60.

9. Y. K. Kim, B. R. Reddy, T. G. George, and R. B. Lal, "Optical Heterodyne Interferometry Technique for Solution Crystal Growth Rate Measurement," *Optical Engineering,* 37, 2, July 1998, pp. 172-180.

10. T. Yoshizawa, *Handbook of Optical Metrology: Principles and Applications*, Boca Raton, CRC Press, 2015.

11. F. Meriaudeau, "Real Time Multispectral High Temperature Measurement: Application to Control in the Industry," *Image and Vision Computing*, **25**, 7, July 2007, pp. 1124-33.

12. C. W. Farley III, and B. R. Reddy, Interferometric Measurement of Laser Heating in Praseodymium-Doped YAG Crystal," *Applied Optics*, **50**, 4, February 2011, pp. 526-531.

13. M. Sheik-Bahae and R. I. Epstein, "Laser Cooling of Solids," *Laser & Photonics Reviews*, **3**, 1-2, February 2009, pp. 67-84.

14. D. V. Seletskiy, S. D. Melgaard, S. Bigotta, A. Di Lieto, M. Tonelli, and M. Sheik-Bahae, "Laser Cooling of Solids to Cryogenic Temperatures," *Nature Photonics*, **4**, 3, March 2010, p. 161.

15. G. Nemova and R. Kashyap, "Laser Cooling of Solids," *Reports on Progress in Physics*, **73**, 8, July 2010, pp. 086501.

16. Pooja Munjal and Kamal P. Singh, "A Single-Lens Universal Interferometer: Towards a Class of Frugal Optical Devices," *Applied Physics Letters*, **115**, 11, September 2019, pp. 111102.

17. A. S. Usmani, J. M. Rotter, S. Lamont, A. M. Sanad, and M. Gillie, "Fundamental Principles of Structural Behaviour Under Thermal Effects," *Fire Safety Journal*, **36**, 8, November 2001, pp. 721-744.

18. B. S. Yilbas and N. Al Aqeeli, "Analytical Investigation into Laser Pulse Heating and Thermal Stresses," *Optics & Laser Technology*, **41**, 2, March 2009, pp. 132-139.

A Theoretical Model for the Generation of Kinetic Alfvén Waves in the Earth's Magnetosphere by Ion Beam and Velocity Shear

K. C. Barik, S. V. Singh, and G. S. Lakhina

Indian Institute of Geomagnetism
Navi Mumbai 410218, India
E-mail: kcbarik17@gmail.com

Abstract

A generation mechanism for kinetic Alfvén waves (KAWs) by ion-beam and velocity shear is discussed. For this, a three-component plasma model, consisting of cold background ions, hot electrons, and hot ion beams is considered. The model is very general in the sense that all of the three species have drifting Maxwellian distributions, nonuniform streaming, and velocity shear, and can be applied to magnetospheric regions where velocity shear is present. The effects of the ion beam alone and the combined effect of the ion beam as well as the velocity shear in exciting the kinetic Alfvén waves are discussed. It is found that the ion beam alone can excite these kinetic Alfvén waves. However, in the presence of an anti-parallel ion beam and positive shear, the wave growth is much larger as compared to the ion-beam case alone. For a set of plasma parameters, waves are excited for $\lambda_B < 1$ for the case of the ion beam alone, whereas for the combined case (an anti-parallel ion beam and positive velocity shear), these waves are excited for $\lambda_B > 1$. The present model is applied to the polar cusp/auroral region of the Earth's magnetosphere, and it can explain several characteristic properties of the observed ultra-low-frequency waves. The mechanism presented here can excite the kinetic Alfvén waves up to a frequency of ≈ 65 mHz, which can explain the ultra-low-frequency waves observed in the auroral/polar cusp region.

1. Introduction

Kinetic Alfvén waves (KAWs) are low-frequency electromagnetic waves that propagate nearly perpendicular to the ambient magnetic field, and have an electric-field component along the ambient magnetic field. The acceleration of charged particles in space plasmas is related to the presence of parallel electric fields. Due to the presence of a parallel electric field, kinetic Alfvén waves play a major role in the transfer of energy to particles and auroral acceleration of the electrons [1-5]. In the low-β plasmas, this parallel electric field arises in the magneto-hydrodynamic (MHD) waves under two aspects. First, when electron inertia is taken into account, the shear Alfvén waves will come into the picture and will satisfy conditions in a region where with β being the (thermal pressure/magnetic pressure) [3]. Second, when the ion gyro radius is taken into account, kinetic Alfvén waves will play a major role and satisfy conditions in a region where $\beta \gg m_e/m_i$ [6]. At the auroral altitudes of 4-5 R_E, where is the radius of the Earth, the shear Alfvén wave plays a major role [7], and beyond that, the kinetic Alfvén waves are important. Observationally, kinetic Alfvén waves appear as broadband enhancements in electric and magnetic field wave power that become increasingly electrostatic at higher frequencies [8-11]. These waves have been reported inside the plasmasphere in conjunction with, and modulated by, ultra-low-frequency (ULF) oscillations driven by an impulsive solar-wind pressure enhancement, and are identified as Doppler-shifted kinetic Alfvén waves. Furthermore, kinetic Alfvén waves may significantly impact particle dynamics in the inner magnetosphere through enhanced ion transport and heating [2, 12]. Observations carried out onboard the S3-3, DE1, AUREOL 3, VIKING, CLUSTER, THEMIS, Van Allen Probes, and MMS spacecraft have given evidence for intense electromagnetic turbulence in the solar wind and magnetosphere [13-20].

Ultra-low-frequency waves have been observed in various regions of the Earth's magnetosphere, e.g., the magnetopause, magnetosheath, plasma-sheet boundary layer (PSBL), polar cusp, and on auroral field lines for decades [8, 21-26]. These ULF waves can be generated

by several mechanisms [8, 21, 22, 24]. Instabilities/waves such as the Kelvin-Helmholtz (K-H) instability [21, 27, 28], kinetic Alfvén waves [1, 3, 5, 29-31], field-line resonance [28], etc., are some of the phenomena that can explain the generation of ULF waves. More recent observations in the terrestrial magnetosphere and reconnection region have shown that kinetic Alfvén waves facilitate the generation of ULF waves and wave-particle energy exchange [20, 32]. Lakhina [31] discussed the excitation of kinetic Alfvén waves by velocity shear and explained the observed generation of ULF waves by kinetic Alfvén waves. Ion beams have also been observed in various regions of the magnetosphere such as the plasma-sheet boundary layer, polar cusp, auroral zone, etc. [24, 27]. Here, we are proposing a three-component plasma model for the excitation of kinetic Alfvén waves by ion-beam and velocity shear as a possible mechanism for the generation of ULF waves in the Earth's magnetosphere. The combined effect of ion-beam and velocity shear in exciting the kinetic Alfvén waves for resonant instability has been studied. This model is able to explain some of the observed characteristics of ULF waves in the magnetosphere.

2. Theoretical Model for Kinetic Alfvén Waves Excited by Ion-Beam and Velocity Shear

A three-component theoretical plasma model is considered, having background ions, beam ions, and electrons as its species. All the three species have nonuniform streaming along the ambient magnetic field $\mathbf{B}_0 = B_0\hat{z}$, where $X = x + v_y/\omega_{cj}$, $\omega_{cj} = \dfrac{q_j B_0}{m_j c}$ is the gyro frequency of the jth species, q_j and m_j are the charge and mass of the jth species, c is the light speed, and the subscript is e, i, or B for electrons, ions, and beam ions, respectively. The equilibrium charge neutrality is obtained from the relation , where N_j represents the number density of the jth species. To proceed further, we have assumed a drifting Maxwellian distribution, given by

$$f_{0j} = \left(\pi\alpha_j^2\right)^{-3/2} N_j \exp\left[-\left\{v_\perp^2 + \left[v_\parallel - V_j(X)\right]^2\right\}\Big/\alpha_j^2\right] \qquad (1)$$

where $v_\perp = \sqrt{v_x^2 + v_y^2}$ and $v_\parallel = v_z$ define the perpendicular and parallel velocity components with respect to the ambient magnetic field, $\alpha_j = \sqrt{\dfrac{2T_j}{m_j}}$ is the thermal speed of the jth species, and T_j is the temperature of the jth species.

Since we are assuming a low-beta plasma (thermal pressure/magnetic pressure) for our study, the wave is assumed to be magnetically incompressible. This means that the z component of the wave's magnetic field, B_z, is zero. This fact allows us to use the two electric potentials to describe the wave's electric field, as done by Hasegawa [1]. The electric field of the electromagnetic wave can thus be written as

$$\mathbf{E} = -\nabla_\perp\phi + E_\parallel\hat{z}\,, \qquad (2)$$

where $E_\parallel = -\nabla_\parallel\psi$. The basic equations used for our calculations are Poisson's equation and the z component of Ampere's law. Respectively, they are given by

$$-\nabla_\perp^2\phi + \frac{\partial E_\parallel}{\partial z} = 4\pi\sum_j e_j n_j\,, \qquad (3)$$

$$\frac{\partial\nabla_\perp^2\phi}{\partial z} + \nabla_\perp^2 E_\parallel = \frac{4\pi}{c^2}\frac{\partial}{\partial t}\sum_j J_{zj}\,. \qquad (4)$$

Here, n_j and J_{zj} are respectively the perturbed number and the z component of the current densities, and can be computed from the expressions

$$n_j = \int d^3v f_{1j}\,, \qquad (5)$$

$$J_{zj} = \int d^3v e_j v_z f_{1j}\,,$$

where f_{1j} is the perturbed distribution function, which can be obtained from the linearized Vlasov's equation using a local approximation ($L_v k \gg 1$). Here, k is the wavenumber and $L_v = V_B\left(dV_B/dx\right)^{-1}$ is the velocity gradient scale length. For this, the perturbation is assumed to be of the form $f_{1j} = \exp(ik_\perp y + ik_\parallel z - i\omega t)$, where ω is the frequency of the wave, and $k_\parallel$ and $k_\perp$ are respectively the parallel and perpendicular components of the wave vector $\mathbf{k}$. The generalized perturbed distribution can now be written as [33, Equation (4.169)]

$$f_1(\mathbf{r},\mathbf{v},t) = -\frac{q}{m}\int_{-\infty}^{t} dt'\left[\mathbf{E} + \frac{(\mathbf{E}\cdot\mathbf{v}')\mathbf{k} - \mathbf{E}(\mathbf{v}'\cdot\mathbf{k})}{\omega}\right]$$

$$\cdot\nabla_{v'} f_0(\mathbf{v}')\, e^{i(\mathbf{k}\cdot\mathbf{r}' - \omega t')} \qquad (6)$$

which has to be integrated along the unperturbed orbits. Following the standard procedure and algebraic manipulations, the perturbed distribution function for low-frequency kinetic Alfvén waves can be written as [31,34]

$$f_{1j} = \frac{e_j}{m_j}\sum_{n=-\infty}^{+\infty}\sum_{m=-\infty}^{+\infty}\frac{e^{i(n-m)\theta}}{\left(k_\parallel v_z - \omega + n\omega_{cj}\right)} J_n(\xi_j) J_m(\xi_j)$$

$$\times\left(k_\perp M_j\phi + k_\parallel L_j\psi\right) \qquad (7)$$

where coefficients M_j and L_j can be expressed as

$$M_j = \left(1-\frac{k_{\|}v_z}{\omega}\right)\left[\frac{\partial f_{0j}}{\partial v_{\perp}}\frac{n\omega_{cj}}{k_{\perp}v_{\perp}}+\frac{1}{\omega_{cj}}\frac{\partial f_{0j}}{\partial x}\right]+\frac{\partial f_{0j}}{\partial v_z}\frac{n\omega_{cj}k_{\|}}{k_{\perp}\omega} \quad (8)$$

$$L_j = \frac{k_{\perp}v_z}{\omega}\left[\frac{\partial f_{0j}}{\partial v_{\perp}}\frac{n\omega_{cj}}{k_{\perp}v_{\perp}}+\frac{1}{\omega_{cj}}\frac{\partial f_{0j}}{\partial x}\right]+\left(1-\frac{n\omega_{cj}}{\omega}\right)\frac{\partial f_{0j}}{\partial v_z} \quad (9)$$

Here, $J_n(\xi_j)$ and $J_m(\xi_j)$ are the Bessel functions of the order n and m, respectively, with the arguments $\xi_j = \left(k_{\perp}v_{\perp}/\omega_{cj}\right)$. For the calculation of velocity integrals, we use cylindrical coordinates, i.e., $\mathbf{v} = \left(v_{\perp}, \theta, v_{\|}\right)$, where θ represents the angular coordinate of the velocity vector. Substituting f_{1j} from Equation (7) into Equation (5) and evaluating the integrals, we obtain the perturbed number density, n_j, and the parallel component (z component) of the current density, J_{zj}. Furthermore, these number and current densities are substituted into Equations (3) and (4), respectively, to get the following:

$$\begin{pmatrix} D_{11} & D_{12} \\ D_{21} & D_{22} \end{pmatrix}\begin{pmatrix} \phi \\ \psi \end{pmatrix} = 0 \quad (10)$$

where the coefficients are given by the expressions

$$D_{11} = k_{\perp}^2\left[1+\sum_j \frac{2\omega_{pj}^2}{k_{\perp}^2\alpha_j^2}\frac{\bar{\omega}}{\omega}\left(1-b_j\right)\right], \quad (11)$$

$$D_{12} = k_{\|}^2\left[1-\sum_j \frac{\omega_{pj}^2 b_j}{k_{\|}^2\alpha_j^2}Z'\left(\frac{\bar{\omega}}{k_{\|}\alpha_j}\right)\left(1-S_j\frac{k_{\perp}}{k_{\|}}\right)\right], \quad (12)$$

$$D_{21} = k_{\|}k_{\perp}^2\left[1+\sum_j \frac{\omega_{pj}^2 b_j}{c^2k_{\perp}^2}S_j\frac{k_{\perp}}{k_{\|}}\right], \quad (13)$$

$$D_{22} = -k_{\|}k_{\perp}^2\left\{1+\sum_j \frac{\omega_{pj}^2}{c^2k_{\perp}^2}\left[\frac{b_j\omega^2}{k_{\|}^2\alpha_j^2}Z'\left(\frac{\bar{\omega}}{k_{\|}\alpha_j}\right)\left(1-S_j\frac{k_{\perp}}{k_{\|}}\right)+S_j\frac{k_{\perp}}{k_{\|}}\right]\right\}, \quad (14)$$

where $\omega_{pj} = \left(\frac{4\pi N_j e_j^2}{m_j}\right)^{1/2}$ is the plasma frequency, $\bar{\omega} = \left(\omega - k_{\|}V_j\right)$ is the Doppler-shifted frequency of the jth species, and $b_j = I_0\left(\lambda_j\right)\exp\left(-\lambda_j\right)$, where $I_0\left(\lambda_j\right)$ is the zeroth-order modified Bessel function. The coefficients D_{ij} are obtained by assuming low-frequency waves ($\omega^2 \ll \omega_{cj}^2$) propagating nearly perpendicular to $\mathbf{B}_0$, i.e., $k_{\|}^2 << k_{\perp}^2$. We get the following generalized dispersion relation from Equation (10) by equating the determinant of the coefficients of ϕ and ψ to zero:

$$1+\sum_j \frac{\omega_{pj}^2}{k^2\alpha_j^2}\left[\frac{2\bar{\omega}}{\omega}\left(1-b_j\right)-b_j\left(1-S_j\frac{k_{\perp}}{k_{\|}}\right)Z'\left(\frac{\bar{\omega}}{k_{\|}\alpha_j}\right)\right]$$

$$+\sum_j \frac{2\omega_{pj}^2}{k^2\alpha_j^2}\frac{\bar{\omega}}{\omega}\left(1-b_j\right)$$

$$\sum_j \frac{\omega_{pj}^2}{c^2k_{\perp}^2}\left[\frac{b_j\omega^2}{k_{\|}^2\alpha_j^2}Z'\left(\frac{\bar{\omega}}{k_{\|}\alpha_j}\right)\left(1-S_j\frac{k_{\perp}}{k_{\|}}\right)+S_j\frac{k_{\perp}}{k_{\|}}\right]$$

$$-\sum_j \frac{\omega_{pj}^2 b_j}{k^2\alpha_j^2}\left(1-S_j\frac{k_{\perp}}{k_{\|}}\right)Z'\left(\frac{\bar{\omega}}{k_{\|}\alpha_j}\right)\sum_j \frac{\omega_{pj}^2 b_j}{c^2k_{\perp}^2}S_j\frac{k_{\perp}}{k_{\|}} = 0. \quad (15)$$

3. Resonant Instability of Kinetic Alfvén Waves

In this section, we study the resonant instabilities of the kinetic Alfvén waves excited by hot-ion beams and velocity shear. The dispersion relation is here restricted to a hot-ion beam with drift velocity V_B and shear in the flow of $S = S_B$, whereas other species have $V_i = 0 = V_e$ $S_i = 0 = S_e$. Under the assumptions of a hot-ion beam, $\omega \ll k_{\|}\alpha_e$, $\lambda_e \ll 1$, hot electrons, $\omega \ll k_{\|}\alpha_e$, $\lambda_e << 1$, and cold background ions, $\omega^2 \gg k_{\|}^2\alpha_i^2$, the dispersion relation obtained from Equation (15) is given by

$$\frac{b_i N_i}{N_e}\left[1+a_1-\frac{\omega^2}{k_{\|}^2v_A^2}\frac{N_i}{N_e}\frac{1-b_i}{\lambda_i}Aq_0\right]$$

$$-\frac{\omega^2}{k_{\|}^2c_s^2}\left[C_R'+i\left(1+a_1\right)C_I-\frac{\omega^2}{k_{\|}^2v_A^2}\frac{N_i}{N_e}\frac{1-b_i}{\lambda_i}A\left(C_R+iC_I\right)\right]$$

$$=\frac{2\omega^2}{k_{\|}^2\alpha_i^2}\frac{\left(1-b_i\right)N_i}{N_e}, \quad (16)$$

where

$$a_1 = \frac{N_B}{N_e}\frac{\beta_B b_B}{2\lambda_B} S\frac{k_\perp}{k_\parallel}, \quad (17)$$

$$q_0 = 1 + \frac{N_B}{N_i}\frac{m_i}{m_B}\frac{Sk_\perp}{b_i k_\parallel}, \quad (18)$$

$$A = 1 + \frac{N_B}{N_i}\frac{T_i}{T_B}\frac{\bar{\omega}}{\omega}\frac{(1-b_B)}{(1-b_i)}, \quad (19)$$

$$C_R = 1 + \frac{N_B}{N_e}\frac{T_e}{T_B} b_B\left(1 - S\frac{k_\perp}{k_\parallel}\right), \quad (20)$$

$$C_R' = 1 + \frac{N_B}{N_e}\frac{T_e}{T_B}\left[b_B\left(1-\frac{\bar{\omega}}{\omega}\right) + \left(\frac{\bar{\omega}}{\omega} - b_B S\frac{k_\perp}{k_\parallel}\right)\right] + a_1 C_R \quad (21)$$

$$C_I = \sqrt{\pi}\,\frac{\omega}{k_\parallel \alpha_e}\left[\exp\left(-\frac{\omega^2}{k_\parallel^2\alpha_e^2}\right) + b_B\frac{N_B}{N_e}\left(\frac{T_e}{T_B}\right)^{3/2}\left(\frac{m_B}{m_e}\right)^{1/2}\right.$$

$$\left.\frac{\bar{\omega}}{\omega}\left(1 - S\frac{k_\perp}{k_\parallel}\right)\exp\left(-\frac{\bar{\omega}^2}{k_\parallel^2\alpha_B^2}\right)\right]. \quad (22)$$

The expression C_I here represents the damping terms due to hot electrons and beam ions, and $c_s = \left(T_e/m_i\right)^{1/2}$ is the ion acoustic speed, $v_A = \left(B_0^2/4\pi N_e m_i\right)^{1/2}$ is the Alfvén velocity, and $\beta_i = \left(8\pi N_e T_i/B_0^2\right)$ and $\beta_B = \left(8\pi N_e T_B/B_0^2\right)$ are the ion and beam plasma betas, respectively. In the absence of ion beam ($N_B = 0$) and neglecting the damping due to electron and beam ions, we will reach the usual dispersion relation for kinetic Alfvén waves in a two-component plasma, as obtained by Hasegawa and Chen [1] and Lakhina [31]. We can write the general dispersion relation, Equation (16), as a combination of real and imaginary parts:

$$D_R(\omega,k) + iD_I(\omega,k) = 0 \quad (23)$$

where

$$D_R(\omega,k) = \frac{\omega^4}{k_\parallel^4 V_A^4}\left[\frac{N_i}{N_e}\frac{(1-b_i)}{\lambda_i} AC_R\right]$$

$$- g_1\frac{\omega^2}{k_\parallel^2 V_A^2} + \frac{N_i}{N_e}\frac{b_i\beta_i}{2}(1+a_1), \quad (24)$$

$$D_I(\omega,k) = -\frac{\omega^2}{k_\parallel^2 V_A^2}\left[1 + a_1 - \frac{\omega^2}{k_\parallel^2 V_A^2}\frac{(1-b_i)}{\lambda_i}\frac{N_i}{N_e}A\right]C_I, \quad (25)$$

$$g_1 = \left\{C_R' + \frac{N_i}{N_e}(1-b_i)\left[\frac{T_e}{T_i} + \frac{N_i}{N_e}\frac{b_i\beta_i}{2\lambda_i}Aq_0\right]\right\} \quad . (26)$$

The real frequency can be obtained by equating $D_R(\omega,k) = 0$, which contains both shear and beam velocity. In the absence of streaming, $V_B = 0$, and assuming $C_I \approx 0$, one can also obtain the real frequency from Equation (24) for non-resonant instability [31].

The growth/damping rate, γ, of the resonant kinetic Alfvén waves can be obtained from Equations (24) and (25) as

$$\gamma = -\frac{D_I(\omega_r,\mathbf{k})}{\dfrac{\partial D_R(\omega_r,\mathbf{k})}{\partial\omega_r}}$$

$$= \omega_r^2\left[1 + a_1 - \frac{\omega_r^2}{k_\parallel^2 v_A^2}\frac{(1-b_i)}{\lambda_i}\frac{N_i}{N_e}A\right]C_I$$

$$\left\{\omega_r\left[2\left(g_1^2 - 4g_0\right)^{1/2}\right] + V_B\frac{N_B}{N_e}(1-b_B)\right.$$

$$\left.\left[\frac{\omega_r^2}{k_\parallel v_A^2}\frac{T_i}{T_B}\frac{C_R}{\lambda_i} - k_\parallel\frac{T_e}{T_B}\left(1 + \frac{N_i}{N_e}\frac{T_i}{T_e}\frac{b_i\beta_i}{2\lambda_i}q_0\right)\right]\right\}^{-1} \quad (27)$$

where

$$g_0 = \left(\frac{N_i}{N_e}\right)^2\frac{b_i\beta_i}{2}\frac{(1-b_i)}{\lambda_i}(1+a_1)AC_R. \quad (28)$$

This is a general expression for the growth/damping rate of the kinetic Alfvén waves in the presence of ion beam and velocity shear. It has been obtained after making use of the assumption $\omega = \omega_r + i\gamma$, where ω_r is the real frequency and $\gamma \ll \omega_r$ is the growth/damping rate.

The numerical computations were next carried out for real frequency, Equation (24), and growth/damping rate,

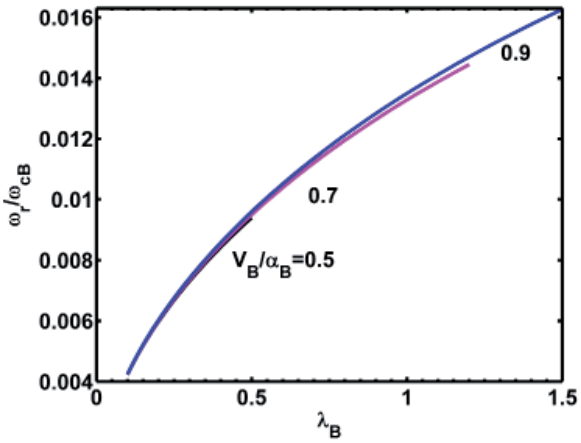

Figure 1a. The resonant instability of kinetic Alfvén waves driven by an ion beam alone: the normalized real frequency, ω_r/ω_{cB}, as a function of $\lambda_B = \frac{k_\perp^2\alpha_B^2}{2\omega_{cB}^2}$ for $\frac{N_B}{N_e} = 0.4$, $\beta_i = 0.001$, $\frac{k_\parallel}{k_\perp} = 0.04$, $S = 0$, and for $\frac{V_B}{\alpha_B} = 0.5$, 0.7, and 0.9, respectively.

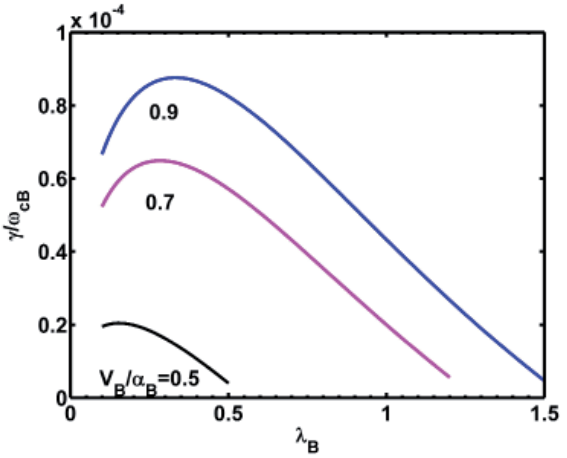

Figure 1b. The resonant instability of kinetic Alfvén waves driven by an ion beam alone: the normalized growth rate, γ/ω_{cB}, as a function of $\lambda_B = \frac{k_\perp^2\alpha_B^2}{2\omega_{cB}^2}$ for $\frac{N_B}{N_e} = 0.4$, $\beta_i = 0.001$, $\frac{k_\parallel}{k_\perp} = 0.04$, $S = 0$, and for $\frac{V_B}{\alpha_B} = 0.5$, 0.7, and 0.9, respectively.

Equation (27), for the relevant plasma parameters. We made sure that all the assumptions that were made in arriving at the theoretical results were satisfied. The normalization procedure that we adopted for our numerical computations were as follows: frequencies, ω_r, were normalized with respect to the cyclotron frequency of the ion beam, ω_{cB}; temperatures with the ion beam temperature, T_B; streaming velocity, V_B, with the thermal speed of the ion beam, α_B. The normalized real frequency and the growth rates of the resonant instability as calculated numerically from Equation (24) and Equation (27), respectively, were plotted against $\lambda_B = k_\perp^2\alpha_B^2/2\omega_{cB}^2$ (the square of the perpendicular wave number normalized with the gyro radius of the beam ions). From the numerical analysis, it was found that for the resonant instability of the kinetic Alfvén waves, $C_R > 0$ and $C_I < 0$ should be satisfied. From the condition $C_R > 0$ an upper limit for the velocity shear was obtained from Equation (20) as

$$S_{max} = \frac{k_\parallel}{k_\perp}\left(1 + \frac{N_e}{N_B}\frac{T_B}{b_B T_e}\right). \qquad (29)$$

The $C_I < 0$ contains terms corresponding to ion beam as well as velocity shear, and hence it was difficult to analytically obtain a combined threshold or upper limit for which growth of the wave occurred. However, in the absence of velocity shear (i.e., $S = 0$), from the condition $C_I < 0$, we obtained an expression for the threshold value of ion beam velocity above which the growth of the waves was possible. This is given by

$$V_{Bth} = \frac{\omega}{k_\parallel}\left[1 + \frac{N_e}{N_B}\frac{1}{b_B}\left(\frac{T_B}{T_e}\right)^{3/2}\left(\frac{m_e}{m_B}\right)^{1/2}\right]. \qquad (30)$$

Figures 1a and 1b represent the normalized real frequency and the normalized growth rate as functions of the square of the normalized perpendicular wave number, $\lambda_B = \frac{k_\perp^2\alpha_B^2}{2\omega_{cB}^2}$, in the absence of velocity shear ($S = 0$). The waves were excited by an ion beam alone. It was observed that when the ion-beam velocity was increased from $\frac{V_B}{\alpha_B} =$ 0.5 to 0.9, the real frequency marginally increased, whereas the growth rate significantly increased. The growth rate first increased up to a certain extent, reached its maximum value, and then fell back. The value of λ_B for which the growth rate was maximum is called λ_{Bmax}. It was observed that with an increase in beam velocity, the λ_{Bmax} shifted towards higher values, i.e., higher wave numbers. The extent of wave numbers for which kinetic Alfvén waves were excited also increased with an increase in ion-beam velocity. It is emphasized here that in the absence of velocity shear, an ion beam alone can excite the kinetic Alfvén waves with reasonable growth rate. The *threshold value* of the beam velocity was found to be $V_B/\alpha_B \approx 0.42$, below which no growth was possible.

In Figures 2a and 2b, plots of normalized real frequency and growth rate in the presence of finite shear ($S = 0.4$) and the ion beam streaming parallel to the ambient magnetic field (positive velocity) are shown. The ion-beam velocity was increased from $\frac{V_B}{\alpha_B} = 0.15$ to 0.45. It was observed that with an increase in beam velocity in the parallel direction, the real frequency increased, although marginally. However, there was slight growth at $\frac{V_B}{\alpha_B} = 0.15$ which diminished with the further increase in ion-beam

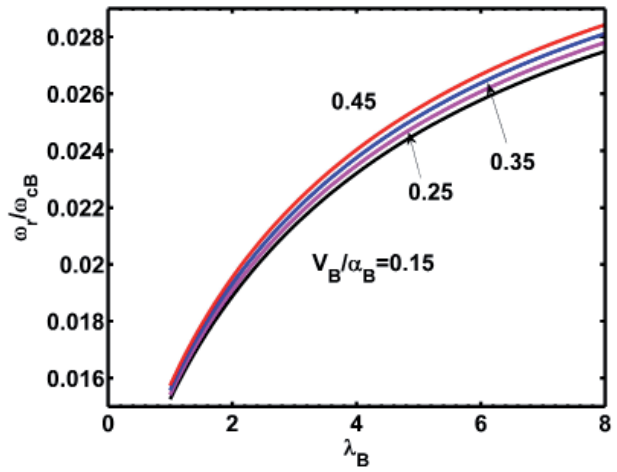

Figure 2a. The resonant instability of kinetic Alfvén waves driven by an ion beam and velocity shear: the normalized real frequency, ω_r/ω_{cB}, as a function of $\lambda_B = \frac{k_\perp^2 \alpha_B^2}{2\omega_{cB}^2}$ for $\frac{N_B}{N_e} = 0.4$, $\beta_i = 0.001$, $\frac{k_\parallel}{k_\perp} = 0.04$ $S = 0.4$, and for $\frac{V_B}{\alpha_B} = 0.15$, 0.25, 0.35, and 0.45, respectively.

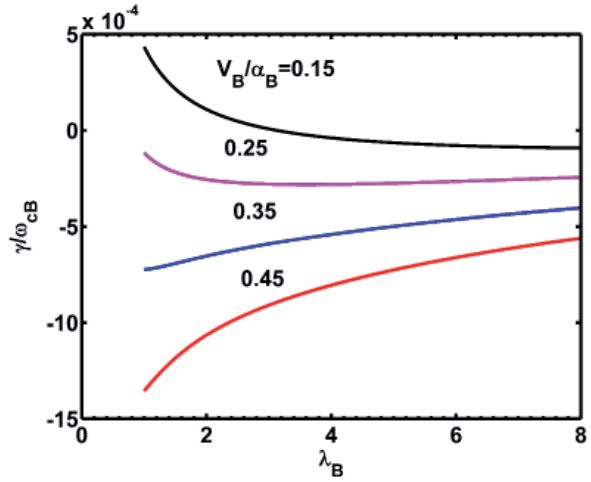

Figure 2b. The resonant instability of kinetic Alfvén waves driven by an ion beam and velocity shear: the normalized growth rate, γ/ω_{cB}, as a function of $\lambda_B = \frac{k_\perp^2 \alpha_B^2}{2\omega_{cB}^2}$ for $\frac{N_B}{N_e} = 0.4$, $\beta_i = 0.001$, $\frac{k_\parallel}{k_\perp} = 0.04$ $S = 0.4$, and for $\frac{V_B}{\alpha_B} = 0.15$, 0.25, 0.35, and 0.45, respectively.

velocity considered here. The waves were thus being damped at higher values of ion-beam velocity. This indicated that positive shear with parallel streaming of ions will have a stabilizing effect on the kinetic Alfvén waves. Due to the damping of the wave, there may be a transfer of energy from the wave to the particles, and hence energy transfer to the particles. Positive velocity shear along with parallel streaming of the ion beam therefore creates a favorable condition for energy transfer to the particles.

In Figures 3a and 3b, the variation of the normalized real frequency and growth rate with the normalized perpendicular wave number in the presence of positive shear ($S = 0.4$) and the ion beam anti-parallel to the ambient magnetic field are shown for $\frac{V_B}{\alpha_B} = -0.15$ to -0.45. With the increase in beam velocity in the anti-parallel direction, the real frequency marginally decreased, whereas the growth rate slightly increased. The growth rate fell off

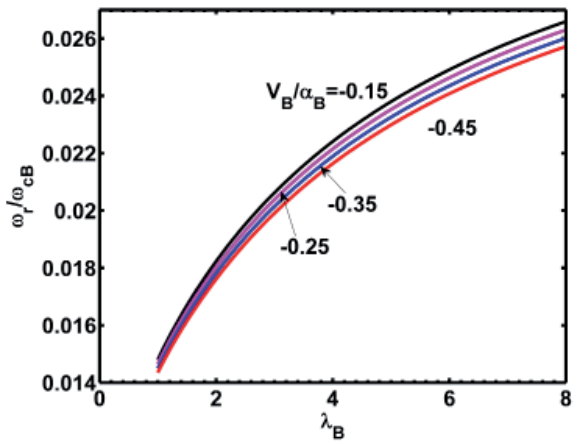

Figure 3a. The resonant instability of kinetic Alfvén waves driven by an ion beam and velocity shear: the normalized real frequency, ω_r/ω_{cB}, as a function of $\lambda_B = \frac{k_\perp^2 \alpha_B^2}{2\omega_{cB}^2}$ for $\frac{N_B}{N_e} = 0.4$, $\beta_i = 0.001$, $\frac{k_\parallel}{k_\perp} = 0.04$ $S = 0.4$, and for $\frac{V_B}{\alpha_B} = -0.15$, -0.25, -0.35, and -0.45, respectively.

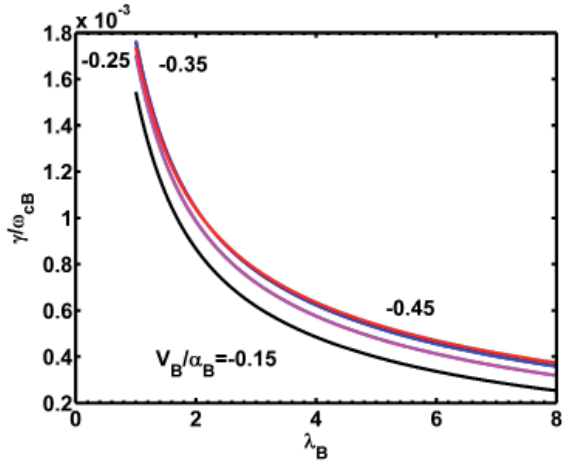

Figure 3b. The resonant instability of kinetic Alfvén waves driven by an ion beam and velocity shear: the normalized growth rate, γ/ω_{cB}, as a function of $\lambda_B = \frac{k_\perp^2 \alpha_B^2}{2\omega_{cB}^2}$ for $\frac{N_B}{N_e} = 0.4$, $\beta_i = 0.001$, $\frac{k_\parallel}{k_\perp} = 0.04$ $S = 0.4$, and for $\frac{V_B}{\alpha_B} = -0.15$, -0.25, -0.35, and -0.45, respectively.

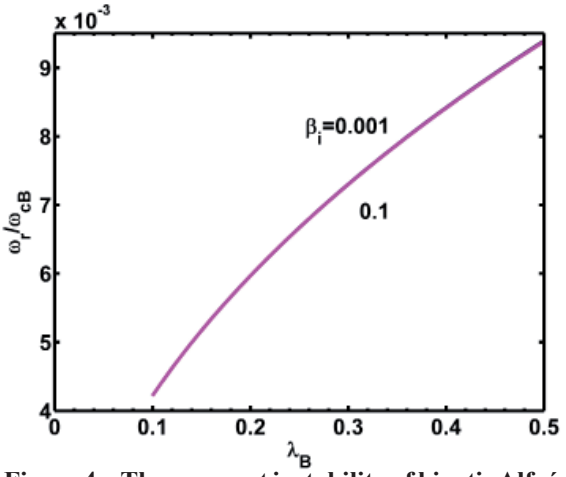

Figure 4a. The resonant instability of kinetic Alfvén waves driven by an ion beam: the normalized real frequency, ω_r/ω_{cB}, as a function of $\lambda_B = \frac{k_\perp^2 \alpha_B^2}{2\omega_{cB}^2}$ for $\frac{N_B}{N_e} = 0.4,$, $\frac{k_\parallel}{k_\perp} = 0.04$, $\frac{V_B}{\alpha_B} = 0.5$, $S = 0.0$, and for $\beta_i = 0.001$ and 0.1, respectively.

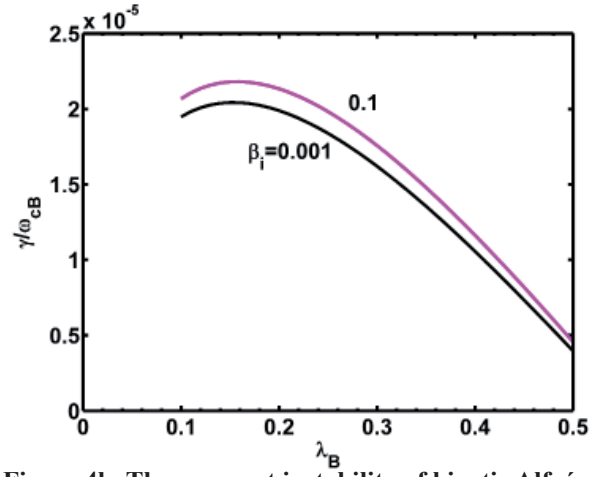

Figure 4b. The resonant instability of kinetic Alfvén waves driven by an ion beam: the normalized growth rate, γ/ω_{cB}, as a function of $\lambda_B = \frac{k_\perp^2 \alpha_B^2}{2\omega_{cB}^2}$ for $\frac{N_B}{N_e} = 0.4,$, $\frac{k_\parallel}{k_\perp} = 0.04$, $\frac{V_B}{\alpha_B} = 0.5$, $S = 0.0$, and for $\beta_i = 0.001$ and 0.1, respectively.

sharply with λ_B. The growth rate was significantly higher than for the case of the ion beam alone (Figure 1b) and for the ion beam and positive velocity shear (Figure 2b). This indicated that an ion-beam streaming anti-parallel to the ambient magnetic field in the presence of a finite shear can excite kinetic Alfvén waves with a larger growth rate compared to other two cases discussed above. From the above analysis, it was evident that in the presence of a finite shear, the ion-beam streaming should be anti-parallel to the ambient magnetic field to make the condition more favorable for excitation of kinetic Alfvén waves.

In Figures 4a and 4b, the variations of the normalized real frequency and growth rate with λ_B for different β_i values (shown on the curves) are depicted for the plasma parameters of Figure 1 and $V_B/\alpha_B = 0.5$. Here, waves were excited by ion-beam streaming alone. It was seen that the effect of β_i was negligible on the real frequency of the kinetic Alfvén waves. However, the growth rate of the wave decreased with a decrease in β_i without any change in the λ_B range for the set of parameters considered here. It was noticed that the waves were excited for $\lambda_B < 1$.

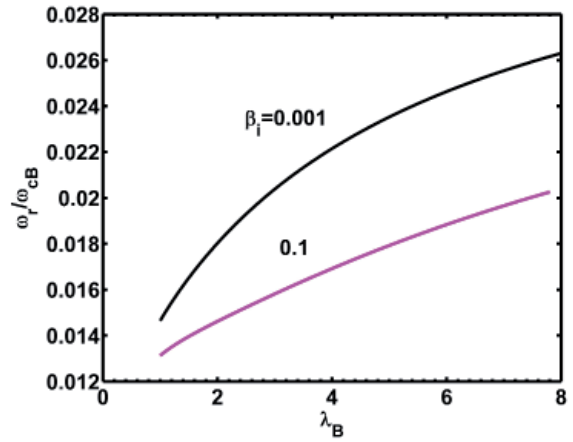

Figure 5a. The resonant instability of kinetic Alfvén waves driven by an ion beam and velocity shear: the normalized real frequency, ω_r/ω_{cB}, as a function of $\lambda_B = \frac{k_\perp^2 \alpha_B^2}{2\omega_{cB}^2}$ for $\frac{N_B}{N_e} = 0.4$, $\frac{V_B}{\alpha_B} = -0.25$, $\frac{k_\parallel}{k_\perp} = 0.04$ $S = 0.4$, and for $\beta_i = 0.001$ and 0.1, respectively.

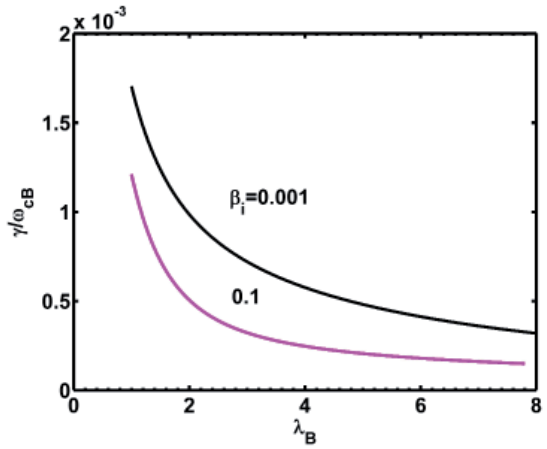

Figure 5b. The resonant instability of kinetic Alfvén waves driven by an ion beam and velocity shear: the normalized growth rate, γ/ω_{cB}, as a function of $\lambda_B = \frac{k_\perp^2 \alpha_B^2}{2\omega_{cB}^2}$ for $\frac{N_B}{N_e} = 0.4$, $\frac{V_B}{\alpha_B} = -0.25$, $\frac{k_\parallel}{k_\perp} = 0.04$ $S = 0.4$, and for $\beta_i = 0.001$ and 0.1, respectively.

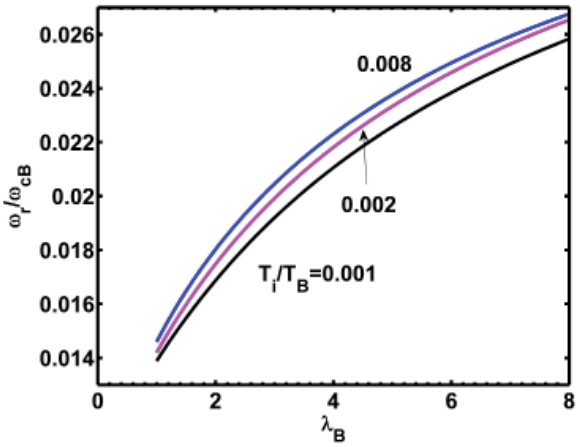

Figure 6a. The resonant instability of kinetic Alfvén waves driven by an ion beam and velocity shear: the normalized real frequency, ω_r/ω_{cB}, as a function of $\lambda_B = \frac{k_\perp^2 \alpha_B^2}{2\omega_{cB}^2}$ for $\frac{N_B}{N_e} = 0.4$, $\frac{V_B}{\alpha_B} = -0.25$, $\frac{k_\parallel}{k_\perp} = 0.04$ $S = 0.4$, $\beta_i = 0.001$, and for $T_i/T_B = 0.001,\ 0.002$, and 0.008, respectively.

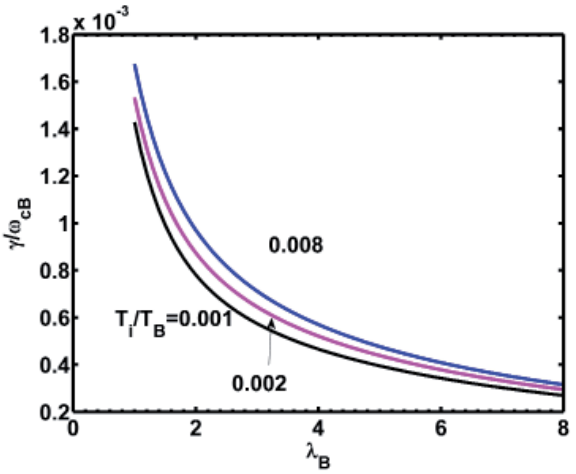

Figure 6b. The resonant instability of kinetic Alfvén waves driven by an ion beam and velocity shear: the normalized growth rate, γ/ω_{cB}, as a function of $\lambda_B = \frac{k_\perp^2 \alpha_B^2}{2\omega_{cB}^2}$ for $\frac{N_B}{N_e} = 0.4$, $\frac{V_B}{\alpha_B} = -0.25$, $\frac{k_\parallel}{k_\perp} = 0.04$ $S = 0.4$, $\beta_i = 0.001$, and for $T_i/T_B = 0.001,\ 0.002$, and 0.008, respectively.

Here we show the effect of β_i on the waves in the presence of both a finite positive shear ($S = 0.4$) and anti-parallel streaming of the ion beam ($\frac{V_B}{\alpha_B} = -0.25$). The normalized real frequency and growth rate are shown in Figures 5a and 5b for values of $\beta_i = 0.001$ and 0.1. Other plasma parameters were as in Figure 3. A significant enhancement was observed in both the real frequency and growth rate with a decrease in the β_i value, and the wave could also grow for a larger range of wave numbers. The decrease in β_i had a reverse effect on the growth rate of kinetic Alfvén waves for the combined case of an ion beam and velocity shear as compared to the ion-beam case alone. In this case, the waves were excited for

In Figures 6a and 6b, we show the effect of the temperature variation, T_i/T_B, on the real frequency and growth rate of kinetic Alfvén waves for the parameters of Figure 3 and $\frac{V_B}{\alpha_B} = -0.25$. The real frequency as well as the growth rate increased with an increase in the temperature's T_i/T_B values.

4. Discussion and Conclusions

This paper discussed a three-component plasma model for the excitation of kinetic Alfvén waves by ion beam and velocity shear. It was observed that an ion beam solely streaming parallel to the ambient magnetic field could excite kinetic Alfvén waves for a significant growth. The ion beam streaming anti-parallel to the ambient magnetic field in the presence of a finite positive shear will also excite kinetic Alfvén waves more efficiently as compared to the ion-beam case alone.

An enhancement in the growth rate of kinetic Alfvén waves was observed with a decrease in β_i value for a combination of anti-parallel streaming ion beam and positive velocity shear, whereas a reverse trend was obtained in the absence of shear and ion-beam streaming parallel to the magnetic field, i.e., a reduction in the growth rate of kinetic Alfvén waves was found. For the case of an ion beam alone, these waves were excited for $\lambda_B < 1$. On the other hand, for the case of combined sources (an anti-parallel ion beam and velocity shear), these waves were excited for $\lambda_B > 1$. An increase in temperature, T_i/T_B, had a positive impact on the real frequency and growth rate of kinetic Alfvén waves, i.e., both increased with an increase in temperature.

For our computational purposes, we considered some typical plasma parameters observed on the auroral/polar-cusp field lines at an altitude of $5R_E$ to $7R_e$, where R_E is the radius of the Earth [22, 23, 31]. The values reported were ion-beam densities $N_B/N_e = (0.01 \text{ to } 0.2)$; beam speed $V_B/\alpha_B < 2$; $\frac{\omega_{cB}}{2\pi} \approx (2.2-3)$ Hz, more common at auroral altitude; whereas we used $N_B/N_e = (0.1 \text{ to } 0.4)$, $V_B/\alpha_B = (-0.5 \text{ to } 0.9)$, $\beta_i = (0.001 \text{ to } 0.1)$, $\frac{\omega_{cB}}{2\pi} = 2.5$ and $S = (0.1 \text{ to } 0.4)$ for our numerical experiments. For the temperature of the species we assumed the following: for the hot electrons, $T_e \approx 100$eV; for the background cold ions, $T_i \approx 10$eV; and for the ion beam, $T_B \approx 1$keV to 2keV.

For the case of the excitation of the kinetic Alfvén waves by the ion beam alone, the normalized peak growth rate was found to be 0.00009 at $\lambda_B = 0.33$, and the corresponding real frequency peak was 0.008, whereas the wave was excited for $\lambda_B = (0.1 \text{ to } 1.5)$. The corresponding un-normalized growth rate and real frequency were 0.00023 Hz and 0.02 Hz, respectively.

The un-normalized real frequency had a range of 10 mHz to 40 mHz, and the corresponding growth rate fell in the range of 0.013 mHz to 0.23 mHz for the whole range of our computations. The transverse wave number was found to be in the range $k_\perp \approx 0.02\text{km}^{-1}$ to 0.04km^{-1}. The corresponding perpendicular wavelength fell in the range 314 km to 157 km. The parallel wave number, which can be obtained from the relation $k_\parallel / k_\perp = 0.04$, was found to be $k_\parallel \approx 0.08\times10^{-2}\,\text{km}^{-1}$ to $0.16\times10^{-2}\,\text{km}^{-1}$, and the parallel wavelength value was 78×10^2 km to 39×10^2 km. In the presence of finite shear and anti-parallel ion-beam streaming, the peak of the normalized growth rate significantly increased in comparison to the ion-beam case alone, and was found to be 0.0018 for $\lambda_B = 1.0$. The corresponding real frequency was found to be 0.015, whereas the kinetic Alfvén waves were excited in the λ_B range of 1.0 to 8.0. The respective un-normalized growth rate and real frequency had values of 0.0045 Hz and 0.04 Hz, respectively. The un-normalized real frequency fell in the range of 37.5 mHz to 65 mHz, and the growth rate had a range of 0.9 mHz to 4.5 mHz. The perpendicular wavenumber was found to be 0.03km^{-1} to 0.10km^{-1}. From this, the perpendicular wave length was obtained to be 209 km to 62 km. The respective parallel wave number was found to be $0.12\times10^{-2}\,\text{km}^{-1}$ to $0.4\times10^{-2}\,\text{km}^{-1}$, which gave the parallel wavelength values as 52×10^2 km to 15×10^2 km. The numerically calculated perpendicular wavelengths of 62 km to 314 km matched well with the observed values of 20 km to 120 km in the auroral region [8].

The theoretical model developed here provides insight into the generation mechanism of kinetic Alfvén waves by an ion beam alone, as well as by both the ion beam and velocity shear. Our model can excite kinetic Alfvén waves up to a frequency of ≈ 10 mHz to ≈ 65 mHz for the auroral-region parameters. It can explain some of the characteristics (perpendicular wavelengths) of observed ULF waves in the Earth's magnetosphere [8].

5. Acknowledgements

GSL thanks the Indian National Science Academy, New Delhi, for the support under INSA-Honorary Scientist Scheme. KCB would like to thank AP-RASC for providing the financial support under the Student Paper Competition (SPC) program to present his results. KCB would also like to thank the Indian Institute of Geomagnetism (IIG) for the financial support to attend the AP-RASC.

6. References

1. A. Hasegawa and L. Chen, "Kinetic Processes in Plasma Heating by Resonant Mode Conversion of Alfvén Wave," *Physics of Fluids*, **19**, 1976, pp. 1924-1934.

2. A. Hasegawa and K. Mima, "Anomalous Transport Produced by Kinetic Alfvén Wave Turbulence," *Journal of Geophysical Research*, **19**, 1978, pp. 1117-1123.

3. C. K. Goertz and R. W. Boswell, "Magnetosphere-Ionosphere Coupling," *Journal of Geophysical Research*, **84**, 1979, pp. 7239.

4. R. L. Lysak, and Christian T. Dum, "Dynamics of Magnetosphere-Ionosphere Coupling Including Turbulent Transport," *Journal of Geophysical Research: Space Physics*, **88.A1**, 1983, pp. 365-380.

5. B. J. Thompson and R. L. Lysak, "Electron Acceleration by Inertial Alfvén Waves," *Journal of Geophysical Research: Space Physics*, **101**, 1996, pp. 5359-5369.

6. A. Hasegawa, "Particle Acceleration by MHD Surface Waves and Formation of Aurora," *Journal of Geophysical Research*, **81**, 1976, pp. 5083.

7. R. L. Lysak and C.W. Carlson, "Effect of Microscopic Turbulence on Magnetosphere and Ionosphere Coupling," *Geophysical Research Letters*, **8**, 1981, pp. 269.

8. J. R. Wygant, A. Keiling, C. A. Cattell, R. L. Lysak, M. Temerin, F. S. Mozer, C. A. Kletzing, J. D. Scudder, V. Streltsov, W. Lotko, et al., "Evidence for Kinetic Alfvén Waves and Parallel Electron Energization at 4-6 R_E Altitudes in the Plasma Sheet Boundary Layer," *Journal of Geophysical Research: Space Physics*, **107** , 2002.

9. C. C. Chaston, L. M. Peticolas, C. W. Carlson, J. P. McFadden , F. Mozer , M. Wilber, G. K. Parks, A. Hull, R. E. Ergun, R. J. Strangeway and M. Andre, "Energy Deposition by Alfvén Waves into the Dayside Auroral Oval: Cluster and FAST Observations," *Journal of Geophysical Research: Space Physics*, **110(A2)**, 2005.

10. C. C. Chaston, G. Vincent , J. W. Bonnell, C. W. Carlson, J. P. McFadden, R. E. Ergun, R. J. Strangeway, E. J. Lund, and K. J. Hwang, "Ionospheric Erosion by Alfvén Waves," *Journal of Geophysical Research: Space Physics*, **111.A3**, 2006.

11. C. C. Chaston, J. W. Bonnell, and C. Salem, "Heating of the Plasma Sheet by Broadband Electromagnetic Waves," *Geophysical Research Letters*, **41.23**, 2014, pp. 8185-8192.

12. T. Izutsu, H. Hasegawa, T. K. M. Nakamura, and M. Fujimoto, "Plasma Transport Induced by Kinetic Alfvén Wave Turbulence," *Physics of Plasmas*, **19.10**, 2012, pp. 102305.

13. D. A. Gurnett, K. L. Huff, D. Menieti, L. Burch, D. Winningham, and S. D. Shawhan, "Correlated Low-Frequency Electric and Magnetic Noise Along Auroral Field Lines," *Journal of Geophysical Research: Space Physics*, **89**, 1984, pp. 8971.

14. A. Berthelier, J-C. Cerisier, J-J. Berthelikr, and L. Rnzeau, "Low-Frequency Magnetic Turbulence in the High-Latitude Topside Ionosphere: Low-Frequency

Waves or Field-Aligned Currents," *Journal of Atmospheric and Terrestrial Physics*, **53.3-4**, 1991, pp. 333-341.

15. J. R. Johnson, and C. Z. Cheng, "Kinetic Alfvén Waves and Plasma Transport at the Magnetopause," *Geophysical Research Letters*, **24.11**, 1997, pp. 1423-1426.

16. J. R. Johnson, C. Z. Cheng, and P. Song, "Signatures of Mode Conversion and Kinetic Alfvén Waves at the Magnetopause," *Geophysical Research Letters*, **28.2**, 2001, pp. 227-230.

17. C. S. Salem, G. G. Howes, D. Sundkvist, S. D. Bale, C. C. Chaston, C. H. K. Chen, and F. S. Mozer, "Identification of Kinetic Alfvén Wave Turbulence in the Solar Wind," *The Astrophysical Journal Letters*, **745.1**, 2012, pp. L9.

18. S. Duan, Z. Liu, and V. Angelopoulos, "Observations of Kinetic Alfvén Waves by THEMIS Near a Substorm Onset," *Chinese Science Bulletin*, **57.12**, 2012, pp. 1429-1435.

19. P. S. Moya, V. A. Pinto, A. F. Viñas, D. G. Sibeck, W. S. Kurth, G. B. Hospodarsky, and J. R. Wygant, "Weak Kinetic Alfvén Waves Turbulence During the 14 November 2012 Geomagnetic Storm: Van Allen Probes Observations," *Journal of Geophysical Research: Space Physics*, **120.7**, 2015, pp. 5504-5523.

20. Daniel J. Gershman, F. Adolfo, John C. Dorelli, Scott A. Boardsen, Levon A. Avanov, Paul M. Bellan, Steven J. Schwartz, et al, "Wave-Particle Energy Exchange Directly Observed in a Kinetic Alfvén-Branch Wave," *Nature Communications*, **8**, 2017, pp. 14719.

21. N. D'Angelo, "Ultralow frequency fluctuations at the polar cusp boundaries," *Journal Geophysical Research*, **78**, 1973, pp. 1206-1209.

22. N. D'Angelo, A. Bahnsen, and H. Rosenbauer, "Wave and Particle Measurements at the Polar Cusp," *Journal Geophysical Research*, **79**, 1974, pp. 3129-3134.

23. D. A. Gurnett and L. A. Frank, "Plasma Waves in the Polar Cusp: Observations from Hawkeye 1," *Journal Geophysical Research: Space Physics*, **83**, 1978, pp. 1447-1462.

24. B. Grison, F. Sahraoui, B. Lavraud, T. Chust, N. Cornilleau-Wehrlin, H. Reme, A. Balogh, and M. Andre, "Wave Particle Interactions in the High-Altitude Polar Cusp: A Cluster Case Study," *Annales Geophysicae*, **23**, 2005, pp. 3699-3713.

25. D. Sundkvist, A. Vaivads, M. Andre, J.-E. Wahlund, Y. Hobara, S. Joko, V. Krasnosel-skikh, Y. Bogdanova, S. Buchert, N. Cornilleau-Wehrlin, et al., "Multi-Spacecraft Determination of Wave Characteristics Near the Proton Gyrofrequency in High-Altitude Cusp," *Annales Geophysicae*, **23**, 2005, pp. 983-995.

26. T. Takada, K. Seki, M. Hirahara, M. Fujimoto, Y. Saito, H. Hayakawa, and T. Mukai, "Statistical properties of low-frequency waves and ion beams in the plasma sheet boundary layer: Geotail observations," *Journal of Geophysical Research: Space Physics*, **110**, 2005.

27. N. D'Angelo, "Plasma Waves and Instabilities in the Polar Cusp: A Review," *Reviews of Geophysics*, **15**, 1977, pp. 299-307.

28. L. Chen and A. Hasegawa, "A Theory of Long-Period Magnetic Pulsations: 1. Steady State Excitation of Field Line Resonance," *Journal of Geophysical Research*, **79**, 1974, pp. 1024-1032.

29. G. S. Lakhina, "Low-Frequency Electrostatic Noise Due to Velocity Shear Instabilities in the Regions of Magnetospheric Flow Boundaries," *Journal of Geophysical Research: Space Physics*, **92**, 1987, pp. 12161-12170.

30. G. S. Lakhina, "Generation of ULF Waves in the Polar Cusp Region by Velocity Shear-Driven Kinetic Alfvén Modes," *Astrophysics and Space Science*, **165**, 1990, pp. 153-161.

31. G. S. Lakhina, "Generation of Kinetic Alfvén Waves by Velocity Shear Instability on Auroral Field Lines," *Advances in Space Research*, **41**, 2008, pp. 1688-1694.

32. David M. Malaspina, Seth G. Claudepierre, Kazue Takahashi, Allison N. Jaynes, Scot R. Elkington, Robert E. Ergun, John R. Wygant, Geoff D. Reeves, and Craig A. Kletzing, "Kinetic Alfvén Waves and Particle Response Associated with a Shock-Induced, Global ULF Perturbation of the Terrestrial Magnetosphere," *Geophysical Research Letters*, **42**, 2015, pp. 9203-9212.

33. D. G. Swanson, *Plasma Waves*, Boca Raton, FL, CRC Press, 075030927X, 2003.

34. K. C. Barik, S. V. Singh, and G. S. Lakhina, "Kinetic Alfvén Waves Generated by Ion Beam and Velocity Shear in the Earth's Magnetosphere," *Physics of Plasmas*, **26.2**, 2019, pp. 022901.

A Considerable Level of Correlation Between SID-Monitoring Time Series and GPS-Derived TEC Observations Taken During Development of a Massive Ionospheric Storm

Mia Filić[1,2] and Renato Filjar[3]

[1]Independent Statistical Learning, Satellite Navigation,
and Space Weather Scientist
Sesvete
Zagreb, Croatia

[2]University of Ljubljana
Faculty of Computer and Information Science
Ljubljana, Slovenia
E-mail: filicmia@gmail.com

[3]Zagreb University of Applied Sciences
Zagreb, Croatia
E-mail: renato.filjar@gmail.com

Abstract

Space weather, geomagnetic, and ionospheric conditions are the most prominent causes of degradation in the positioning performance of the Global Navigation Satellite System (GNSS), through introduction of ionospheric delay in the GNSS signal. This affects numerous GNSS-based technologies and socio-economic systems and services. Analyses of case studies of GNSS positioning-performance degradation contribute to the characterization of GNSS positioning error, and support error-correction methods and model development. A case study of a rapidly developing ionospheric storm is examined here, with the aim of characterizing the event using a low-cost sudden ionospheric disturbance (SID) monitor observation of lower-ionospheric-level conditions through continuous reception of very-low-frequency (VLF) signal-strength values. Time series of observations, taken in Croatia during the St. Patrick 2015 event of the fast development of the large ionospheric storm, were compared with the time series of the dual-frequency GPS-derived observations of total electron content (TEC), a parameter linearly related to GNSS ionospheric delay. A comparison framework was developed in the open-source *R* programming framework for statistical computing. Time series of SID and GNSS-based TEC observations were examined for cross-correlation. The research revealed correspondences between the two time series. Although not linear, the correspondences identified may be used as an early warning for potential GNSS positioning-performance deterioration. Furthermore, this may serve as the foundation for understanding the lower-ionosphere contribution to the over-all TEC, and thus to the formation of the GNSS ionospheric delay. Our team intends to explore both research directions in forthcoming studies.

1. Introduction

Detection of an approaching ionospheric storm with potential effects on GNSS positioning performance and subsequently on GNSS-based applications is of utmost importance for sustainable provision of the core GNSS and GNSS-related services [1]. An SID monitor is a low-cost low-ionosphere-activity sensor, developed by a Stanford University (California) team to facilitate scientific activity in the space-weather field across the globe [2]. We hypothesized that using sudden ionospheric disturbances (SID) to monitor observations might serve as early warnings for the development of ionospheric disturbances that increase TEC, thus affecting the accuracy of GNSS positioning performance of single-frequency GNSS receivers, which dominate the market [1]. To validate this hypothesis, we here examined the case of the rapid development of the St. Patrick's Day (DOY076) 2015

ionospheric storm. The time series of Dst (disturbance storm time), TEC, and SID monitoring observations during the storm were assessed in this study, with the aim of characterizing the relationships among the cause (ionospheric-storm development, described by Dst [3]), the effect (GNSS ionospheric delay, and, consequently, GNSS pseudo-range measurement error, described by TEC), and a candidate descriptor for the forecasting of and alerting for ionospheric-storm development (SID monitoring observations).

The disturbance storm time (Dst) index [4, 5] measures the level of the globally symmetrical equatorial electrojet, also known as the "ring current." It has additionally been recognized as an accurate descriptor of ionospheric conditions, especially in sub-equatorial regions. Dst observations are calculated from experimental observations from the network of near-equatorial observatories using the methodology developed by Kyoto University, Japan.

The total electron content (TEC) [4, 5] is defined as the over-all free-electron density encountered by a satellite signal on its path from a GNSS satellite's aerial towards a GNSS receiver's aerial, as traditionally defined by Equation (1), with $N(h)$ denoting the vertical ionospheric profile:

$$TEC = \int_{\text{lower ionospheric boundary}}^{\text{upper ionospheric boundary}} N(h)\,dh\,. \qquad (1)$$

Considering recent developments in identification of the additional sources of temporal ionization (thunderstorms, earthquakes, volcanic eruptions), we recently extended the definition of TEC to account for contributions of layers below the ionosphere, as presented in Equation (2) [5]:

$$TEC = \int_{0}^{\text{upper ionospheric boundary}} N(h)\,dh\,. \qquad (2)$$

Utilization of dual-frequency GNSS observations allows for accurate estimation of TEC as expressed in Equation (3), where f_1 and f_2 denote different GNSS carrier frequencies (as an example, for GPS, $f_1 = 1575.42$ MHz and $f_2 = 1227.60$ MHz), respectively, and ρ_1 and ρ_2 are the measured pseudoranges at related frequencies [4, 5]:

$$TEC = \frac{1}{40.3}\left[\frac{f_1^2 f_s^2}{f_1^2 - f_s^2}\right](\rho_2 - \rho_1)\,. \qquad (3)$$

TEC serves as an essential estimator of GNSS pseudorange measurement error, as expressed in Equation (4) [4, 5], with $2\pi f$, where f denotes the carrier frequency, $e = 1.60217662\times10^{-19}\,C$, $\varepsilon_0 = 8.854187817\times10^{-12}$ V/m $m = 9.109\times10^{-31}$ kg, and $c = 2.99792458\times10^{8}$ m/s. Integration is conducted for heights ranging from sea level ($h = 0$) to the upper (top) boundary of the ionosphere ($h = h_{max}$):

$$\Delta t = \frac{e^2}{2\varepsilon_0 m\omega^2 c}\int_0^{h_{max}} N(h)\,dh\,. \qquad (4)$$

The GNSS pseudorange measurement error propagates into the GNSS position-estimation error [5-7]. The error-propagation model varies with the selection of the position-estimation method [5-8]. It can be shown that the error-propagation model can be expressed for the case of the weighted-least-square (WLS) position-estimation method [7, 8] using the *information matrix* $\mathbf{H}^T\mathbf{R}^{-1}\mathbf{H}$, and the *information state* $\mathbf{H}^T\mathbf{R}^{-1}\mathbf{y}$, as expressed in Equation (5) [5-7], with $\boldsymbol{H}$ denoting the geometry matrix, $\boldsymbol{R}$ being the weighting matrix, $\Delta\hat{\mathbf{x}}$ being the GNSS positioning-error vector, and $\Delta\mathbf{y}$ being the vector of GNSS pseudorange measurement errors:

$$\Delta\hat{\mathbf{x}} = \left(\mathbf{H}^T\mathbf{R}^{-1}\mathbf{H}\right)\mathbf{H}^T\mathbf{R}^{-1}\Delta\mathbf{y}\,. \qquad (5)$$

The model of Equation (5) reveals a direct relationship between the GNSS pseudorange observation errors and the GNSS position-estimation vector components [5, 7]. The research presented was founded on the space weather-GNSS performance coupling model we established [5].

2. Data Description

This section outlines the details of the three data sets examined in the study, as follows: (1) the disturbance storm-time (Dst) index, determined by the Kyoto University methodology; (2) the total electron content (TEC) as an ionospheric condition index; and (3) sudden ionospheric disturbance (SID) monitor observations.

Dst index observations were taken as products of the Kyoto University's processing facility, without further consideration of the original calculation methodology. Observations were provided at hourly sampling intervals, and are available at http://wdc.kugi.kyoto-u.ac.jp/wdc/Sec3.html.

Time series of TEC observations were derived from dual-frequency GPS pseudorange observations at the SONEL (data available at http://www.sonel.org/-GPS-.html?lang=en) network reference station Poreč, Croatia ($\varphi = 45.22601300°$N, $\lambda = 13.59504100°$E), at 30 s sampling intervals. We used an open-source software tool for TEC estimation using the process defined by Equation (1),

Figure 1. The locations of GPS-TEC Poreč, Croatia (blue), and SID Požega, Croatia (red), observation sites, and the VLF broadcasting station at Rosnel, France (magenta).

developed by Dr. Gopi Seemala [9]. TEC estimates defined by Equation (1) are compromised by satellite and receiver bias. The former were mitigated using differential-code-bias (DCB) data provided by the University of Bern, Switzerland, at ftp://ftp.aiub.unibe.ch/CODE/. The latter, presented in the form of an additive model with receiver and receiver inter-channel biases, were left uncorrected.

The time series of SID monitor observations (available through http://sid.stanford.edu/database-browser/calendar.jsp) consisted of data collected at the Požega, Croatia, observation site ($\varphi = 45.331032°\text{N}$, $\lambda = 17.676991°\text{E}$). The data sets contained signal-strength observations of the VLF signal broadcast by the Rosnel, France, station ($\varphi = 46.713129°\text{N}$, $\lambda = 1.245248°\text{E}$). SID monitor observations were taken at 5 s sampling intervals.

The locations of the observing and transmitting stations involved in the study are shown in Figure 1.

3. Methodology

The time series of the Dst, TEC, and SID monitoring observations were examined with the aim of characterizing the relationships among the cause (ionospheric storm – Dst), effect (ionospheric dynamics, and, consequently, GNSS pseudorange measurement error – TEC), and potential indication in lower-ionospheric dynamics, as a candidate descriptor for forecasting of, and alerting for, ionospheric storm development (SID monitor observations) [5, 10, 11].

The time series of SID observations comprised the observation samples of the received VLF signal strength at the observing station at Požega, Croatia. VLF signals were continuously transmitted by the Rosnel, France, transmitter. The SID monitoring observations comprised the readings of the radio signal strength in $\left[\text{W/m}^2\right]$, as observed at the reception station.

A software-based data-processing framework was developed by the authors in the *R* open-source environment for statistical computing [12]. Dst observations were used as a control data set that described the ionospheric-storm development. The SID monitoring and the GPS-derived TEC observations were re-sampled to a one-minute sample interval to allow for their interrelationship analysis. Additional procedures, such as data smoothing, were not employed. We performed the examination of the SID monitoring and TEC time series [13] for DOY076 (17 March) in the 2015 data to identify prospects for utilization of SID observations for identification of TEC enhancement due to ionospheric-storm development, including analysis of: (1) time-series diagrams (waveforms) comparison, (2) kernel density plots, (3) Q-Q diagrams, and (4) anomaly assessment.

Time-series comparison was performed with the aim of examining potential consistency in the observed time delay between the two time-series responses to particular ionospheric disturbances.

Table 1. Algorithm 1: Time-Difference Determination Algorithm

Data: Subset of both time series around the approximate central time of candidate disturbance of duration *d*, to x_s, $s = 1,..., p$, and $y_s = 1,..., p$, with $p = 2d$

Result: Time difference (delay) between subsets of x_i and y_i related to a short-term ionospheric disturbance

```
1    count := 0
2    for i:= 1 to p do
6        calculate correlation coefficient corr(x(s), y(s+p))
7        if(corr(x,y) == 1) do
8            time_diff = count
9        else do
10           count = count + 1
11       end;
12   end;
```

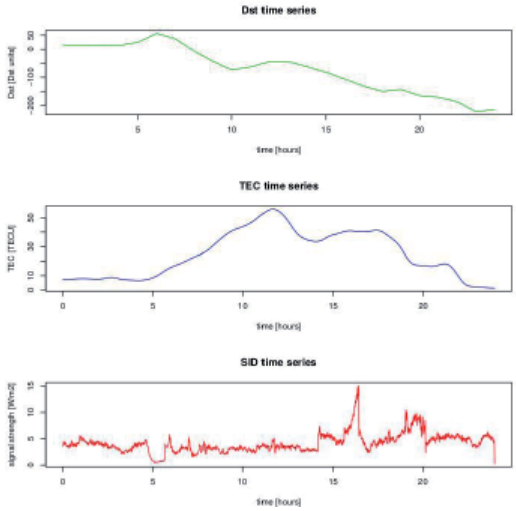

Figure 2. The time series of Dst (green), TEC (blue), and SID monitoring (red) observations during the 2015 St. Patrick ionospheric event.

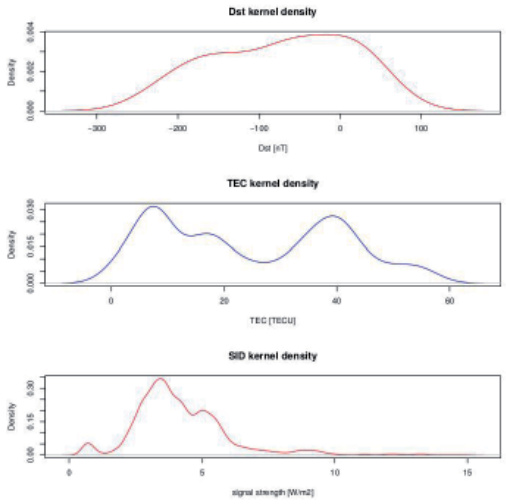

Figure 3. Kernel density plots of Dst (green), TEC (blue), and SID monitoring (red) observations during the 2015 St. Patrick ionospheric event.

The time-delay derivation algorithm was used for every candidate short-term ionospheric disturbance of duration *d*, as presented below. Algorithm 1 (given in Table 1) determined the time difference based on the waveform-similarity-examination approach. More subtle and accurate algorithms may be devised.

4. Study Results

We performed time-series analysis as outlined in Section 3 with the results presented in this section. The data-preparation phase involved the re-sampling of the SID and TEC observations to the same sampling rate, thus allowing for the alignment of samples for the common time-stamp identification and time-difference determination. Data-smoothing procedures were not considered during data preparation.

The properties of the SID and TEC time series were examined, followed by assessment of their inter-relationships, and the prospects for utilization for detection and forecasting of ionospheric-disturbance development that might affect technology systems, in particular, GNSS positioning performance.

The Dst waveform analysis revealed the development of a massive and fast-developing ionospheric storm (Figure 2, green, top). The TEC and SID waveforms (Figure 2, blue and red, middle and bottom, respectively) depicted a sudden commencement of ionospheric activity immediately after 1400 UTC that lasted with considerable variations until the end of the day in observation.

The kernel-density plot (Figure 3) analysis of the TEC and SID time series revealed a non-Gaussian TEC distribution and a skewed Gaussian-like SID distribution.

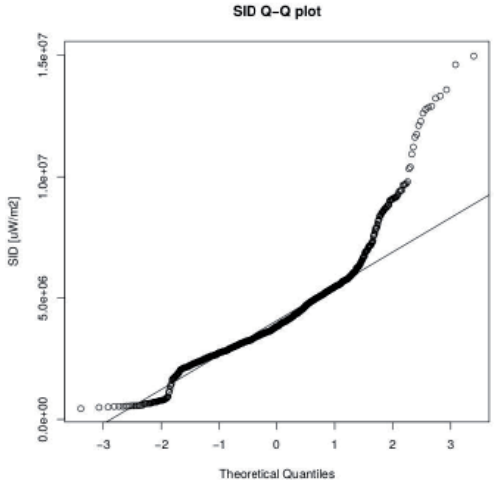

Figure 4. A Q-Q normal plot of the SID time series.

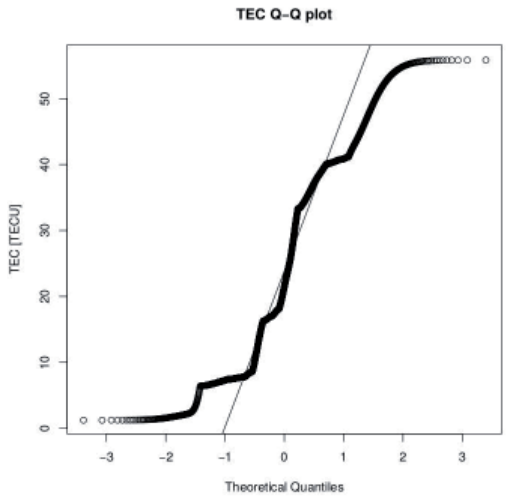

Figure 5. A Q-Q normal plot of the TEC time series.

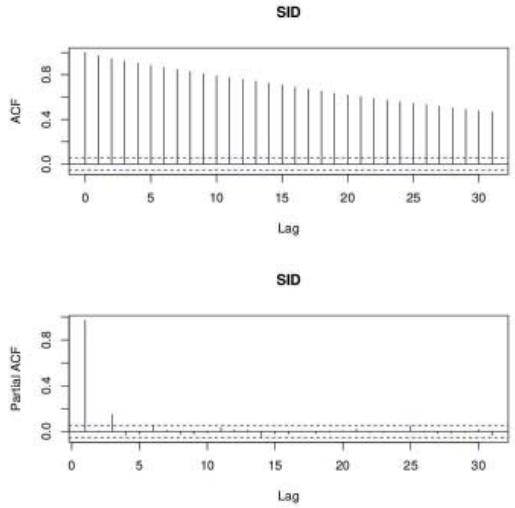

Figure 6. Plots of the auto-correlation function (*acf*) and partial auto-correlation function (*pacf*) estimates of the SID time series observations.

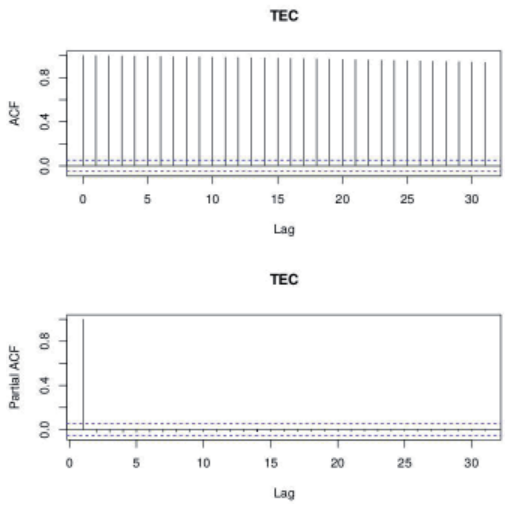

Figure 7. Plots of the auto-correlation function (*acf*) and partial auto-correlation function (*pacf*) estimates of the TEC time series observations.

These findings were confirmed with examination of the Q-Q normal plots depicted in Figures 4 and 5 for SID and TEC time series, respectively. The properties of the SID and TEC time series were further examined through estimates of the autocorrelation function (*acf*) and the partial autocorrelation function (*pacf*), with the related plots presented in Figures 6 and 7 for the SID and TEC time series, respectively. The *acf* and *pacf* analysis results confirmed the occurrence of a massive nonlinear disturbance in the SID and TEC time series. We intend to explore the prospects of the utilization of the *acf* and *pacf* analysis results for ionospheric-storm development identification and forecasting further in our forthcoming research.

Finally, an assessment of anomalies in the observed SID and TEC time series compared with the waveforms in stable (unperturbed) ionospheric conditions revealed notable time-/phase-shift (advancement) in the SID waveform compared with the TEC-related waveforms. Throughout the morning hours of DOY076 of 2015, the SID and TEC values followed the daily pattern characteristics for unperturbed space weather and ionospheric conditions. However, the rapid development of the ionospheric storm commenced on the day under observation soon after 1400 UTC. The event caused an immediate anomaly in the observed SID time series, followed by the occurrence of an anomaly later in the TEC time series, as evident from a visual comparison of the observed waveforms of Dst, SID, and TEC time series (Figure 8).

The observed waveform time-/phase shift was consistent in the cases of two separated major ionospheric

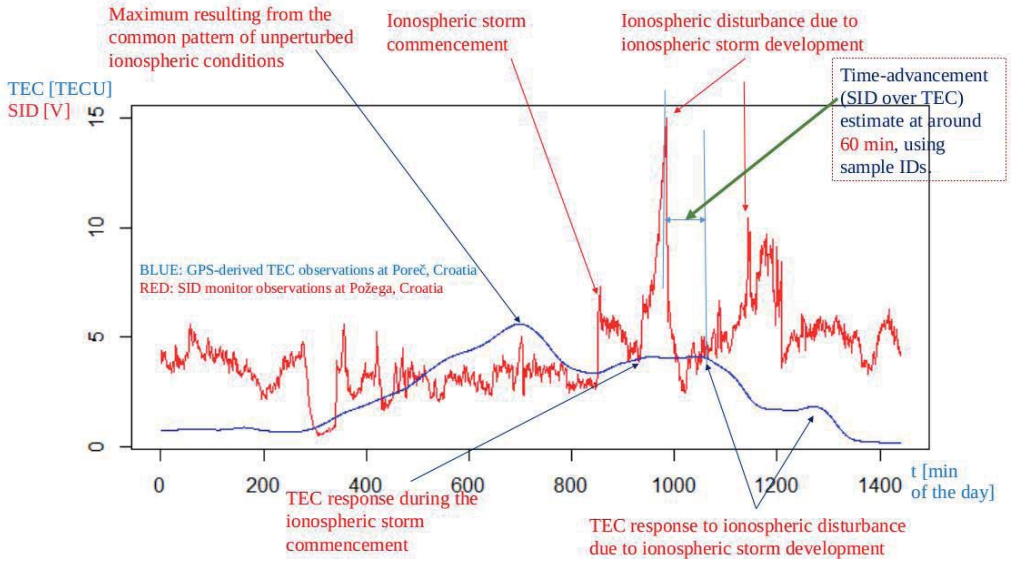

Figure 8. The observed consistent time/phase advancement of the SID time series over the TEC time series.

disturbances, one around 1400 UTC and the other at around 1830 UTC, identified during the rapid development of the St. Patrick's Day 2015 ionospheric storm (Figure 8) through deployment of Algorithm 1. Using sample IDs, we were able to estimate the time-advancement value at approximately 60 minutes. We intend to examine variations of the observed time shift (advancement) further in planned studies of similar events.

5. Discussion and Conclusion

The Dst observations clearly depicted a textbook case of ionospheric storm development. The St. Patrick's Day 2015 storm commenced suddenly during the afternoon hours of DOY076 in 2015, foundering immediately into its negative phase, according to available Dst data.

The ionosphere responded to the storm development, as evident from the dynamics of the SID and TEC time series. Individual disturbances related to the storm's development were followed by SID and TEC responses.

A consistent time advance of the SID time series observations over the TEC time series was observed to the extent of approximately 60 minutes. This research outcome was based on two candidate ionospheric disturbances observed during the same ionospheric event.

The observed time advance allows for precious time to be utilized for the issuance of an ionospheric storm alert for the benefit of the growing community of the human population affected by space-weather events due to the increased utilization of technology.

In particular, established models define the mechanism for propagation of ionospheric disturbance effects into GNSS pseudorange measurements and GNSS position-estimation results, thus affecting a wide range of GNSS-related and GNSS-based applications. The identification of the time-advancement of SID time series over TEC time series renders the former a valuable descriptor candidate for forecasting model development for GNSS-positioning performance.

We intend to pursue and exploit the prospects of the utilization of SID observations in our forthcoming research. Additionally, evidence points to the assumption that the clear SID-based identification of an individual disturbance may result from the correspondence between the SID monitoring site selection and the direction of the ionospheric-disturbance propagation. We intend to address the prospects for exploitation of the VLF propagation-direction-related impact on the quality of SID-based ionospheric-storm observation for TEC and GNSS-positioning-performance forecasting models in our future research. Additionally, we intend to continue research activities in the development and tuning of alternatives to Algorithm 1, using statistical analysis and statistical learning. We believe an advanced algorithm would not only more precisely determine the duration of the ionospheric disturbance, but would also allow us to detect the occurrence of the ionospheric disturbance, thus providing a framework for both detection and characterization of the ionospheric disturbance and its effects on technology and socio-economic systems.

Wisely crafted as equipment aimed at raising the awareness of and engaging more people in scientific activities, SID monitors have already been recognized as invaluable scientific equipment in numerous studies worldwide, including ours. We intend to further exploit them as an invaluable source of information for advanced understanding of both the ionospheric processes and the causes and nature of degradation in GNSS-positioning performance.

6. References

1. UK Government Office for Science, *Satellite-Derived Time and Position: A Study of Critical Dependencies, HM Government of the United Kingdom and Northern Ireland*, 2018, available at https://bit.ly/2E2STnd.

2. D. Scherrer, et al., "Distributing Space Weather Monitoring Instruments and Educational Materials Worldwide for IHY 2007: The AWESOME and SID Project," *Adv in Space Research*, **42**, 2007, pp. 1777-1785, doi: 10.1016/j.asr.2007.12.013.

3. R. Filjar, S. Kos and S. Krajnović, "Dst Index as a Potential Indicator of Approaching GNSS Performance Deterioration," *J. of Nav.*, **66**, 2013, pp. 149-160, doi: 10.1017/S037346331200029X.

4. T. Fuller-Rowell, E. Yizengaw, P. H. Doherty, and S. Basu (eds,), *Ionospheric Space Weather: Longitude Dependence and Lower Atmosphere Forcing*, Washington, DC, AGU and John Wiley & Sons, 2016, ISBN: 978-1118929209.

5. M. Filić and R. Filjar, *Forecasting Model of Space Weather-Driven GNSS Positioning Performance*, Riga, Latvia, Lambert Academic Publishing, 2018, ISBN 978-613-9-90118-0.

6. F. Gustafsson, *Statistical Sensor Fusion*, Linkoepping, Sweden, Studentlitteratur, 2010.

7. M. Filić, *Analysis of the Position Estimation Procedure Based on Given GNSS Pseudoranges in a GNSS SDR Receiver* (MSc thesis, in Croatian), Department for Mathematics, Faculty of Science, University of Zagreb, 2017, available at https://zir.nsk.hr/islandora/ object/pmf%3A3230.

8. M. Filić, L. Grubišić, and R. Filjar, "Improvement of Standard GPS Position Estimation Algorithm Through Utilization of Weighted-Least-Square Approach," Proceedings of 11th Annual Baška GNSS Conference, May 7-18, 2017, Baška, Krk Island, Croatia, available at https://bit.ly/2sLuR82.

9. G. Semaala, *GPS-TEC* program, software, and documentation, 2017, available at http://seemala.blogspot.com.

10. M. Filić, "On Development of the Forecasting Model of GNSS Positioning Performance Degradation Due to Space Weather and Ionospheric Conditions," Proceedings of the Second URSI AT-RASC, Gran Canaria, Spain, May 2018.

11. M. Filić, "A Comparative Study of Forecasting Methods for Space Weather-Caused GNSS Positioning Performance Degradation," UN/USA Workshop on ISWI, Boston College, Chestnut Hill, MA, August 2017.

12. R-project team, "R Programming Environment for Statistical Computing," 2018, available at https://www.r-project.org/.

13. T. C. Mills, *Applied Time Series Analysis: A Practical Guide to Modeling and Forecasting*, London, UK, Academic Press, 2019, ISBN: 978-0-12-813117-6.

Matched Waves and Unexpected Resonances: Variety of Boundary Conditions

Ari Sihvola and Ismo V. Lindell

Aalto University
Department of Electronics and Nanoengineering
Box 15500, 00076, Finland
E-mail: Ari.Sihvola@aalto.fi, Ismo.Lindell@aalto.fi

Abstract

This article discusses certain interesting findings about phenomena that take place when electromagnetic fields interact with a surface on which given boundary conditions are enforced. In particular, the concept of matched waves is analyzed and illustrated. Furthermore, observations are made on resonance spectra that may accompany sub-wavelength scatterers with an isotropic impedance boundary condition. This invited article, reviewing some of our studies on boundary conditions during the past decades, is based on the Commission B (Fields and Waves) keynote presentation of the 2019 URSI Asia-Pacific Radio Science Conference held in New Delhi, India, March 9-15, 2019.

1. Introduction

To solve electromagnetic problems – in other words, for electric and magnetic fields in a given domain – fields need to be found that satisfy Maxwell equations. The freedom of solutions that the equations allow is restricted by boundary conditions that the fields need to fulfill on the boundary of the domain of interest. Boundary conditions are indeed essential in electromagnetics, and they are in the focus of this article.

In electromagnetics, a concept related to a boundary is an interface. The interface is a two-dimensional surface that separates two homogeneous media. On an interface, continuity conditions between the tangential components of the electric and magnetic fields are enforced, and likewise the continuity of the normal components of the flux densities is required [1]. However, despite the continuity of certain components over the interface, the total vectors are in general changed in each of the four cases, the magnitude of the change being determined by the contrasts of the permittivity and permeability between the two media.

For the interface problem, fields hence exist on both sides of the surface. This marks a qualitative difference from the boundary problem, where the fields are only in the domain to be considered. The space beyond this boundary is irrelevant: fields have no meaning there. Another way to look at the situation is to replace the boundary problem by an equivalent free-space problem where sources (electric and magnetic charge and current densities) exist on that two-dimensional surface that was the boundary in the original problem. These sources (together with the primary sources of the original problem) create the correct fields in the original domain, but they radiate zero fields into the domain on the non-interesting side of the boundary.

In classical electromagnetics, much-used boundary conditions are the PEC (perfect electric conductor) and PMC (perfect magnetic conductor) boundaries, on which the tangential components of the electric or tangential components of the magnetic field vector have to vanish, respectively. Such conditions are rather powerful in their "short-circuiting" capability, which leads to the fact that electromagnetic waves hitting such boundaries will be very strong reflected. Another boundary condition that is used to approximate highly conducting structures is the so-called impedance-boundary condition, which was introduced in the 1940s [2, 3] with the objective of facilitating the analysis of radiowave propagation over ground or sea. Towards the end of the century, different ways of approximating layered and other types of structures with effective boundary conditions were developed and documented [4-6].

However, due to the vectorial character of the electric and magnetic fields, the variety of different possibilities of boundary conditions is very large. Let us take a look on their diversity in the following, drawing on our past and recent research on this topic. A detailed exposition on the topic is contained in our forthcoming monograph [7].

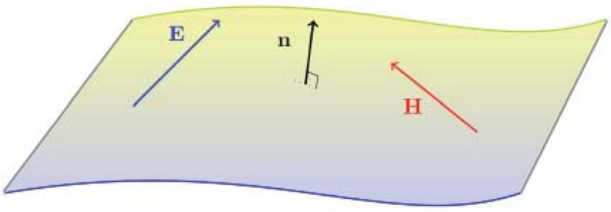

Figure 1. A boundary surface represented by a two-dimensional sheet with unit normal vector $\mathbf{n}$.

2. Classification of Boundary Conditions

Boundary conditions are given as relations of the tangential and/or normal components of the electric and magnetic fields, $(\mathbf{E},\mathbf{H})$, or flux densities, $(\mathbf{D},\mathbf{B})$, at the boundary under consideration. The unit normal vector, $\mathbf{n}$ of the boundary (see Figure 1) is used to project these components: the dot product of $\mathbf{n}$ with the field vector gives the normal component, and the cross product returns the (90° rotated) tangential component.

The classification of boundary conditions can be done using different principles. An obvious way to put the conditions into an order from simple conditions to more-complex conditions is by the number of degrees of freedom that they contain. Another possibility, to be followed here, is to look at classes with similar character, without consideration of the number of free parameters of a given boundary condition. Nevertheless, in the following we start from the well-known conditions.

2.1 PEC, PMC, and PEMC Boundaries

As already mentioned above, the perfect-electric-conductor boundary forces the tangential part of the electric field to vanish:

$$\mathbf{n}\times\mathbf{E}=0\,,\ \text{(PEC)} \tag{1}$$

while the perfect-magnetic-conductor boundary is its dual:

$$\mathbf{n}\times\mathbf{H}=0\,.\ \text{(PMC)} \tag{2}$$

A generalization of these two boundary conditions is the *perfect-electromagnetic-conductor* (PEMC) boundary, which appears at the boundary of the PEMC medium. This medium was introduced in 2005 [8], defined by the following fundamental constitutive relations:

$$\mathbf{D}=M\mathbf{B}\,,$$

$$\mathbf{H}=-M\mathbf{E}\,, \tag{3}$$

where M is the PEMC parameter, having an admittance character. The PEMC boundary condition hence reads

$$\mathbf{n}\times\left(\mathbf{H}+M\mathbf{E}\right)=0\,,\ \text{(PEMC)} \tag{4}$$

which form immediately shows that PEC and PMC are special cases ($1/M=0$ and $M=0$, respectively) of the PEMC boundary condition. [1]

2.2 Impedance Boundaries

The so-called impedance boundary condition (IBC) requires that the tangential electric and magnetic fields stand in a given relation. Due to the fact that the tangential components of the fields have a two-dimensional interconnection, the space of the impedance boundary condition has to be described by four scalars. Formally, the impedance condition is written

$$\mathbf{E}_t=\overline{\overline{Z}}_s\bullet\left(\mathbf{n}\times\mathbf{H}_t\right) \tag{5}$$

between the tangential electric and magnetic fields at the boundary:

$$\mathbf{E}_t=-\mathbf{n}\times\left(\mathbf{n}\times\mathbf{E}\right),$$

$$\mathbf{H}_t=-\mathbf{n}\times\left(\mathbf{n}\times\mathbf{H}\right). \tag{6}$$

Here, the surface impedance dyadic, $\overline{\overline{Z}}_s$, is two-dimensional in the plane perpendicular to $\mathbf{n}$: in other words, $\mathbf{n}\bullet\overline{\overline{Z}}_s=0$ and $\overline{\overline{Z}}_s\bullet\mathbf{n}=0$.

As for PEMC, the IBC condition of Equation (5) also gives, as special cases, the PEC boundary condition $\left(\overline{\overline{Z}}_s=0\right)$, and the PMC boundary condition $\left(\overline{\overline{Z}}_s^{\,-1}=0\right)$.

A two-dimensional dyadic can be decomposed into a physically interpretable manner using the following four elementary base dyadics [12]:

[1] In the four-dimensional electromagnetic formalism, the PEMC condition has been shown to have a natural connection to axion electrodynamics [9-11].

$$\bar{\bar{I}}_t = \mathbf{uu} + \mathbf{vv}\,,$$

$$\bar{\bar{J}} = \mathbf{n} \times \bar{\bar{I}}_t = \mathbf{vu} - \mathbf{uv}\,, \tag{7}$$

$$\bar{\bar{K}} = \mathbf{uu} - \mathbf{vv}\,,$$

$$\bar{\bar{L}} = \mathbf{uv} + \mathbf{vu}\,,$$

where the unit vectors, $\mathbf{u}$ and $\mathbf{v}$, span the two-dimensional plane under consideration, and $\mathbf{u}, \mathbf{v}, \mathbf{n}$ form an orthonormal set.

The simplest isotropic IBC arises from $\bar{\bar{Z}}_s = Z_s \bar{\bar{I}}_t$ where Z_s is a complex scalar. For such an impedance surface to be lossless, Z_s has to be purely imaginary [12, Section 3.6]. If the real part of Z_s is positive, the surface is dissipative, and correspondingly, the negative real part means an active surface.

The case $\bar{\bar{Z}}_s = Z_s \bar{\bar{J}}_t$ leads to the PEMC surface (Equation (4)), with the connection $M\, Z_s = 1$ to the PEMC admittance parameter. For a PEMC boundary to be lossless, the Z_s (or M) parameter has to be real. Note that despite the fact that the dyadic $\bar{\bar{J}}$ is antisymmetric, this boundary is also of isotropic character because there is no special direction in the plane of the boundary.

In contrast to $\bar{\bar{I}}_t$ and $\bar{\bar{J}}$, the two remaining base dyadics, $\bar{\bar{K}}$ and $\bar{\bar{L}}$, are anisotropic. Any surface-impedance dyadic with non-zero component of $\bar{\bar{K}}$ or $\bar{\bar{L}}$ hence has a dependence on the direction of the fields in the plane of the surface. The "losslessness" requirement for such surfaces is that Z_s is purely imaginary in the expansions $\bar{\bar{Z}}_s = Z_s \bar{\bar{K}}$ or $\bar{\bar{Z}}_s = Z_s \bar{\bar{L}}$.

Reciprocity is an important property in electromagnetics [13], and also for boundary conditions. The mathematical requirement that an impedance boundary be reciprocal is that the dyadic $\bar{\bar{Z}}_s$ is symmetric [12]. $\bar{\bar{I}}_t, \bar{\bar{K}}$, and $\bar{\bar{L}}$ are therefore allowed components in the dyadic $\bar{\bar{Z}}$ for a reciprocal IBC. Indeed, the PEMC boundary is non-reciprocal, since $(1/M)\mathbf{n} \times \bar{\bar{I}}_t$ is not symmetric.

2.3 Boundary Conditions with Normal Components of Fields

While the impedance boundary condition linked the *tangential* components of the electric and magnetic fields with each other, a complementary approach is to enforce a condition on their *normal* components. Such a non-traditional viewpoint has been shown to lead into interesting conceptual interpretations of phenomena appearing in the wave interaction with such a boundary (such as matched waves, to be discussed more closely later in this article), as well as promising application perspectives for scattering by objects with this type of boundary (such as zero-backscattering objects [14]).

Probably the simplest of such boundary conditions is one in which the normal components of the electric and magnetic flux densities vanish:

$$\mathbf{n} \cdot \mathbf{D} = 0\,, \tag{8}$$

$$\mathbf{n} \cdot \mathbf{B} = 0\,.$$

Originally introduced already in 1959 [15], this boundary condition has received attention in recent years under the label of the "DB boundary condition" [16-18]. For isotropic media (such as free space in Figure 1), conditions such as Equation (8) are tantamount to corresponding conditions for the fields:

$$\mathbf{n} \cdot \mathbf{E} = 0\,, \tag{9}$$

$$\mathbf{n} \cdot \mathbf{H} = 0\,.$$

A related boundary condition with focus on normal components of the displacements is the D′B′ condition, where the normal derivatives of the normal components vanish. For a planar boundary, this means

$$(\mathbf{n} \cdot \nabla)(\mathbf{n} \cdot \mathbf{D}) = \partial_n D_n = 0\,, \tag{10}$$

$$(\mathbf{n} \cdot \nabla)(\mathbf{n} \cdot \mathbf{B}) = \partial_n B_n = 0\,.$$

An interesting connection back to PEC and PMC boundaries comes from the "mixed boundaries:" referring to the normal derivative with the prime, the D′B condition is equivalent to PEC, and the DB′ condition is equivalent to PMC [19].

It is essential to note the fundamental character of DB and D′B′ boundary conditions: they do not contain any free parameter. In that respect (sharing with PEC and PMC the vanishing number of degrees of freedom), they are more primary than impedance boundary conditions.

A further generalization from DB and D′B′ is the so-called "mixed-impedance boundary," in which the conditions combine the normal component and its derivative separately for the electric and magnetic flux densities [20].

2.4 Hybrid Boundary Conditions

Combining the tangential and normal components of the fields into the same boundary condition takes us deeper into the multidimensional space of boundary conditions. A very general representation of such hybrid boundary conditions is the following [21]:

$$\alpha_1 \mathbf{n}\bullet c\mathbf{B} + \beta_1 \mathbf{n}\bullet c\eta_0\mathbf{D} + \mathbf{a}_{1t}\bullet\mathbf{E} + \mathbf{b}_{1t}\bullet\eta_0\mathbf{H} = 0\,, \qquad (11)$$

$$\alpha_2 \mathbf{n}\bullet c\mathbf{B} + \beta_2 \mathbf{n}\bullet c\eta_0\mathbf{D} + \mathbf{a}_{2t}\bullet\mathbf{E} + \mathbf{b}_{2t}\bullet\eta_0\mathbf{H} = 0\,,$$

where the normalization with constants $\eta_0 = \sqrt{\mu_0/\varepsilon_0}$ and $c = 1/\sqrt{\mu_0\varepsilon_0}$ makes the parameters of the boundary condition, $\alpha_i, \beta_i, \mathbf{a}_{it}, \mathbf{b}_{it}$, dimensionless. Here, the vectors $\mathbf{a}_{it}$ and $\mathbf{b}_{it}$ are transversal: $\mathbf{n}\bullet\mathbf{a}_{it} = \mathbf{n}\bullet\mathbf{b}_{it} = 0$.

Due to the fact that the electric and magnetic fields and flux densities are connected, and that the equations in Equation (11) are homogeneous, there are only eight free boundary parameters in these equations. Nevertheless, this corresponds to a very large space of potential boundary conditions. As an example of hybrid boundary conditions that connect the tangential and normal components of the fields, we can mention the SHDB boundary [22]. This is a one-parameter boundary with the following conditions:

$$\mathbf{a}_t\bullet\mathbf{E} + \alpha\mathbf{n}\bullet\eta_0\mathbf{H} = 0\,, \qquad (12)$$

$$\alpha\mathbf{n}\bullet\mathbf{E} - \mathbf{a}_t\bullet\eta_0\mathbf{H} = 0\,.$$

Obviously, the choice for the parameter $\alpha^{-1} = 0$ returns the DB boundary (Equation (9)). The other limit ($\alpha = 0$) gives the condition $\mathbf{a}_t\bullet\mathbf{E} = 0, \mathbf{a}_t\bullet\mathbf{H} = 0$, which is the so-called soft-and-hard surface (SH). This boundary condition, coined by Per-Simon Kildal [23], can be approximated by a corrugated conducting surface, and finds plenty of applications in microwave components and antenna technology.

Further examples of hybrid boundary conditions are the generalized SHDB surface, in which the transversal vectors, $\mathbf{a}_t$, in the two conditions in Equation (12) can point in two different transversal directions [24], and the E boundary [21], for which the conditions are $\mathbf{a}_1\bullet\mathbf{E} = 0$ and $\mathbf{a}_2\bullet\mathbf{E} = 0$; here, $\mathbf{a}_1$ and $\mathbf{a}_2$ are arbitrary vectors that satisfy $\mathbf{a}_1\times\mathbf{a}_2 \neq 0$. (When these two vectors are tangential to the boundary, the E condition becomes equal to the special case of PEC.)

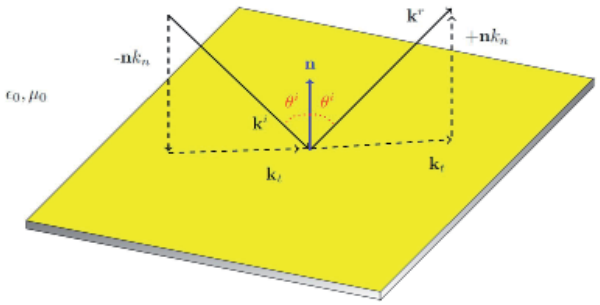

Figure 2. The incident and reflected wave vectors $\mathbf{k}^i$, $\mathbf{k}^r$.

3. Matched Waves

An interesting concept in connection to boundary conditions is that of a matched wave. The way to solve a problem of the reflection of a plane wave from a boundary or interface is to find such a reflected wave such that the sum of the incident and reflected waves satisfies the boundary conditions. By a matched wave, we mean an incident wave with such a polarization state that the boundary condition is already satisfied without any reflected wave. The matched wave is a single wave that can have phase velocity towards the surface ("incident" wave), or away from the surface ("reflected" wave). In the former case, the boundary is absorbing, and in the latter case, it is active. The concept of a matched wave in connection with a boundary condition was coined in 2017 [24].

Let us treat the reflection problem of a plane wave from a general planar boundary. The incident, $\mathbf{E}^i(\mathbf{r})$, and reflected, $\mathbf{E}^r(\mathbf{r})$, electric field functions read

$$\mathbf{E}^i(\mathbf{r}) = \mathbf{E}^i\,\mathrm{e}^{-\mathrm{j}\mathbf{k}^i\bullet\mathbf{r}}\,, \qquad (13)$$

$$\mathbf{E}^r(\mathbf{r}) = \mathbf{E}^r\,\mathrm{e}^{-\mathrm{j}\mathbf{k}^r\bullet\mathbf{r}}\,,$$

where we assume the time-harmonic dependence $\exp(\mathrm{j}\omega t)$ The magnetic fields come from Faraday's law as

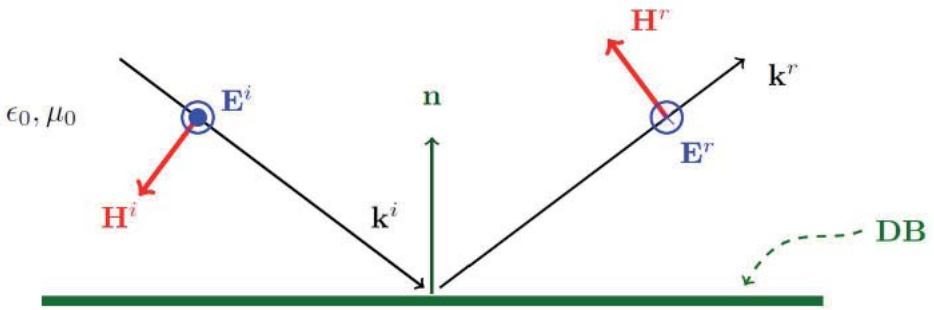

Figure 3. The reflection of a perpendicularly polarized plane wave from the DB boundary. The boundary condition only restricts the magnetic field, forcing its normal component to vanish. The reflection is equivalent to a reflection from a PEC plane.

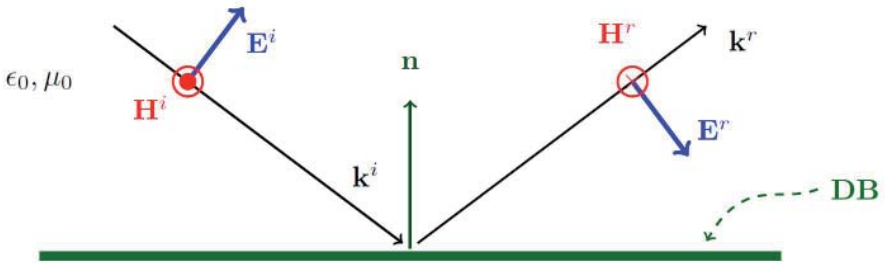

Figure 4. As in Figure 3 for parallel-polarization incidence. The boundary condition now applies on the electric field, forcing its normal component to vanish. The reflection is the same as from a PMC boundary.

$$k_0\eta_0\mathbf{H}^i(\mathbf{r}) = \mathbf{k}^i \times \mathbf{E}^i(\mathbf{r}) \,, \tag{14}$$

$$k_0\eta_0\mathbf{H}^r(\mathbf{r}) = \mathbf{k}^r \times \mathbf{E}^r(\mathbf{r}) \,.$$

Figure 2 shows the geometry of the reflection problem. The incident and reflected wave vectors have the same transversal component, $\mathbf{k}_t$, and opposite normal components, k_n:

$$\mathbf{k}^i = \mathbf{k}_t - k_n\mathbf{n} \,, \tag{15}$$

$$\mathbf{k}^r = \mathbf{k}_t + k_n\mathbf{n} \,,$$

and their magnitudes are the same:

$$\mathbf{k}^i \bullet \mathbf{k}^i = k_0^2 = \omega^2\mu_0\varepsilon_0 \,, \tag{16}$$

$$\mathbf{k}^r \bullet \mathbf{k}^r = k_0^2 = \omega^2\mu_0\varepsilon_0 \,.$$

3.1 Matched Waves at a DB Boundary

For an illustrative view of matched waves, consider plane-wave reflection from a DB boundary, which forces the normal components of both fields to vanish (Equation (9)). The plane wave, with wave vector $\mathbf{k}^i$, impinges at an oblique angle on the boundary, and the wave vector of the reflected wave, $\mathbf{k}^r$, has the same transversal component, $\mathbf{k}_t$, as the incident wave vector, $\mathbf{k}^i$.

In Figure 3, the polarizations of the incident (and reflected) wave are perpendicular (TE polarization). The electric field hence does not have any normal component, and the DB condition applies only on the magnetic field: the reflected wave needs to have a normal component that is opposite to that of the incident wave. The result is that the electric field changes sign in reflection: the reflection is equal to that from a PEC surface.

On the other hand, the complementary phenomenon takes place for a parallel-polarized plane wave (TM polarization) reflecting from a DB boundary, illustrated in Figure 4. The DB condition requires that the normal components of the incident and reflected electric fields have to be equal in magnitude and opposite in direction. This leads to the situation that the magnetic field is short-circuited at the boundary, which is equivalent to a reflection from a PMC boundary.

The DB boundary therefore acts as a PEC boundary for TE waves, and as a PMC boundary for TM waves. The question arises, what happens for a TEM wave, in other words, a wave with normal incidence for which both the electric and magnetic fields are in the plane of the boundary and do not have any normal component? The answer is that there is no reflected wave. The DB boundary condition is already satisfied by the incident wave. A normally incident wave is a wave matched to the DB boundary.

3.2 Matched Waves at a General Boundary

Matched waves can be found for all types of boundary conditions. It may happen that some matched waves are inhomogeneous plane waves, such as surface or leaky waves, but there still exists a systematic wave to determine conditions for wave vectors that correspond to matched waves for any arbitrary boundary condition [21].

The general hybrid boundary condition of Equation (11) can be written in the form

$$\mathbf{a}_1 \bullet \mathbf{E} + \mathbf{b}_1 \bullet \eta_0\mathbf{H} = 0 \,, \tag{17}$$

$$\mathbf{a}_2 \bullet \mathbf{E} + \mathbf{b}_2 \bullet \eta_0\mathbf{H} = 0 \,,$$

with

$$\mathbf{a}_1 = \beta_1\mathbf{n} + \mathbf{a}_{1t} \,,$$

$$\mathbf{a}_2 = \beta_2\mathbf{n} + \mathbf{a}_{2t} \,, \tag{18}$$

$$\mathbf{b}_1 = \alpha_1 \mathbf{n} + \mathbf{b}_{1t} ,$$

$$\mathbf{b}_2 = \alpha_2 \mathbf{n} + \mathbf{b}_{2t} .$$

The wave vector for matched waves for this boundary obeys the condition

$$\mathbf{k}^i \bullet \left(\mathbf{k}^i \times \mathbf{b}_1 - k_0 \mathbf{a}_1 \right) \times \left(\mathbf{k}^i \times \mathbf{b}_2 - k_0 \mathbf{a}_2 \right) = 0 , \qquad (19)$$

where the free-space wave number is $k_0 = \omega \sqrt{\mu_0 \varepsilon_0}$. Likewise, a reflected wave can be matched to the boundary, whence we require a similar condition for the reflected wave vector, $\mathbf{k}^r$:

$$\mathbf{k}^r \bullet \left(\mathbf{k}^r \times \mathbf{b}_1 - k_0 \mathbf{a}_1 \right) \times \left(\mathbf{k}^r \times \mathbf{b}_2 - k_0 \mathbf{a}_2 \right) = 0 . \qquad (20)$$

3.3 Matched Waves at an Impedance Boundary

For the special case of an impedance boundary with impedance dyadic $\overline{\overline{\mathsf{Z}}}_s$ in Equation (5), the condition for a matched wave becomes

$$\eta_0 \left(\overline{\overline{\mathsf{Z}}}_s : \mathbf{k}_t \mathbf{k}_t + k_n^2 \, \mathrm{tr} \overline{\overline{\mathsf{Z}}}_s \right) = \pm k_0 k_n \left(\eta_0^2 + \det{}_t \overline{\overline{\mathsf{Z}}}_s \right) , \quad (21)$$

where tr denotes the trace and $\det_t$ is the two-dimensional determinant of the dyadic. Here, the double-dot product is a short-hand notation for the trace of the dyadic product where one of the dyadics is transposed:

$$\overline{\overline{\mathsf{A}}} : \overline{\overline{\mathsf{B}}} = \mathrm{tr} \left(\overline{\overline{\mathsf{A}}} \cdot \overline{\overline{\mathsf{B}}}^T \right) = \mathrm{tr} \left(\overline{\overline{\mathsf{A}}}^T \cdot \overline{\overline{\mathsf{B}}} \right) . \qquad (22)$$

3.4 Matched Waves at an Isotropic Impedance Boundary

The simplest IBC is the isotropic boundary with symmetric impedance dyadic:

$$\overline{\overline{\mathsf{Z}}}_s = Z_s \, \overline{\overline{\mathsf{I}}}_t . \qquad (23)$$

Equation (21) allows four solutions, which in this case read

$$\frac{k_n}{k_0} = \pm \frac{Z_s}{\eta_0} \text{ (parallel polarization)}, \qquad (24)$$

$$\frac{k_n}{k_0} = \pm \frac{\eta_0}{Z_s} \text{ (perpendicular polarization).} \qquad (25)$$

Here, the upper signs correspond to a matched incident wave, and the lower signs correspond to a matched reflected wave. This is in agreement with the direction of the incident wave: for positive k_n (see Figure 2), a matched incident wave is absorbed into the boundary, requiring a positive real part of the surface impedance, Z_s , which corresponds to a dissipative boundary, and vice versa for the matched reflected wave, which requires an active boundary and a negative surface resistance.

Because for real wave vectors the incidence angle, θ^i , is related to the components of the wave vector, $\mathbf{k}^i$, by $k_n = k_0 \cos\theta^i$, the parallel-polarized (TM) wave can be matched for $Z_s < \eta_0$, and the perpendicular polarization (TE) can be matched for $Z_s > \eta_0$. It is also geometrically obvious that for the parallel (perpendicular) polarization, the ratio of the tangential component of the electric (magnetic) field to the total field is $k_n / k_0 = \cos\theta^i$, which is in agreement with the boundary condition $\mathbf{E}_t = Z_s \mathbf{n} \times \mathbf{H}_t$.

3.5 Matched Waves at a PEMC Boundary

Another isotropic boundary is the PEMC boundary with antisymmetric impedance dyadic. For a PEMC boundary, the condition between the tangential fields is $\mathbf{H}_t = -M \mathbf{E}_t$, meaning that

$$\mathbf{E}_t = \overline{\overline{\mathsf{Z}}}_s \bullet \left(\mathbf{n} \times \mathbf{H}_t \right) \qquad (26)$$

with $\overline{\overline{\mathsf{Z}}}_s = (1/M) \mathbf{n} \times \overline{\mathsf{I}} = (1/M) \overline{\mathsf{J}}$.

This leads to the following condition for matched waves:

$$k_n \left(\eta_0^2 + \frac{1}{M^2} \right) = 0 . \qquad (27)$$

Equation (27) allows two types of solutions. The first one is a lateral wave: $k_n = 0$ and $\mathbf{k}^i = \mathbf{k}_t$. The polarization of such a wave is along the vector

$$\mathbf{E} \propto \mathbf{n} + \frac{\mathbf{n} \times \mathbf{k}}{k_0 M \eta_0} . \qquad (28)$$

The second solution for Equation (27) is $M \eta_0 = \pm \mathrm{j}$. This is a particular case, in the sense that it forces no limitation for the wave vector. It only fixes the magnitude of the PEMC parameter, which is complex-valued. This is in agreement

with the matched wave being either absorbed (dissipative boundary) or existent without incidence (active boundary), depending on the sign of the imaginary part of M.

The polarization of these matched waves is

$$\mathbf{E} \propto k_t^2 \mathbf{n} \mp jk_0 \mathbf{n} \times \mathbf{k} + k_n \mathbf{k}_t , \tag{29}$$

where $k_t^2 = \mathbf{k}_t \bullet \mathbf{k}_t$. Due to the fact that the vector in Equation (29) satisfies $\mathbf{E} \bullet \mathbf{E} = 0$, it is circularly polarized.

3.6 Matched Waves at PEC and PMC Boundaries

The PEC and PMC boundaries can be seen as special cases of both the isotropic symmetric boundary, Equation (23), and the isotropic antisymmetric PEMC boundary, Equation (26). In the first case, PEC and PMC correspond to $Z_s = 0$ and $Z_s^{-1} = 0$, respectively, and in the latter case, they arise from $M^{-1} = 0$ and $M = 0$, respectively.

The matched waves also hence appear from the previous results. Assuming homogeneous plane waves ($\mathbf{k}^i$ and $\mathbf{k}^r$ real-valued vectors), we can see that Equation (24) gives $k_n = 0$ for $Z_s = 0$ for the PEC boundary. This is a parallel-polarized lateral wave traveling along the boundary, in full agreement with Equation (28) for $M^{-1} = 0$, leading to the polarization $\mathbf{E} \propto \mathbf{n}$. Analogously, the PMC boundary supports a perpendicularly polarized matched wave, seen from Equation (25) for $Z_s^{-1} = 0$ and from Equation (28) for $M = 0$.

Note that matched waves can also be inhomogeneous plane waves, for example such as in the case where $k_t > k_0$, or where both k_n and k_t are complex, thereby corresponding to leaky or surface waves.

4. Scattering by Spheres with Boundary Conditions

Another interesting area of electromagnetics problems in which boundary conditions play a significant role is scattering by objects with a given surface characterization. Let us consider here plane-wave scattering from a sphere as a function of the boundary condition assigned on the sphere's surface.

A rigorous full-wave solution of the scattering problem by an isotropic homogeneous dielectric sphere has a long history, starting from the works of L. V. Lorenz [25] and G. Mie [26] over a hundred years ago.[2] Excellent treatments of the analysis and computation of scattering by penetrable spheres can be found in textbooks [28-30], and the analysis has been applied not only to dielectric but also magnetic, plasmonic, chiral, and multilayer spherical scatterers.

The scattering problem of spheres with boundary conditions has received less attention. Apart from early treatments on PEC bodies, boundary-condition scatterers have been analyzed only recently. Let us review some of these results.

4.1 Scattering by PEC, DB, and D′B′ Spheres

When a plane wave hits an object, part of its forward-propagating energy will be lost. Two mechanisms are responsible for this loss: energy will be scattered toward directions around the object, and also some part of the energy may be absorbed into the object, which happens in the case of dissipative scatterers. The measure for the magnitude of these losses is the cross section. The scattering

[2] For a review of the history of Lorenz-Mie scattering, see [27, Section 1.1].

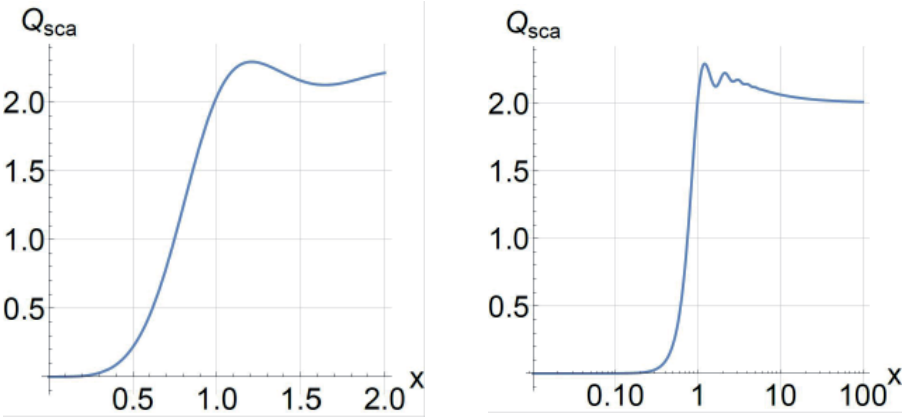

Figure 5. The scattering efficiency of a PEC sphere as a function of its size parameter, x, on linear and logarithmic size-parameter dependence

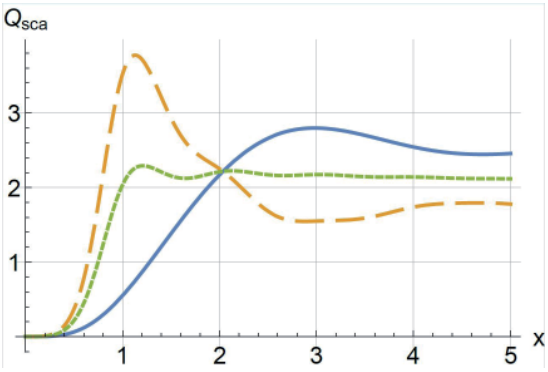

Figure 6. The scattering efficiency of DB (solid blue), D′B′ (dashed orange), and PEC/PMC (dotted green) spheres as functions of the size parameter of the sphere, x.

cross section of an object is equal to the area from which one needs to collect the power density of the incident wave such that this power equals the total scattered power in all directions. In a similar manner, the absorption cross section is defined. The dimension of the cross section is hence area, and the unit is m^2. For a general scatterer, the cross sections are functions of (in addition to the size, shape, and constitution of the scatterer itself) the incident wave direction, its polarization and frequency.

Often, the cross sections are normalized by the geometric cross section of the object, which leads to useful dimensionless quantities called *efficiencies*: the scattering efficiency, Q_{eff}, the absorption efficiency, Q_{abs}, and the extinction efficiency, Q_{ext}, which is the sum of the two other efficiencies:

$$Q_{ext} = Q_{sca} + Q_{abs} . \tag{30}$$

For spherical scatterers, the efficiencies can be computed as summations of the electric and magnetic multipole contributions, each of these so-called Lorenz–Mie scattering terms being rational expansions that contain spherical Bessel and spherical Hankel functions. Depending on the size of the sphere, a certain number of these terms need to be computed in order to have an accurate estimate of the efficiencies. The Wiscombe criterion [31]

$$N = x + 4x^{1/3} + 1 \tag{31}$$

is commonly applied to estimate the necessary number of multipole terms in the expansions. Here, $x = k_0 a$ is the size parameter for the sphere with radius a.[3]

A PEC scatterer is lossless. Its absorption efficiency hence vanishes, and the extinction equals the scattering. Figure 5 displays the behavior of $Q_{sca} = Q_{ext}$ as function of its size parameter. In the region $x \ll 1$, the PEC sphere is a weak Rayleigh scatterer [32] the efficiency of which

[3] The criterion of Equation (31) is used for size parameters x less than 8; for higher values, the formula is slightly modified. The Wiscombe criterion is fairly strict: for example, to estimate the scattering efficiency of a PEC sphere with size parameter $x = 1$, the number of required terms using Equation (31) is 6. This leads to a tremendous accuracy: a six-term approximation of Q_{sca} gives a number for which the relative error is less than 10^{-21}!

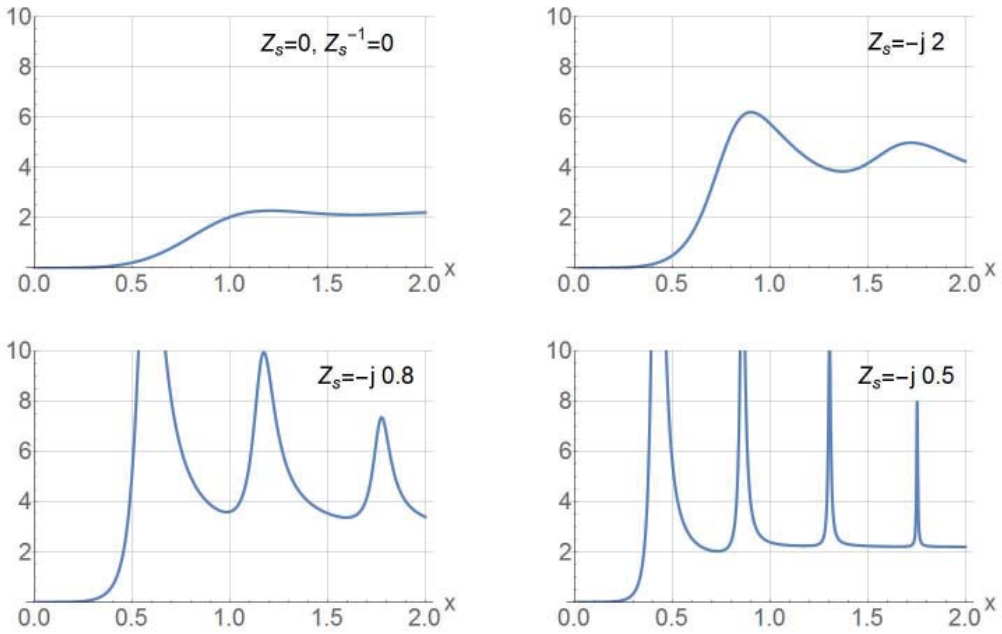

Figure 7. The scattering efficiency of lossless impedance-boundary spheres as functions of the size parameter of the sphere, x, for different surface reactances $\mathrm{Im}\{Z_s\}$.

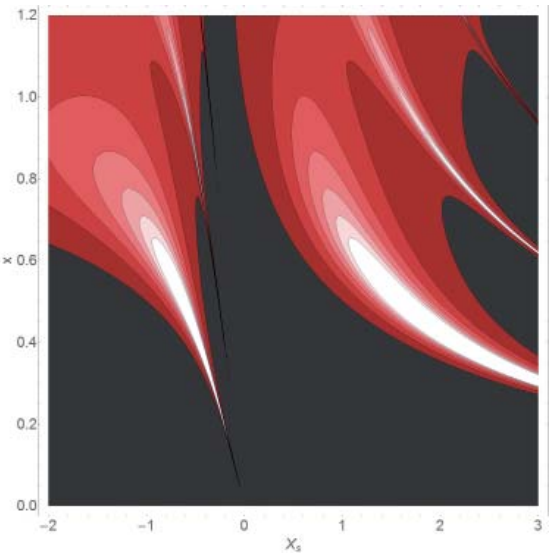

Figure 8. A contour plot of the scattering efficiency of lossless impedance-boundary spheres as functions of the size parameter of the sphere, x, and the surface reactance, $\mathrm{Im}\{Z_s\}$. Dark regions correspond to small values of Q_{sca}, while the white regions show the highest amplitudes.

is proportional to x^4. For high frequencies, the extinction cross section approaches the value of twice the geometrical cross section, which property is valid for all scatterers according to the so-called extinction paradox [33].

The scattering efficiency only takes into account the integrated scattered energy into different directions, and not the details of the scattering patterns in different scattering planes. Due to duality between electric and magnetic fields, the scattering efficiency of a PMC sphere hence follows the same curve as the curve for the PEC in Figure 5. In fact, this is also valid for the PEMC sphere with any PEMC admittance parameter M.

However, the scattering characteristics of DB (Equation (9)) and D′B′ (Equation (10)) boundary spheres are different than the PEC/PMC cases. These are shown in Figure 6. These types of scatterers show larger dynamics than the rather smooth efficiency curve of the PEC sphere: the maximum values of Q_{sca} are higher: 2.80 for DB and 3.77 for D′B′, while the largest value for PEC/PMC is 2.29. Another interesting observation is that in the Rayleigh scattering region (small x values), the D′B′ sphere clearly scatters more strongly than the DB sphere.

4.2 Scattering by Impedance Boundary Spheres

Even if the curves for the scattering efficiencies in Figures 5 and 6 were rather smooth, the situation is utterly different for spheres with impedance boundary conditions, as was recently pointed out [34]. Let us review those results and consider the scattering efficiencies of spheres with isotropic symmetric impedance boundary dyadic $\overline{\overline{Z}}_s = Z_s\,\overline{\overline{I}}$, in other words, the tangential fields on the surface of the sphere are connected by

$$\mathbf{E}_t = Z_s \mathbf{n} \times \mathbf{H}_t \,. \tag{32}$$

The scattering, absorption, and extinction efficiencies can be computed using the modified Mie scattering coefficients [34], and now they are functions of not only the electrical size of the sphere, x, but also of the impedance scalar, Z_s. The surface impedance can be split to the real part (surface resistance, R_s) and the imaginary part (surface reactance, X_s):

$$Z_s = R_s + \mathrm{j}X_s \,. \tag{33}$$

For lossless scatterers, the impedance is purely imaginary: $R_s = 0$. Such scatterers behave interestingly. Figure 7 shows the drastic effect of the surface reactance X_s on the scattering efficiency. While for the values $Z_s = 0$ and $Z_s^{-1} = 0$ (PEC and PMC) the smooth curve of Figure 5 is reproduced, very sharp resonances start to develop for small negative X_s values (capacitive reactances). These peaks grow larger and narrower as $|X_s|$ decreases, and, at the same time, the size x at which the resonance takes place decreases.

Another illustration of the wild behavior of Q_{sca} for lossless impedance scatterers is shown in Figure 8. The contour plot of the efficiency as functions of the size parameter, x, and the surface reactance, X_s, (positive for inductive surfaces, negative for capacitive surfaces) shows the landscape of the resonances.

Indeed, as already seen in Figure 7, there appear ever-sharper peaks in the negative reactance range that accumulate towards the small-x, small-X_s range. However, at the same time, another range of resonances can be observed in the positive-X_s domain. These inductive resonances move into larger and larger X_s values as the size of the scatterer decreases. Between these two "mountain ranges," the vertical line at $X_s = 0$ is seen to form a peaceful valley. This is the efficiency function of the PEC sphere.

It is counterintuitive that a small sphere would display a resonant electromagnetic behavior. However, this phenomenon is also known in plasmonic studies. Penetrable homogeneous spheres with negative permittivity (such as silver nanoparticles) also can support localized surface plasmons that can be very sharp, even if the particle itself is deeply sub-wavelength [35].

However, qualitative differences exist between the plasmonic resonances and those in the impedance spheres. The localized resonances in plasmonic nanoparticles are due only to electric multipoles (dipole, quadrupole, etc.). On the

other hand, in Figure 8, the resonances clustering towards zero are of magnetic type, the most dominant being the magnetic dipole. Electric multipoles also form resonances in impedance spheres: these are due to the second tier that turns towards large positive X_s values in Figure 8.

5. Conclusion

The focus in the present article has been on the variety of boundary conditions in electromagnetics that extends far beyond the classical perfect-electric-conductor or perfect-magnetic-conductor cases. We have highlighted some very fundamental boundary conditions, such as, for example, the perfect electromagnetic conductor (PEMC) condition and conditions that bind the normal components of the electric and magnetic fields, such as the DB and D′B′ boundaries. Hybrid boundary conditions that combine the tangential and normal components of fields form another large class of interesting conditions, with examples such as SHDB and E boundaries.

It is important to note that while many of the boundary conditions presented here have their inspiration from theoretical considerations and may seem even esoteric at first sight, many of those have found experimental realizations. For example, the PEMC boundary was demonstrated by graphene-ferrite metamaterial structures [36, 37] (see also the realizability computations [38]), and the practical fabrication of a DB surface was reported in references [39, 40].

The concept of a matched wave is an essential underlying concept in connection with boundary conditions. This means a wave – propagating either into or away from the boundary – that by itself satisfies the boundary condition. No reflection is hence generated, nor is no incidence required. The properties of matched waves were discussed in connection with the most important boundary conditions.

Finally, a fascinating phenomenon of resonant structure in the scattering spectrum in sub-wavelength impedance-boundary scatterers was analyzed. The origin of the resonance modes can be traced to the poles of the magnetic and electric multipole coefficients, and is especially visible for lossless scatterers. As in the case of localized surface plasmons in negative-permittivity-penetrable particles, these sharp resonance modes in impedance-boundary spheres can be supported by sub-wavelength objects. Obviously, the richness of such electromagnetic responses may be immensely amplified once the surface of these scatterers is endowed with more complicated boundary conditions.

6. References

1. J. A. Kong, *Electromagnetic Wave Theory*, Cambridge, MA, EMW Publishing, 2000.

2. A. N. Shchukin, *Propagation of Radio Waves*, Moscow, Svyazizdat, 1940.

3. M. A. Leontovich, "Methods of Solution for Problems of Electromagnetic Wave Propagation Along the Earth Surface," *Bulletin of the Academy of Sciences of USSR, Physics Ser.*, **8**, 1, 1944, pp. 16-22.

4. D. J. Hoppe and Y. Rahmat-Samii, *Impedance Boundary Conditions in Electromagnetics*, Washington, D.C., Taylor and Francis, 1995.

5. T. B. A. Senior and J. L. Volakis, *Approximate Boundary Conditions in Electromagnetics*, London, IEE, 1995.

6. S. A. Tretyakov, *Analytical Modeling in Applied Electromagnetics*, Boston and London, Artech House, 2003.

7. I. V. Lindell and A. Sihvola, *Boundary Conditions in Electromagnetics*, IEEE Press/Wiley, to appear.

8. I. V. Lindell and A. H. Sihvola, "Perfect Electromagnetic Conductor," *Journal of Electromagnetic Waves and Applications*, **19**, 7, 2005, pp. 861-869.

9. F. W. Hehl and Yu. N. Obukhov, *Foundations of Classical Electrodynamics*, Boston, MA, Birkhäuser, 2003.

10. I. V. Lindell, *Multiforms. Dyadics, and Electromagnetic Media*, Hoboken, New Jersey, IEEE Press and Wiley, 2015.

11. A. Sihvola and I. V. Lindell, "Perfect Electromagnetic Conductor Medium," *Annalen der Physik (Berlin)*, **17**, 9-10, 2008, pp. 787-802.

12. I. V. Lindell, *Methods for Electromagnetic Field Analysis, Second Edition*, New York, Wiley and IEEE Press, 1995.

13. V. H. Rumsey, "Reaction Concept in Electromagnetic Theory," *Physical Review*, **94**, 6, 1954, pp. 1483-1491.

14. I. V. Lindell, A. Sihvola, P. Ylä-Oijala, and H. Wallén, "Zero Backscattering from Self-Dual Objects of Finite Size," *IEEE Transactions on Antennas and Propagation*, **57**, 9, September 2009, pp. 2725-2731.

15. V. H. Rumsey, "Some New Forms of Huygens' Principle," *IRE Transactions on Antennas and Propagation, Special Supplement*, **7**, December 1959, pp. S103-S116.

16. I. V. Lindell and A. H. Sihvola, "Electromagnetic DB Boundary," Proceedings XXXI Finnish URSI Convention, Espoo, October 2008, pp. 81-82.

17. I. V. Lindell and A. Sihvola, "Electromagnetic Boundary Condition and its Realization with Anisotropic Metamaterial," *Physical Review E*, **79**, 2, 026604, 2009.

18. I. V. Lindell and A. Sihvola, "Uniaxial IB-Medium Interface and Novel Boundary Conditions," *IEEE Transactions on Antennas and Propagation*, **57**, 3, March 2009, pp. 694-700.

19. I. V. Lindell and A. Sihvola, "Electromagnetic Boundary Conditions Defined in Terms of Normal Field Components," *IEEE Transactions on Antennas and Propagation,* **58**, 4, April 2010, pp. 1128-1135.

20. H. Wallén, I. V. Lindell, and A. Sihvola, "Mixed-Impedance Boundary Conditions," *IEEE Transactions on Antennas and Propagation*, **59**, 5, May 2011, pp. 1580-1586.

21. I. V. Lindell and A. Sihvola, "Electromagnetic Wave Reflection from Boundaries Defined by General Linear and Local Conditions," *IEEE Transactions on Antennas and Propagation*, **65**, 9, September 2017, pp. 4656-4663.

22. I. V. Lindell and A. Sihvola, "SHDB Boundary Conditions Realized by Pseudochiral Media," *IEEE Antennas Wireless Propagation Letters*, **12**, 2013, pp. 591-594.

23. P.-S. Kildal, "Definition of Artificially Soft and Hard Surfaces for Electromagnetic Waves," *Electronics Letters*, **24**, 1988, pp. 168-170.

24. I. V. Lindell and A. Sihvola, "Generalized Soft-and-Hard/DB Boundary," *IEEE Transactions on Antennas and Propagation*, **65**, 1, January 2017, pp. 226-233.

25. L. Lorenz, "Lysbevægelser i og uden for en af plane Lysbolger belyst Kugle," *Kongelige Danske Videnskabernes Selskabs Skrifter, (Denmark)*, **6**, 1890, pp. 2-62.

26. G. Mie, "Beiträge zur Optik trüber Medien, speziell kolloidaler Metallösungen," *Annalen der Physik*, **25**, 1908, pp. 377-445.

27. D.C. Tzarouchis, "Resonant Scattering Particles – Morphological Characteristics of Plasmonic and Dielectric Resonances on Spherical, Superquadric, and Polyhedral Inclusions," Aalto University publication series, Doctoral Dissertations, 38/2019, March 2019. https://aaltodoc.aalto.fi/handle/123456789/36611.

28. J. A. Stratton, *Electromagnetic Theory,* New York and London, McGraw-Hill, 1941.

29. H. C. van de Hulst, *Light Scattering by Small Particles*, New York, Wiley; London, Chapman and Hall, 1957.

30. C. F. Bohren and D. R. Huffman, *Absorption and Scattering of Light by Small Particles*, New York, Wiley, 1983.

31. W. J. Wiscombe, "Improved Mie Scattering Algorithm," *Applied Optics,* **19**, 9, May 1980, pp. 1505-1509.

32. A. Sihvola, *Electromagnetic Mixing Formulas and Applications*, London, IEE/IET Publishing, 1999.

33. L. Brillouin, "The Scattering Cross Section of Spheres for Electromagnetic Waves," *Journal of Applied Physics*, **20**, 1949, pp. 1110-1125.

34. A. Sihvola, D. C. Tzarouchis, P. Ylä-Oijala, H. Wallén, and B. B. Kong, "Resonances in Small Scatterers with Impedance Boundary," *Physical Review B*, **98**, 235417, 2018.

35. S. A. Maier, *Plasmonics: Fundamentals and Applications,* New York, Springer, 2007.

36. C. Caloz, A. Shahvarpour, D. L Sounas, T. Kodera, B. Gurlek, and N. Chamanara, "Practical Realization of Perfect Electromagnetic Conductor (PEMC) Boundaries Using Ferrites, Magnetless Non-Reciprocal Metamaterials (MNMs) and Graphene," Proceedings 2013 URSI Electromagnetic Theory Symposium (EMTS2013), Hiroshima, Japan, May 2013, pp. 652-655.

37. A. Shahvarpour, T. Kodera, A. Parsa, and C. Caloz, "Arbitrary Electromagnetic Conductor Boundaries Using Faraday Rotation in a Grounded Ferrite Slab," *IEEE Transactions on Microwave Theory and Techniques*, **58**, 11, 2010, pp. 2781-2793.

38. H. Wallén and A. Sihvola, "How Well Can a PEC-Backed Gyrotropic Layer Approximate the Ideal PEMC Boundary?" Proceedings European Conference on Antennas and Propagation (EuCAP 2006), Nice, France, November 6-10, 2006.

39. D. Zaluski, D. Muha, and S. Hrabar, "DB Boundary Based on Resonant Metamaterial Inclusions," Proceedings Fifth International Congress on Advanced Electromagnetic Materials in Microwaves and Optics (Metamaterials'2011), Barcelona, Spain, October 2011, pp. 820-822.

40. D. Zaluski, S. Hrabar, and D. Muha, "Practical Realization of DB Metasurface," *Applied Physics Letters*, **104**, 234106, 2014.

XXXIII General Assembly and Scientific Symposium of the International Union of Radio Science

Union Radio Scientifique Internationale

August 29 - September 5, 2020 - Rome, Italy

www.URSI2020.org

Preliminary Call for Papers and Sessions

The **XXXIII General Assembly and Scientific Symposium** (GASS) of the International Union of Radio Science (URSI, www.ursi.org) will take place in Rome, Italy from August 29 to September 5, 2020. The scientific programme will be organized around the ten URSI Commissions (see below) and will comprise oral sessions, poster sessions, plenary and public lectures, and tutorials, with both invited and contributed papers. In addition, there will be **workshops, short courses, special programmes for young scientists, a student paper competition, programmes for accompanying persons, and an industrial exhibition**. More than 1,500 scientists from more than 50 countries are expected to participate.

Scientists and researchers are invited to submit papers **as well as proposals for sessions** (that may include both invited and contributed papers), workshops and short courses. Detailed information will be posted on the GASS 2020 web site.
Any topic concerning the scientific domains of URSI Commissions is potentially acceptable. Session/workshop/short-course proposals covering multidisciplinary aspects will be assigned to several Commissions.

Workshops are expected to promote interactive exchanges, with enhanced organization flexibility.

Paper Submission

All papers should be submitted electronically via the link provided on the GASS 2020 web site, to be checked prior to submission regarding latest instructions, templates, and sample formats. Accepted papers presented at the GASS 2020 may be submitted for posting on IEEE Xplore, if the author chooses so.

Important Deadlines:

Session, workshop and short course proposals: **August 31, 2019**
Paper submission opening: **October 15, 2019**
Paper submission closing: **January 31, 2020**
Notification of acceptance: **March 15, 2020**

URSI Commissions

Commission A: Electromagnetic Metrology
Commission B: Fields and Waves
Commission C: Radiocommunication and Signal Processing Systems
Commission D: Electronics and Photonics
Commission E: Electromagnetic Environment and Interference
Commission F: Wave Propagation and Remote Sensing
Commission G: Ionospheric Radio and Propagation
Commission H: Waves in Plasmas
Commission J: Radio Astronomy
Commission K: Electromagnetics in Biology and Medicine

Young Scientists Program and Student Paper Competition

A limited number of grants are available for young scientists to help them attend the GASS. Information on this program and on the Student Paper Competition will be available on the Web site.

INTERNATIONAL UNION OF RADIO SCIENCE
UNION RADIO-SCIENTIFIQUE INTERNATIONALE
info@ursi.org www.ursi.org

URSI YOUNG SCIENTIST AWARDS

A limited number of awards are available to assist young scientists from both developed and developing countries to attend the General Assembly and Scientific Symposium of URSI in Rome, 29 August – 5 September 2020.

To qualify for an award, the applicant:

1. must be less than 35 years old on September 1, 2020;
2. should have a paper, of which he or she is the principal author, submitted and accepted for oral or poster presentation at a regular session of the General Assembly and Scientific Symposium.

Applicants should also be interested in promoting contacts between developed and developing countries. Applicants from all over the world are welcome, including from regions that do not (yet) belong to URSI. All successful applicants are expected to fully participate in the scientific activities of the General Assembly and Scientific Symposium. They will receive free registration, and financial support for board and lodging at the General Assembly and Scientific Symposium. Limited funds will also be available as a contribution to the travel costs of young scientists from developing countries.

All Young Scientist applicants must submit a Summary Paper (2 to 4 pages) meeting the requirements of the Summary Paper Template (https://www.ursi2020.org/author-info-abstract-submission/), together with a CV and a list of publications in PDF format. The Summary Papers will be submitted to IEEE Xplore unless the author opts out.

The application needs to be done electronically by going to the same Web site used for the submission of abstracts/papers via http://www.ursi2020.org/. After entering the author and submission details, authors will be asked if they want to apply for the Young Scientist Award. If they check the box "Yes," additional questions will pop up for them to answer. Submissions must use the following file-naming convention, where "Lastnameauthor" text is replaced by the student's surname:

- YSASummaryLastnameauthor.pdf
- YSACVLastnameauthor.pdf
- YSAPubListLastnameauthor.pdf

The deadline for paper submission is **31 January 2020**.

Applications will be assessed by the URSI Young Scientist Committee, taking account of the national ranking of the application and the technical evaluation of the Summary Paper by the relevant URSI Commission. Awards will be announced on 1 May 2020 on the URSI Web site.

For more information about URSI, the General Assembly and Scientific Symposium, and the activities of URSI Commissions, please look at the URSI Web site at: http://www.ursi.org/ and the GASS 2020 Web site at http://www.ursi2020.org/. Updates will also be posted on our Twitter account @URSI_Radio (https://twitter.com/URSI_Radio) and on our Facebook page @internationalunionofradioscience (https://www.facebook.com/internationalunionofradioscience/).

If you need more information concerning the Young Scientist Program, please contact:

URSI Secretariat Ghent University/INTEC
Technologiepark-Zwijnaarde 126, B-9052 Gent, Belgium
E-mail: ingeursi@ugent.be

IUCAF 2018 Annual Report

1. Introduction

The Scientific Committee on Frequency Allocations for Radio Astronomy and Space Science, IUCAF, was formed in 1960 by its adhering Scientific Unions, IAU, URSI, and COSPAR, at the behest of URSI. The IUCAF brief is to study and coordinate the requirements of radio-frequency spectrum allocations for passive radio sciences – radio astronomy, space research, and remote sensing – and to make these requirements known to the national and international bodies that regulate the use of the radio spectrum. IUCAF operates as an Inter-Disciplinary Body under the auspices of the International Council for Science (ICS, formerly ICSU until 2018). IUCAF is a Sector Member of the International Telecommunication Union's Radiocommunication Sector (ITU-R), with observer status at the Space Frequency Coordination Group (SFCG).

IUCAF is online at http://www.iucaf.org.

2. Membership and Member Affiliations with Other Bodies

IUCAF member Hyun Soo Chung, from the Republic of Korea, announced his inability to continue as an IUCAF member representing the International Astronomical Union, and IUCAF is seeking a replacement IAU committee member. At the end of 2018, the IUCAF membership elected by the three adhering unions was as given in Table 1.

In addition, the Counselor for ITU-R Study Group 7 (Science Services), Mr. Vadim Nozdrin, is an ex-officio member by virtue of his ITU-R position, as specified in IUCAF's terms of reference. IUCAF also has an informal group of correspondents in order to improve its global geographic representation and for consultation on specific issues, for instance, concerning astronomical observations in the optical and infrared domains.

IUCAF member van Driel recently stepped down as the Chair of CRAF, the European Committee on Radio Astronomy Frequencies of the European Science Foundation (https://www.craf.eu/), the members of which also include Tiplady. Tzioumis is Chair of the Radio Astronomy Frequency Committee in the Asia-Pacific region (RAFCAP), the members of which also include Ohishi and Zhang (see http://www.atnf.csiro.au/rafcap/). Tzioumis is Chair of ITU-R Working Party 7D (Radio Astronomy), and Ohishi, IUCAF's immediate past Chair, is the official liaison between the IAU and the ITU. Van Driel is Secretary of IAU Commission B4 on Radio Astronomy and a member of its Organizing Committee. Liszt is a member of the American Astronomical Society's Committee on Light Pollution, Radio Interference and Space Debris, and the IAU Executive Committee on WG Dark and Quiet Sky Protection, and serves on the steering committee of the IAU Inter-Division Commission C.B4 on Protection of Existing and Potential Observatory Sites.

3. IUCAF Terms of Reference (Revised 2015)

A revision to the statement of IUCAF's composition, operating practices, and Terms of Reference (TOR), originally dating to 1972 when IUCAF was the Inter-Union Committee on Allocation of Frequencies, was approved by ICSU's Executive Board in 2015 (see http://www.iucaf.org/IUCAF_Terms_Of_Reference.pdf).

4. International and Regional Spectrum-Management Meetings

During the period January-December 2018, IUCAF members participated in the regional and international meetings shown in Table 2.

In addition, IUCAF members participated in numerous national spectrum-management proceedings, working in their capacities as spectrum managers at their observatories.

5. IUCAF Business Meetings

IUCAF held in-person business meetings during each of the ITU-R sessions of Working Party 7D in Geneva listed in Table 2, and at the IAU General Assembly in Vienna. During the year, IUCAF business was undertaken via e-mail as matters arose.

6. Finances

The IUCAF budget is held at and managed by URSI. Sustaining financial contributions of €5,000, €2,000, and €1,000 were gratefully received from IAU, URSI, and COSPAR, respectively, for calendar year 2018. Annual

expenses of €8785 were incurred in support of the IUCAF Chair's attendance at the IAU General Assembly in August and ITU-R WP 5C in November, and van Driel's participation at the ITU-R TG 5/1 session in Geneva in May.

Exceptionally, an anonymous benefactor stepped forward to provide funds to procure an IUCAF-branded fidget spinner (Figure 1) that has been distributed at meetings attended by IUCAF.

7. The IUCAF Role Protecting Passive Radio Science

IUCAF is a global forum where spectrum management concerns of passive radio science in all ITU-R Regions are regularly addressed in a comprehensive manner. The group is expert in the underlying science, in the spectrum-management needs of the science, and in the workings of the spectrum-regulatory regime that allocates spectrum and makes the rules for spectrum use. IUCAF has been an important contributor to the support of radio astronomy at the ITU-R in Geneva since its inception in 1960, providing the spectrum-management interface between the radio astronomy and space science communities. As such, IUCAF is a unique resource, with a lengthy record of contributions the initial history of which was recounted by a former IUCAF chair in "Frequency Allocation: The First Forty Years," by Brian Robinson, *Annual Reviews of Astronomy and Astrophysics*, **37**, 1999, pp 65-96, available at https://tinyurl.com/y5vsgb6x.

IUCAF will celebrate its 60th birthday in 2020. Several IUCAF members are even older.

8. Contact with ICS, the IUCAF Sponsoring Unions (IAU, URSI, COSPAR) and Other International Organizations

IUCAF maintains regular contact with its adhering Unions and the parent body, ICS. These organizations play a strong supporting role for IUCAF, the members of which are greatly encouraged thereby. A report of IUCAF activities was requested by ICSU in preparation for its 2017 General Assembly (see https://tinyurl.com/y6djyca4). A report to URSI was prepared for the 2017 GASS in Montreal (see https://tinyurl.com/y2j839g8).

IUCAF helped to organize and spoke at a session of the IAU Inter-Division Commission C.B4 on Protection of Existing and Potential Observatory Sites at Kuffner Observatory in Vienna during the August 2018 IAU General Assembly.

Pursuing its brief, IUCAF maintains strong links with other passive radio science communities and with space science, especially the Space Frequency Coordination Group, where IUCAF is an accredited observer and has encouraged coordination with operators of high-powered orbiting Earth-mapping radars.

9. Publications and Outreach

IUCAF has the Web address http://www.iucaf.org, where some basic information on the organization is reported. IUCAF maintains the World Map of Radio Astronomy Sites and Radio Quiet Zones, which has been viewed 48,000 times since its inception in 2008 **(see** http://tinyurl.com/yrvszk**).**

IUCAF's main outreach activities, beyond the ITU-R, are related to the international spectrum-management schools it has organized at four to five year intervals since 2000. The last such school was held in 2014 in Santiago de Chile, and the next is being organized for March 2020 in South Africa. Presentations from the IUCAF schools are available on the IUCAF Web site.

10. IUCAF Activities and Concerns in 2018

Most of IUCAF's work during 2018 was in preparation for the 2019 February ITU-R 2nd Conference Preparatory Meeting (CPM-2) for WRC-19. IUCAF strove to acquire a thorough knowledge of the WRC-19 agenda by participating in the spectrum-sharing and compatibility studies conducted in ITU-R Study Groups 1, 4, 5, and 7, and by participating in the treaty text drafting sessions in those groups. At the end of 2018, IUCAF began the task of creating its customary CPM-2 input document, discussing how administrations might best protect radio astronomy and space research in the face of the methods that are proposed to satisfy the WRC agenda items. IUCAF also began to formulate its work plan and agenda for CPM-2, as expressed in an extensive series of five comprehensive input documents describing suggested modifications of the draft WRC-19 treaty text.

Of particular interest to radio astronomy are WRC-19 Agenda Items 1.6, on fixed-satellite service spectrum for

global wireless broadband in bands at 37 GHz to 43 GHz and 47 GHz to 52 GHz; Item 1.7, on telecom command and control links for short-duration non-GSO satellite missions in the spectrum range 135 MHz to 150 MHz; Item 1.8, on regulatory means to facilitate entry of the strongly-interfering Iridium L-band satellite phone network into IMO's Global Maritime and Disaster Safety System; Items 1.9.1 and 1.9.2 on maritime issues around 160 MHz; Item 1.13 on spectrum identifications and allocations for 5G wireless mobile broadband in the frequency range 24 GHz to 86 GHz; Item 1.14 on high-altitude platform systems for wireless broadband; Item 1.15 for fixed and land mobile service applications at 275 GHz to 450 GHz; and Item 9.1.9 on fixed-service allocations at 51 GHz to 52 GHz.

IUCAF input to CPM-2 included suggested modifications to the draft treaty text for all of the above-mentioned WRC-19 agenda items, with special concentration on Agenda Items 1.8, 1.9.2, 1.14, 1.15, and 9.1.9. The impact of so many WRC-19 Agenda Items upon the small amount of spectrum allocated to radio astronomy is an indication of the complexities and general level of upheaval associated with accommodating new uses of the radio spectrum in a compatible fashion.

Radio transmitters are proliferating in vast numbers in vehicles of all sorts, in handheld and mobile devices, and on satellites, even at frequencies above 70 GHz. Moreover, transmitter bandwidths are envisaged to increase to multiple GHz. For terrestrial transmitters, radio-quiet zones, remoteness and terrain shielding of radio astronomy sites may offer some protection, although it is the rare case that a telescope is so secluded that it is not visible from a public road. However, nothing can shield a terrestrial radio telescope from airborne and satellite-born transmitters. In the near future, multiple constellations numbering in the thousands of satellites will make the sky effectively isotropically bright over large swaths of the spectrum that are not specifically allocated for radio astronomy. Commercial startups are now building constellations of the high-power orbiting Earth-mapping synthetic-aperture radars that formerly existed only in much smaller numbers under the purview of national space agencies. Outside the passive service bands, the only clear spectrum looking up may be that which is most congested and difficult to use from the ground because of terrestrial transmitters.

Closer to home, succession planning is the subject of greatest concern as the IUCAF membership ages, and two members have resigned in successive years. India, Korea, and Canada, nations with major investments in radio astronomy and strong histories of participation in international spectrum management, are currently internationally unrepresented. IUCAF is reaching out to astronomers in Thailand, where radio astronomy is developing for the first time, and has encouraged astronomers in Canada to reengage given the increasingly aggressive tactics of their administration's delegations to ITU-R.

11. Acknowledgements

IUCAF is grateful for the organizational and financial support that has been given by ICS, IAU, URSI, and COSPAR over the past (almost) 60 years. IUCAF also recognizes the support given by radio astronomy observatories, universities and national funding agencies to individual members, allowing them to participate in the vital work of IUCAF.

Respectfully submitted,
Harvey Liszt, Chair
Charlottesville, Virginia, USA
IUCAF Web site: http://www.iucaf.org
IUCAF contact: iucafchair@iucaf.org

In Memoriam: Yakov S. Shifrin

Ukraine lost a rare gem when Prof. Yakov Solomonovich Shifrin, IEEE Life Fellow, passed away on August 6, 2019. Prof. Yakov Shifrin was an outstanding scientist and one of the initiators of IEEE and radio science activity in the fields of antenna theory and technique in Ukraine. Yakov Shifrin was a founder of the IEEE Ukraine Section (Kharkiv) SP/AP/C/EMC/COM Joint Chapter.

Yakov Shifrin was born on April 23, 1920, in the city of Mstislavl, Belarus. He graduated in June 1941 from the Physical Faculty of the Leningrad State University. At the beginning of the Second World War's actions on the territory of the USSR, he was enrolled in the people's volunteer corps. At the end of August 1941, he was seconded to study at the Military Red Banner Academy of Communications (MRAC), named after S. M. Budyonny. In the summer and autumn of 1943, he took part in the battles for the liberation of Ukraine on the Third Ukrainian Front. After graduation with honors from the MRAC Radio Faculty and short courses in radar in 1944, he was appointed the commander of one of the new gun guidance station batteries (GGS), which took part in hostilities until the end of the war.

Between 1946 and 1948, he was the first teacher in radar with the Sevastopol Anti-aircraft artillery college, Zhytomyr, Ukraine. Since 1948, Yakov Shifrin lived and worked in Kharkiv, Ukraine.

From 1948-1980, his service and life were connected with the L. A. Govorov Military Radio Engineering Academy. There, he studied as a military post-graduate student, and then worked as a teacher, professor, and, for 25 years, head of the chair. From September 1980 to March 2019, he worked with the Kharkiv National University of Radio Electronics as a professor, head of the Chair of Technical Electromagnetics and Antennas, and chief researcher.

Yakov Shifrin's contribution to science was in a number of areas of modern radio electronics and radio physics. He was a founder of a new scientific field, the statistical theory of antennas (STA), this being the theory of antennas with random sources. His monograph, "Issues in the Statistical Theory of Antennas" (*Soviet Radio*, 1970), was published in the United States in English (translated by P. Beckmann) as *Statistical Antenna Theory* (Golem Press, 1971). The areas of the scientific research of Yakov Shifrin also covered the long-distance tropospheric propagation of radio waves, the theory of antennas with nonlinear elements, the diagnostics of phased-array antennas, and many others. He was an author and coauthor of over 300 scientific publications, including 16 monographs. About 20 doctors (full doctor degree) and over 50 candidates (PhD degree) of science were prepared under his leadership.

In 1993, he organized the National Antenna Association of Ukraine. He initiated the first international antenna conference in Ukraine, called the International Conferences on Antenna Theory and Technique (ICATT). In 2002, Yakov Shifrin and Carl E. Baum (University of New Mexico, USA) initiated one other conference in cutting-edge science problems of radio physics, the International Conference on Ultrawideband and Ultrashort Impulse Signals (UWBUSIS), at Karazin Kharkiv National University.

In 1983, the Presidium of the Academy of Science USSR awarded him the triennial A. S. Popov Prize, with the citation "For works in the field of Statistical Antenna Theory that fundamentally contributed to the antenna theory and techniques."

Prof. Shifrin became the first scientist in Ukraine elected to the grade of IEEE Fellow for fundamental contributions to antenna theory and technology, in 1998.

In 2014, he was awarded the EuMA Outstanding Career Award. In 2015, he received the prestigious IEEE AESS Pioneer Award for pioneering contributions and accomplishments that have stood the test of time: "For founding contributions to modern radio physics and Statistical Antenna Theory (SAT)." He was honored by State Awards including five orders and 20 medals. Yakov Shifrin was an Honorary Citizen of the city of Kharkiv, Ukraine.

Prof. Shifrin was a charming man of impeccable decency and honesty. He is survived by his second wife, two daughters, four grandchildren, and four great-grandchildren. He was truly beloved by his family, disciples, colleagues, and numerous friends. We will forever remember Yakov Shifrin as an outstanding scientist, brilliant speaker, and very kind, generous, and sociable person. He will be sorely missed.

Mariya Antyufeyeva
Chair of IEEE Ukraine Section (Kharkiv) SP/AP/C/EMC/COM Joint Chapter
E-mail: mariya.antyufeyeva@gmail.com
Nina Maksimova
E-mail: ninamax3@gmail.com

Peter Tokarsky
E-mail: p.tokarsky@rian.kharkov.ua

In Memoriam: Edward J. Smith

Dr. Edward J. Smith, a pioneer of space plasma research, passed away on August 11, 2019, at age 91. Ed received a PhD in Physics (his thesis advisor was Robert E. Holzer, also a space plasma physicist) from UCLA in 1959. Ed spent 1959 to 1961 at the Space Technologies Laboratory (now TRW) in El Segundo, California. He then came to the Jet Propulsion Laboratory (JPL), California Institute of Technology, Pasadena, California, where he spent the remainder of his scientific life. In his early years at JPL, Ed took a sabbatical at the Royal Institute of Technology in Stockholm, Sweden, with Hannes Alfvén. They became lifelong friends from that visit.

Ed was typical of scientists of his age, building both the instruments and making major scientific discoveries. Ed was unique among his peers in that he was the first to not only fly a fluxgate magnetometer and vector helium magnetometers in space (VHMs have lower intrinsic noise than fluxgate magnetometers), but also scalar helium magnetometers and dual vector/scalar mode magnetometers. Ed was also the first to build and fly triaxial-search-coil magnetometers in space for electromagnetic plasma wave studies. Ed gave his design of search-coil magnetometers to Europe and Japan, where the basic designs were copied and flown in space by other scientists. Ed was the "father" for all of these space instruments.

Ed was an "experimenter" on the (fluxgate) magnetic-field investigation on Mariner 2, the first successful mission to a planet (Venus, 1962). The other magnetometer experimenters were Chuck Sonett (NASA), Paul Coleman (NASA), and Leveritt Davis (Caltech). The plasma-instrument experimenters were Marcia Neugebauer and Conway Snyder of JPL. Marcia and Conway used the plasma data to confirm Eugene Parker's prediction of the existence of the solar wind. For Mariner 4, the first mission to Mars (1965), and Mariner 5, a second mission to Venus (1967), Ed was then the Principal Investigator (PI) of the magnetometer (VHM) investigation. From the Mariner 5 interplanetary data, working with Leverett Davis (Caltech) and John Belcher (Davis' PhD student at the time), they identified Alfvén waves in the solar wind. Although much more is now known about these waves, the origins and eventual evolution still remain a mystery.

In the 1960s (launched 1964-1969 and extending into the 1970s), Ed was also Principal Investigator of the search-coil magnetometers onboard the Orbiting Geophysical Observatory (OGO) satellites -1, -3, and -5. From these data, Ed and his colleagues were the first to identify the major electromagnetic plasma waves in the Earth's magnetosphere: plasmaspheric hiss, outer-zone chorus, and magnetosheath lion roars. Ed first worked with Holzer and his students (Chris Russell was one), and then later with Richard Thorne (UCLA) and Bruce Tsurutani (JPL). These are the primary magnetospheric electromagnetic-wave modes still studied today. An analysis technique by Ed's friend, Bengt Sonnerup (Dartmouth College), called "minimum-variance analysis," was found to be extremely useful for analyzing electromagnetic waves. Ed was the first to apply this technique, a method that is the main means of studying plasma-wave details today.

The outer heliosphere was next for Ed. He was Principal Investigator of the magnetometer experiments on the twin spacecraft Pioneers 10 and 11. The spacecraft were built by TRW, and the mission was managed by NASA Ames. These were the first missions to go to the outer heliosphere and to distant planets. The radioisotope thermoelectric generators (RTGs) gave power to these spacecraft going far from the sun (a first). Pioneer 10 encountered Jupiter in 1973, and Pioneer 11 encountered Jupiter in 1974, and then went to Saturn in 1979. Ed was the first to characterize the planetary magnetic fields and the dynamic ever-changing (due to solar-wind pressure fluctuations) magnetospheres of these two planets.

During the transit to these distant planets, Ed and his colleagues made other discoveries. With John Wolfe, they were the first to identify an interaction between high-speed solar-wind streams and slow streams, a region they named "corotating interaction regions" or CIRs. CIRs have been shown to be important for causing geomagnetic activity on Earth. With Pioneers 10 and 11 energetic particle experimenters (John Simpson of the University of Chicago, James Van Allen of the University of Iowa, and Frank McDonald of the Goddard Space Flight Center), they discovered that fast forward and fast reverse collisionless shocks bounding the CIRs were accelerating energetic particles in deep interplanetary space between 3 and 10 AU. With Marcia Neugebauer and Bruce Tsurutani, Ed studied and characterized different types of interplanetary discontinuities.

Pioneer 11 had a close encounter with Saturn, which gave it a gravitational boost to become the first spacecraft to get out of the ecliptic plane. Although it only attained an angular distance of 17°, it was enough for Ed and

colleagues to determine the shape of the heliospheric current sheet (HCS). Ed remembered a somewhat obscure prediction by his old friend Hannes Alfvén. The HCS became known as the "Alfvén ballerina skirt." As the ballerina spins, her skirt will fluctuate up and down, with warps in it.

The International Sun-Earth-Explorers were the first joint NASA-ESA missions to be flown. There were three spacecraft. ISEE-3 was a solar-wind monitor placed in orbit around the L1 libration point (first to have achieved this orbit), and ISEE-1 and -2 were magnetospheric orbiting spacecraft. Ed Smith was the magnetometer PI on the ISEE-3 spacecraft, and a Co-I on the plasma-wave experiments on ISEE-1, -2 and -3.

With combined ISEE-3 magnetometer and plasma data, Ed and colleagues identified and characterized what are now called coronal mass ejections (CMEs), and the causes of magnetic storms on Earth. Ed and Bruce Tsurutani of the ISEE-3 magnetometer team and members of the Los Alamos, New Mexico, plasma team (Jack Gosling and Ron Zwickl; the PI was Sam Bame) were the first to identify and characterize interplanetary fast shocks using observational data.

The ISEE -1, -2, and -3 teams were the first to collectively study the Earth's foreshock regions, where back-streaming energetic electrons and ions propagated into the solar wind, generating plasma waves through in situ instabilities. Ed was also strongly involved in identifying a fundamental magnetosheath wave mode at Earth, Jupiter, and Saturn, called the mirror mode. With Charlie Kennel (UCLA), Ferd Coroniti (UCLA), and Fred Scarf (TRW) (and many other colleagues), Ed studied quasi-parallel shock particle acceleration for the first time.

The ISEE-3 space mission had a very clever design engineer named Bob Farquhar. Bob found that by storing extra hydrazine gas onboard (this gas was used to keep ISEE-3 in orbit about the libration point), after the prime mission was accomplished, the spacecraft could be moved to other regions in space. This was an extremely novel concept at the time! The ISEE-3 team voted (the vote was not unanimous) to move the spacecraft from the L1 orbit to a series of deep magnetotail passes, reaching ~240 Earth radii (R_e). To accomplish this, a series of lunar gravitational assists had to be planned and executed. From this new mission, Ed and colleagues determined that the magnetotail was not "fragmented," but still maintained a two-lobe structure all the way to $240R_e$. They also discovered slow shocks bounding the lobe-plasmasheet boundary, and "plasmoids" flowing down the tail. With Fred Scarf, Charlie Kennel, and Ferd Coroniti, Ed and colleagues identified electrostatic plasma-wave modes in the tail and magnetosphere.

After the deep-tail passes, there was still hydrazine gas available for further spacecraft maneuvers. Farquhar identified an opportunity to go through a comet's tail. The ISEE-3 mission was renamed the International Cometary Explorer (ICE), which encountered comet Giacobini-Zinner in 1985. Ed showed that the cometary magnetic tail had a structure of draped magnetic fields, as predicted (again) by Hannes Alfvén.

One of the biggest surprises with the cometary encounter was the detection of highly nonlinear plasma waves associated with neutral gas sublimated from the comet's nucleus. As the neutral H_2O molecules become ionized by either photoionization or charge exchange from the solar wind, the newly formed ions are instantaneously affected by the solar-wind electric fields, and are accelerated so that they collectively are unstable and generate the waves. Ed and Bruce were the first to make this discovery. A theory by Ching Wu and Ron Davidson of the University of Maryland had clearly predicted this, but was missed by the experimenters.

After the encounter of ICE with comet Grigg-Skjellerup, a spacecraft "armada" was sent to comet Halley (1986 encounter), the most famous of all comets. ICE was a distant participant ~one million km away, but still managed to detect pickup ion waves. Hiroshi Oya (Tohoku University, Japan) invited Ed and Bruce to become Co-Is on the Japanese Sakigake plasma-wave investigation going to Halley.

For the joint NASA-ESA Ulysses mission, Ed not only supplied the Vector Helium Magnetometer as Co-I (Peter Hedgecock of Imperial College was the first PI, and then later, André Balogh), but he was also the NASA Project Scientist for the mission. Ed worked in conjunction with Peter Wenzel, the ESA Project Scientist, to make the mission scientifically successful. By using the magnetometer data, Ed was able to determine that the sun's magnetic field does not simply disappear and then reverse polarity, or simply rotate its dipole every 11 years, but a more complex field dominates during the field-reversal interval.

Ed supplied the (Dual Sensor Scalar) magnetometer for the Argentine Science Application Satellite (SAC-C) in 2000, and a vector/scalar helium magnetometer on the NASA/ESA Cassini mission, which orbited Saturn. Ed also was a Co-I of the JUNO mission to Jupiter (arrival date 2016).

Ed was a member of the American Geophysical Union, the American Association for the Advancement of Science, and the American Astronomical Union. He was a recipient of two NASA medals for Exceptional Scientific Achievement, and a NASA Distinguished Service medal. He was elected a Fellow of the American Geophysical Union. In 2005, he received the Arctowski medal from the US Academy of Sciences in recognition of contributions to solar-terrestrial research. Ed was the author or coauthor of over 500 scientific articles. His research interests included planetary magnetism and magnetospheric and solar-heliospheric physics. The achievements of Dr. Edward J. Smith as a pioneer of space science were truly remarkable.

Bruce T. Tsurutani
E-mail: bruce.tsurutani@gmail.com
Marcia M. Neugebauer, University of Arizona, Tucson
E-mail: mneugeb@lpl.arizona.edu

In Memoriam: Richard Mansergh Thorne

Richard Mansergh Thorne, distinguished Professor Emeritus at the University of California, Los Angeles, passed away peacefully on the July 12, 2019, at the age of 76. He was best known for his work on wave-particle interactions in the radiation belts at the Earth and magnetized planets.

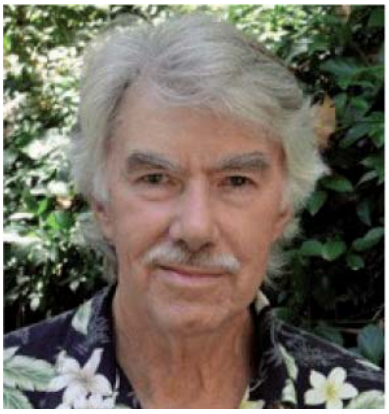

Richard was born in 1942, during an air raid in the second World War. He attended grammar school, where he became captain of the school cricket team, and developed a love for soccer, tennis, badminton, and other competitive sports. He obtained his BSc in Mathematical Physics at the University of Birmingham in 1963, and his PhD at the Massachusetts Institute of Technology in 1968. However, after working at the Avco Everett Research Laboratory in 1965 and 1966, Richard found his real passion: space plasma physics.

In 1968, Richard joined the faculty of the Meteorological Department (he later changed the name to the Department of Atmospheric Sciences) at the University of California, Los Angeles. He was invited to take up this position and stayed at UCLA for the rest of his career. As he once said, "I have never applied for a job in my life." One wonders, could such a thing ever again happen to a young scientist?

Richard started work on wave-particle interactions and applying them to the origin and structure of the Earth's radiation belts: regions of high-energy (relativistic) electrons and protons trapped by the geomagnetic field and which encircle the Earth like a torus. It was known that there was only one proton radiation belt, but the electron belt was spilt into two regions, an inner and outer belt with a gap or "slot" region in between. Richard showed that a special type of electromagnetic plasma wave, called plasmaspheric hiss (Richard named the waves after hearing them played through a loudspeaker), could interact with trapped electrons and precipitate them into the atmosphere. He suggested that these waves would deplete the belts and cause the slot region. This work was profound: we now know that the quiet-time structure of the radiation belts can be explained by inward electron transport from the outer reaches of the geomagnetic field followed by losses due to wave-particle interactions. The model provides our basic understanding of the quiet-time radiation belts at Earth.

Richard also applied similar ideas to Jupiter. At Jupiter, the moon Io has volcanoes associated with gravitational heating, and the resulting gasses become ionized to form the Io torus around the planet. Richard showed the importance of electron precipitation into the Jovian atmosphere caused by plasma instabilities within the torus, and that the precipitation is sufficient to power the diffuse aurora. He went on to suggest that the diffuse aurora would be modulated not just by the wave power, but also by changes in the plasma density arising from volcanic activity. He hence established a connection between volcanoes and diffuse aurora on a distant planet.

Electron precipitation has far-reaching consequences. Richard pointed out that as relativistic electrons penetrate deeper into the Earth's atmosphere, they create various forms of nitric oxide that deplete ozone. This work helped to open up a new area of research: to test whether solar variability can be transmitted to the upper atmosphere through changes in chemistry.

The 1960s and 1970s were a golden age of discovery in space research, and sparked several controversies. Richard was no stranger to a controversy; in fact, he relished controversies, and it would be remiss not to mention at least one. Satellites observed a new type of wave phenomena known as chorus waves, characterized by short bursts of wave power lasting a few tens of milliseconds with a rapidly rising frequency. These signals were at frequencies below the local electron-cyclotron frequency, typically a few kHz, but what could cause such highly nonlinear signals? At kilohertz frequencies, satellites also observed very narrowband signals with a frequency spacing of 50 Hz or 60 Hz or so, which were believed to originate from the power grid: in other words, the power grid was acting as a transmitter, and the high harmonics were being observed in space as power-line harmonic radiation. It had been suggested that the power-line harmonic radiation was triggering a nonlinear interaction that excited chorus waves, but Richard thought otherwise. In a series of papers published in *Science* and elsewhere, the battle raged over the origin of these waves: that the signals should be stronger over land than water; that they should be weaker on a Sunday when there was less power demand; that power-line harmonic radiation was not seen in the outer magnetosphere where chorus was most prevalent; that chorus was observed on field lines that mapped to much higher latitudes than the power grid. Richard was right: we now know that chorus is generated by a natural plasma instability, but the controversy left its mark on the community for several years.

In the late 1980s, Richard Thorne developed a long-lasting collaboration with Richard Horne, publishing over 80 papers on wave-particle interactions and wave propagation at the Earth and planets. These papers gained notoriety as the Thorne and Horne papers by the two Richards (and more often known as the Horney-Thorney papers!). Many of the ideas were conceived in England, over a pint of English beer in a rural Cambridgeshire pub.

As the 1990s drew to a close, it became clear that the electron radiation belts are highly dynamic, and that new theories were required to explain this behavior. While Richard was primarily a theorist, he stayed close to observations as a check on his theoretical predictions. From 1998 onwards, he led many studies to show how plasma waves known as chorus could accelerate electrons to relativistic energies. Testing the wave theory of electron acceleration became one of the primary goals of the NASA Van Allen Probes mission. Launched in 2012, the mission did indeed detect the signatures as predicted by wave theory. It was a tremendous result.

Richard also led other seminal work on wave-particle interactions, showing the relative importance of ground-based radio transmissions (used to communicate with submarines) compared to other types of plasma waves in causing long-term loss of relativistic electrons from the radiation belts. This loss process is most important in the inner electron belt, and for removing some of the electrons injected into the belts by high-altitude nuclear detonations, such as Starfish.

Richard also changed our ideas on the origin of the diffuse aurora: a low-level light emission quite separate from the visible discrete aurora arc. Richard conclusively showed that chorus waves are responsible for electron loss into the atmosphere that causes the diffuse aurora in the Earth's inner magnetosphere. This resolved a controversy that was long-standing since the 1960s.

During his last few years, Richard was keenly interested in identifying the acceleration mechanism of Jovian radiation belts with the help of new data from the Juno mission, where he played a key role. He was excited to see the pronounced peaks in electron phase space density in the Jovian middle magnetosphere from the Juno data, indicative of an internal acceleration source. Even right before his passing, he still showed great passion for science, a role model to the end.

Richard published over 400 research papers, cited over 23,000 times. As a member of the International Union of Radio Science (URSI) since 1971, he always attracted an audience as an excellent speaker. He served the community in many ways, on GEM Working Groups, the NASA Living with a Star Program, and review boards. He was Co-I on the Galileo probe at Jupiter, Van Allen Probes mission, and JUNO at Jupiter. However, first and foremost he was a theorist who took a keen interest in the data. He approached each problem as a mystery, seeking the truth, and not letting politics stand in the way: a rare bird, indeed.

In addition to his outstanding research, Richard will be remembered for his incredible mentorship that has meant so much to so many next-generation scientists. Richard taught them how to have fun in the world of space physics, gave them the freedom to work on the problems they were interested in, and offered to help whenever it was needed. He was a terrific colleague and a friend to so many people from all over the world.

In his early days, Richard was remembered for his flowery shirts, his bell-bottom trousers, a spectacular beard, but most of all for dancing on tables. There were no airs or graces, he had a relaxed manner and was never in awe of anyone who had a title or distinction. What he respected most of all were good scientists who had done, as he would say "something fundamental." He loved his garden, which was an oasis in Los Angeles; sports; English beer; and avidly followed the Manchester United football club. He was renowned for his family hiking trips, not for the faint hearted. In his later years, his group expanded, and many students and post-docs learned his relaxed manner and his focus on fundamental research.

He leaves behind his wife, Moni, his three sons, Peter, Mike, and Tom, and his grandchildren. He was greatly loved, and will be greatly missed.

Richard B. Horne
Bruce Tsurutani
Wen Li
Jacob Bortnik

Submitted by Richard B Horne
British Antarctic Survey
Cambridge, UK
E-mail: rh@bas.ac.uk

Et Cetera

Tayfun Akgül
Istanbul Technical University
Dept. of Electronics and Communications Engineering
Telecommunications Division
80626 Maslak Istanbul, Turkey
Tel: +90 212 285 3605; Fax: +90 212 285 3565
E-mail: tayfunakgul@itu.edu.tr.

Book Review

George Trichopoulos
Electrical, Computer & Energy Engineering ISTB4 555D
Arizona State University
781 E Terrace Road, Tempe, AZ, 85287 USA
Tel: +1 614 364 2090
E-mail: gtrichop@asu.edu

Jan Hendrik Oort – Master of the Galactic System by Pieter C. van der Kruit, Berlin, Springer, Astrophysics and Space Science Library, Volume 459, 2019, ISBN 978-3-030-17800-0, ISBN 978-3-030-17801-7 (eBook), ISSN 0067-0057, ISSN 2214-7985 (electronic).

The early decennia of the twentieth century saw a marked increase in the field of astronomy. New telescopes – in particular, the 100-inch (2.54-m) Hooker Telescope on Mt. Wilson, California, in 1917 – provided a wealth of new data that fostered advances in the understanding of the physics of stars and the dynamics of the stellar system. Just preceding the new century was the birth of Jan Hendrik Oort, in April 1900, in the town of Franeker in the northern province Friesland, The Netherlands. The future science of astronomy would be marked by the exceptional achievements of Oort into the 21st century. He published his first paper while still a student in 1922 ("Some Peculiarities in the Motion of Stars of High Velocity") and his last publication appeared in 1992 ("Exploring the Nuclei of Galaxies"), the year of his death. In the intervening 70 years, he contributed to many aspects of astronomy from comets, stars, and the interstellar medium to the structure and dynamics of our Milky Way system and external galaxies, and ultimately the universe.

The life and work of Jan Oort is the subject of the book under review, written by his one-time student and later colleague, Pieter van der Kruit, Emeritus Professor of Astronomy at the University of Groningen in The Netherlands. The author earlier showed his credentials with a biography of Jacobus Kapteyn, who was a professor of astronomy in Groningen in the early decades of the 20th century. It was Kapteyn who drew young Oort to study astronomy in Groningen instead of Leiden, where Oort lived with his parents. In writing Kapteyn's biography, van der Kruit had already encountered Oort as Kapteyn's student. The author's studies with Oort, including as doctoral-dissertation supervisor, and later as collaborator and colleague, made him almost predestined to write Oort's biography, too. In this task, he was able to exploit a large amount of documentary material in the "Oort Archive" at the University of Leiden, meticulously catalogued by Ms. Jet Katgert-Merkelijn over many years. In addition, van der Kruit interviewed many colleagues of Oort, Oort's students, and family members. They are quoted at length, which gives the narrative a pleasant variability of style. The result is a tome of over 700 pages, richly illustrated with photographs, explanatory drawings, facsimile copies of manuscripts (including some in the tiny but clear handwriting for which Oort was famous), and copies of letters and documents.

The structure of the book is quite unusual, and requires some flexibility of attention and concentration from the reader. Next to the strictly personal and familial aspects, a biography of a scientist needs to illustrate the original scientific achievements and their influence on the development of the field and the community of colleagues and students. The author pays equal attention to the personal and professional aspects of Oort's life. Perhaps due to having taught astronomy over his career, the author decided to add a considerable amount of astronomical material, with the aim of making Oort's specific contributions more accessible to the general reader. It remains to be seen how well this effort will succeed. The "entry level" to this material requires a reasonably good knowledge of basic astronomy and the specific astronomical vernacular, as taught in first- and second-year courses. The mathematical sections are marked by grey shading, and can be skipped without losing track of the presentation. Of the 620 pages of the book's body, some 125 pages are devoted to the "astronomy introduction." The discussion of Oort's own research occupies about twice as many pages. Here, abundant use is made of excerpts and copies of original manuscripts and workbooks. This offers a fascinating look at the style and method of Oort's labor, despite the fact that many of the copies are barely readable because of their printed size and Oort's minute handwriting. A loupe is helpful, here. (E-Book readers can adjust the screen magnification.) The story of Oort's life outside astronomy and his administrative activities are told in some 150 and 100 pages, respectively.

The author has chosen an original way for distributing the different narratives – personal, professional, administrative – over the 15 chapters of the book. The

events are essentially ordered along the timeline, resulting, for instance, in Chapter 5 being titled "Rotation of the Galaxy; Marriage," with the section on "Marriage" sandwiched between "Thesis on High-Velocity Stars" and "Discovery of Galactic Rotation." In this last section, Oort introduced the constants A and B, characterizing Galactic differential rotation that are named after him as "Oort Constants A and B."

The "mixture" of different aspects throughout the text invites the reader to a pause and redirection of the reader's attention. Some may find this annoying, and will need to consult the Table of Contents to follow their main interest. To this reviewer, the change of "landscape" was a rather new and nice feature.

The chapters and sections about Oort's private life are detailed, and filled with quotations from family and friends, and with many photographs. Particularly moving are the passages dealing with the years of World War II, during which the Oort family, with three children, lived "in hiding" in a "vacation home" in the wooded center of the country, without power or running water. He nevertheless regularly went to Leiden to maintain contact with the observatory and actually secretly gave lectures, against the rules imposed by the German occupation.

During his entire career, Oort traveled to foreign observatories, mostly for several months, to make observations and present lectures. His ruminations about these experiences are interesting to read. Despite several honorable and attractive job offers abroad, he decided to remain in Leiden, where he became full Professor of Astronomy and Director of Leiden Observatory in 1945, a few months after the end of the war. Among his first acts was to establish a daily "joint coffee break" for the entire staff at 11:00 o'clock. There, he would appear with a small piece of paper on which he had noted the "chores" he was going to pass on to the attendants. He would note someone's absence within a week and ask for the reason. When this happened to me, and I responded that I had been at the telescope construction site in Westerbork, he nodded approvingly and asked about the progress.

During the war, Oort had read the paper in the *Astrophysical Journal* by Grote Reber, showing the map of radio emission from the sky. Oort immediately saw the prospects of this new component of "cosmic radiation:" not only was it something new, but it could be observed from Holland through the ever-present clouds. He also realized that the presence of a spectral line in the radio regime would enable observations into the far regions of the galaxy that were obscured in the optical domain. At his instigation, Henk van de Hulst attacked this subject and, during a clandestine colloquium at Leiden Observatory in April 1944, predicted that the spectral line of neutral hydrogen at 21 cm wavelength could be observable. Immediately after the war, Oort proposed the construction of a large radio telescope ("some 20-25 m diameter"). His tenacious arguments for development of radio astronomy in Holland were rewarded after Muller and Oort confirmed the detection of the 21 cm line with a 7.5 m diameter German radar antenna in 1951. The 25 m Dwingeloo telescope began operation in 1956, and was for almost a year the largest radio telescope in the world. Its scientific success paved the way for the realization of the Westerbork Synthesis Radio Telescope, which was the primary instrument in the 1970s, and radio astronomy blossomed as a result.

The fact that Oort remained in Leiden for his entire career, apart from a number of visiting-professor positions in the USA, should not be considered as provincialism. On the contrary, Oort was a great promoter of international contacts between astronomers worldwide, and of international collaborations in the area of large and expensive instruments. After the war, he revitalized the International Astronomical Union as its General Secretary and President. He was one of the founders of the European Southern Observatory in the mid-fifties. While staying "at home," Oort also welcomed a steady stream of visitors to Leiden Observatory; some of them stayed forever. On the other hand, quite a number of his brightest students were appointed to influential positions at foreign observatories. Oort's multiple memberships in learned societies, advisory, and review committees made him a true ambassador of Dutch astronomy. At his retirement in 1970, he dislodged himself from all administrative and organizational duties; he only asked to remain a member of the Westerbork Program Committee, because of his scientific interest. He was granted a lifetime place on the committee, which he occupied until 1986, when he resigned at his own initiative at the age of 86.

This is perhaps the strangest book review you have come across. Just copying the contents of the book would have taken more space. I decided to forego any listing of detailed subjects, but to summarize the story about Jan Oort as written by the author van der Kruit, in the hope that you would become curious for more detail. You can be assured that those details are in the book. It is an exhaustive account, well written and solidly backed by references, illustrations, and copies of original documents. In reading this book, you will become familiar with one of the greatest astronomers of the last century, a brilliant scientist, a modest and friendly man in conversation, but with a tenacious will to achieve his goals. Astronomy still enjoys the fruits of this tenacity. You will also learn a lot about astronomy; some of it might be beyond your interest. It is worth a try. Finally, there is lot of interesting material about personalities in astronomy, and the organization and management of science and observatories.

As mentioned before, the author has chosen a somewhat unusual composition of a large amount of available material. The detailed contents list will help to jump through the text. There are quite a number of printing errors, but none of them are serious. Literal quotations are printed in a different, sans-serif font at a point larger size. They "jump out" of the page, which I found annoying. I guess the author's or editor's rationale was the often long length of the quotation. It is a pity that many of the facsimiles of notebook and diary entries were barely readable. On the other hand, the old illustrations and photographs give the book a lively appearance.

Jacob W. M. Baars
Rheinbach, Germany
Max-Planck-Institut für Radioastronomie
E-mail: jacobbaars@arcor.de

Özgür Ergül
Department of Electrical and Electronics Engineering
Middle East Technical University
TR-06800, Ankara, Turkey
E-mail: ozergul@metu.edu.tr

SOLBOX-17: Cylindrical Lens Structures

Hande İbili and and Özgür Ergül

Department of Electrical and Electronics Engineering
Middle East Technical University
TR-06800, Ankara, Turkey
E-mail: ozergul@metu.edu.tr

1. Introduction

Zero-index and near-zero-index (NZI) materials are artificial structures that have recently attracted great interest in the electromagnetics and optics communities, thanks to their potentials in manipulating electromagnetic waves for a plethora of applications [1-5]. As with all other types of metamaterials, NZI structures are built of small unit cells, such as dielectric, metallic, and plasmonic particles, although they are often homogenized and represented by using effective electromagnetic properties in their numerical simulations. In fact, when accurately performed, homogenization can provide excellent analysis abilities, particularly when these structures are integrated with other devices to construct larger systems. At the same time, even when an NZI structure is greatly simplified by using a homogeneous model, the resulting electromagnetic problem may still possess several numerical challenges, considering that the conventional implementations are developed for ordinary materials. Some of these difficulties, e.g., handling numerically small or large values in the computer environment, may be easier to overcome, while there are also challenges that arise due to inherent properties of the developed methods and algorithms and that need more elaborate techniques to solve.

When analyzing an NZI material using implementations based on the Method-of-Moments solutions of surface-integral equations, one can identify two major sources of numerical difficulties [6]. First, since an NZI object must be together with (or at least located in) ordinary materials, integral operators related to the NZI medium are not numerically balanced with the corresponding operators on the other side. Boundary conditions themselves hence involve numerical breakdowns as the permittivity, permeability, or both go to zero, if the underlying formulation is not designed to behave well in such limiting cases. Second, the inner problem that has an extremely large wavelength value causes the well-known dense-discretization breakdown issues, both in terms of formulation and solution algorithm. These issues appear in numerical solutions as inaccuracy, inefficiency, and instability, some of which may be difficult to identify without a rigorous analysis.

In this issue of Solution Box (SOLBOX-17), scattering problems involving various NZI objects are investigated. The objects have homogeneous properties with given permittivity and permeability values, and they have relatively simple geometries (cylindrical lenses). However, the challenge is to obtain numerically accurate results considering the abovementioned issues encountered

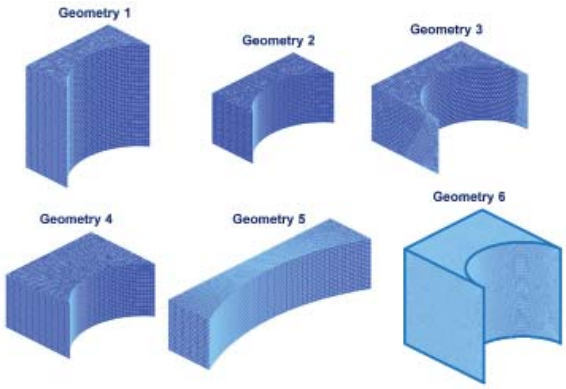

Figure 1. The lens structures with NZI properties considered in SOLBOX-17.

in the conventional implementations. Sample reference solutions are obtained by using conventional and novel integral-equation formulations in the frequency domain, and a broadband implementation of the Multilevel Fast Multipole Algorithm (MLFMA), while we are looking for more accurate and/or efficient solutions for this class of problems. Interested readers are welcome to send their alternative solutions to the described problems, both in this issue and in previous issues.

2. Problems

2.1 Problem SOLBOX-17 (*Handeİbili and Özgür Ergül*)

In SOLBOX-17, we considered six different cylindrical lens structures, labeled Geometry 1-6, as depicted in Figure 1. The geometries can be briefly described as follows (λ is the wavelength in vacuum):

- Geometry 1: $2\lambda \times \lambda \times 2\lambda$ block, cylindrical extraction with 1.25λ radius of curvature
- Geometry 2: $2\lambda \times \lambda \times \lambda$ block, cylindrical extraction with 1.25λ radius of curvature
- Geometry 3: $2\lambda \times 1.5\lambda \times 2\lambda$ block, cylindrical extraction with λ radius of curvature
- Geometry 4: $2\lambda \times 1.5\lambda \times \lambda$ block, cylindrical extraction with 1.25λ radius of curvature
- Geometry 5: $4\lambda \times \lambda \times \lambda$ block, cylindrical extraction with 4.25λ radius of curvature
- Geometry 6: $8\lambda \times 8\lambda \times 8\lambda$ block, cylindrical extraction with 4λ radius of curvature

These lenses were assumed to be located in vacuum and have NZI properties, i.e., 0.1 relative permittivity and 0.1 relative permeability, while smaller values can also be used to test the stability of the implementations. It was desired to investigate near-zone characteristics of the structures, e.g., their focusing properties when they were illuminated by a beam or a plane wave. For this purpose, near-zone electric-field intensity, magnetic-field intensity, and power-density distributions could be sampled in the vicinity of the structures.

3. Solution to Problem SOLBOX-17

3.1 Solution Summary

Solver type (e.g., Noncommercial, commercial): Noncommercial research-based code developed at CEMMETU, Ankara, Turkey
Solution core algorithm or method: Frequency-domain MLFMA
Programming language or environment (if applicable): *MATLAB + MEX*
Computer properties and resources used: 2.5 GHz Intel Xeon E5-2680v3 processors (using 1 core)

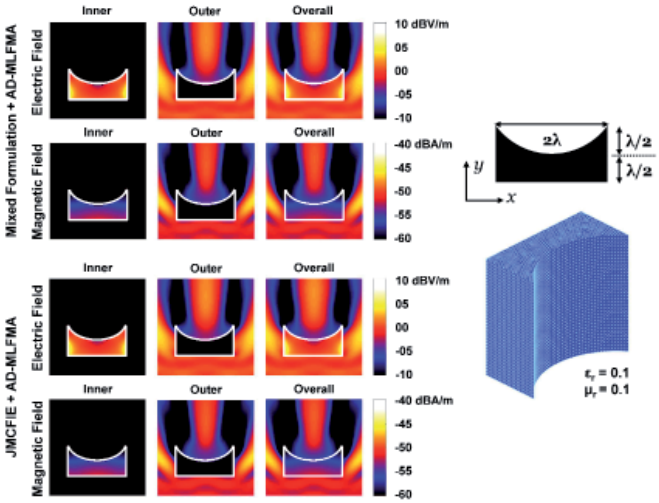

Figure 2. The results (electric-field intensity and magnetic-field intensity) for Geometry 1 of SOLBOX-17 when both relative permittivity and relative permeability of the lens were 0.1.

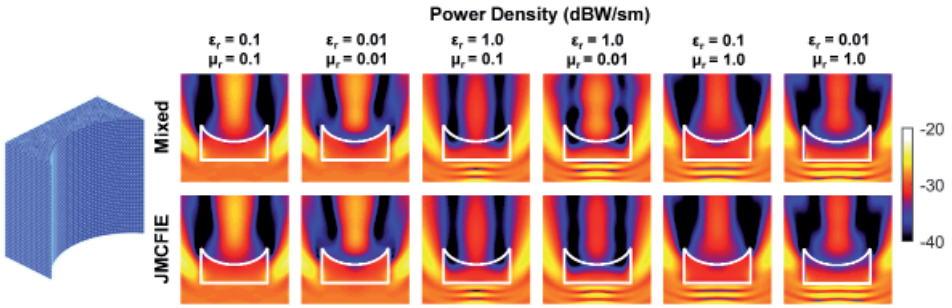

Figure 3. The results (power density) for Geometry 1 of SOLBOX-17 when the lens had various relative permittivity and relative permeability values.

Total time required to produce the results shown (categories: <1 sec, <10 sec, <1 min, <10 min, <1 hour, <10 hours, <1 day, <10 days, >10 days) <1 hour for the smaller problems, and <10 hours for the largest problem

3.2 Short Description of the Numerical Solutions

The problems listed in SOLBOX-17 were solved in the frequency domain by using surface-integral-equation formulations and a broadband MLFMA [7]. The structures were discretized with small triangles ($\lambda/20$ to $\lambda/10$ in size), while the Rao-Wilton-Glisson functions were employed to expand the equivalent electric and magnetic currents. For Geometries 1-6, the numbers of unknowns were 37,794, 22,674, 30,990, 35,052, 44,640, and 255,882, respectively. For numerical comparisons, two different formulations were used: the conventional electric-magnetic current combined-field integral equations (JMCFIE) [8, 9], and a novel mixed formulation that was developed particularly for NZI objects [10]. The structures were illuminated by linearly polarized plane waves that were normally incident on the structures' planar surfaces. The matrix equations that were constructed were iteratively solved using an un-preconditioned no-restart generalized minimal residual algorithm with 0.0001 target residual error. The required matrix-vector multiplications were performed with a broad implementation of MLFMA, based on the approximate diagonalization of the Green's function [7]. Specifically, given an NZI object, a single tree structure was constructed by recursively dividing the triangulated surface into sub-boxes. The outer far-zone interactions (related to the host medium, i.e., vacuum) were then performed via the conventional expansion based on plane waves [11], while the inner far-zone interactions were calculated by using scaled plane waves. In both (outer and inner) cases, far-zone interactions were computed with 1%-2% maximum error, whereas all inner interactions were computed with a maximum of 1% error. Once the expansion coefficients were found, the near-zone field-intensity and power-density distributions were obtained via radiation integrals. In addition to the comparisons of two formulations (JMCFIE and the mixed formulation), inner and outer plots were separately generated to demonstrate the accuracy of the results.

3.3 Results

Figure 2 presents the results for the first lens structure, involving a cylindrical extraction (1.25λ radius of curvature) from a $2\lambda \times \lambda \times 2\lambda$ slab. Both the relative permittivity and relative permeability of the structure were 0.1. The electric-field-intensity and the magnetic-field intensity distributions are given on the x-y plane (E-plane).

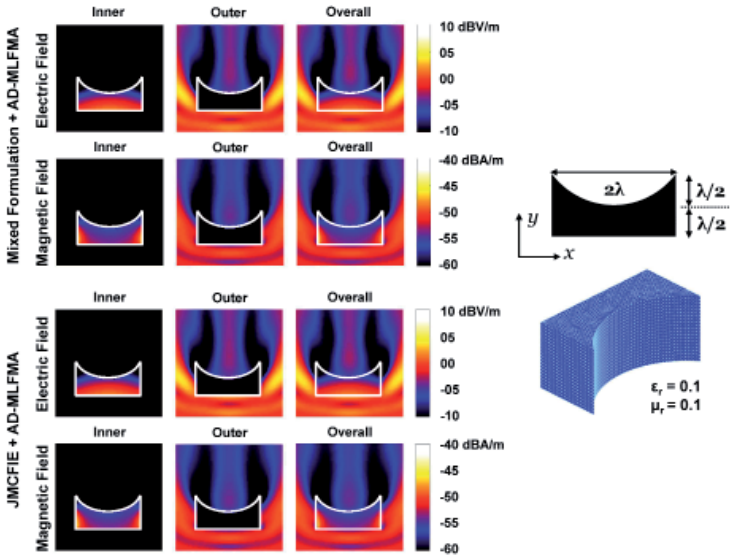

Figure 4. The results (electric-field intensity and magnetic-field intensity) for Geometry 2 of SOLBOX-17 when both relative permittivity and relative permeability of the lens were 0.1.

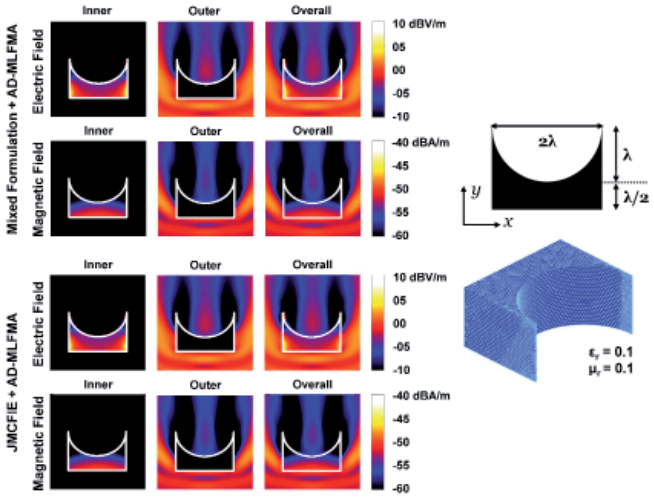

Figure 5. The results (electric-field intensity and magnetic-field intensity) for Geometry 3 of SOLBOX-17 when both relative permittivity and relative permeability of the lens were 0.1.

Inner and outer plots, in addition to their superposition (the overall plot), are included to verify the accuracy. According to the equivalence principle, the equivalent currents should not radiate outside the object for the inner problem (when the NZI material was assumed everywhere). Similarly, they should not radiate inside the object for the outer problem (when everywhere was vacuum). Therefore, after the equivalent currents were numerically found and used in the radiation integrals, vanishingly small fields outside/inside for the inner/outer problem demonstrated the reliability and accuracy of the solutions. In Figure 2, we also observed the consistency between the results obtained with the JMCFIE and the mixed formulation, which further verified the reliability of the results. Regarding the efficiency of the solutions, the JMCFIE required 143 iterations, while the solution of the mixed formulation was slightly faster with 120 iterations.

Figure 3 presents further results for the first lens geometry. The power density was plotted when different values were used for the relative permittivity and relative permeability. Specifically, in addition to cases when both relative permittivity and relative permeability were small (0.1 and 0.01), we considered four different cases when either of them was small but the other one was unity. When both constitutive parameters were 0.01, the number of iterations increased to 336 for the JMCFIE, while it was only 136 for the mixed formulation, which demonstrated its better stability. Despite that the results obtained with the JMCFIE and the mixed formulation were generally consistent, the differences in the fourth case (when the relative permeability was 0.01) were remarkable. This problem required 201 iterations with the JMCFIE and 123 iterations with the mixed formulation, which may be considered as another measure of the stability of the latter.

We next considered the solutions of the second lens structure (with 0.1 relative permittivity and 0.1 relative permeability), as presented in Figure 4. This structure was simply half of the first one, leading to a weaker focus in the electric- and magnetic-field intensity distributions. Good accuracy of the simulations could be verified by both inspecting the inner/outer plots and comparing the results obtained with the JMCFIE and the mixed formulation. In terms of efficiency, the two formulations led to similarly efficient simulations, i.e., the JMCFIE required 137 iterations, while the solution of the mixed formulation was slightly faster, with 111 iterations. Similar results for

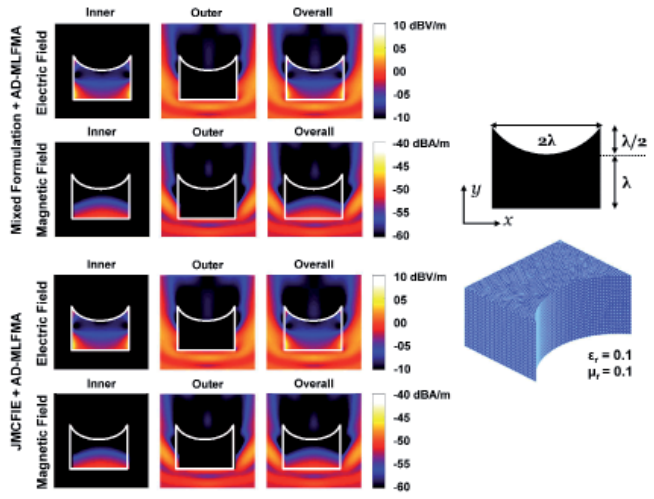

Figure 6. The results (electric-field intensity and magnetic-field intensity) for Geometry 4 of SOLBOX-17 when both relative permittivity and relative permeability of the lens were 0.1.

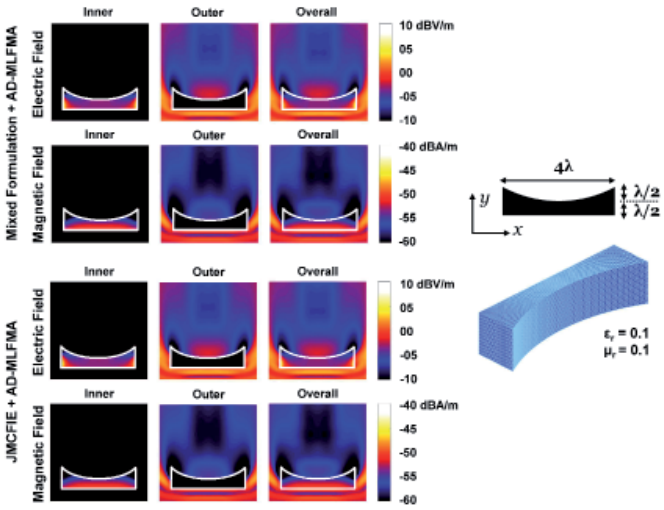

Figure 7. The results (electric-field intensity and magnetic-field intensity) for Geometry 5 of SOLBOX-17 when both relative permittivity and relative permeability of the lens were 0.1.

Geometry 3 are presented in Figure 5. This structure had a larger cross-sectional area and an extraction with a smaller radius of curvature, but its focusing ability was more or less similar to the focusing ability of Geometry 2. On the other hand, while they provided similar near-zone distributions, the mixed formulation led to significantly more efficient simulations, with 161 iterations compared to the JMCFIE, which required 364 iterations for this problem.

Geometry 4 (with 0.1 relative permittivity and 0.1 relative permeability) was a modified version of Geometry 3, where the radius of curvature was increased to 1.25λ . As shown in Figure 6, this lens structure did not possess any focusing ability. The results obtained with the JMCFIE and the mixed formulation were consistent with each other, requiring 143 and 123 iterations, respectively.

Geometry 5 differed from the previous structures, with its long and thin shape. Interestingly, again using 0.1 relative permittivity and 0.1 relative permeability, this structure had a visible focusing ability with relatively increased field-intensity values in the close vicinity of the curved surface, as shown in Figure 7. The number of iterations required to analyze this structure were 196 for the JMCFIE and 138 for the mixed formulation, respectively. To further investigate the geometry, Figure 8 depicts the electric-field-intensity distributions when the relative permittivity/permeability values were set to 0.01 and 0.001, in addition to 0.1. We observed that the results obtained with the JMCFIE and the mixed formulation slightly deviated for the case of 0.001, while the corresponding number of iterations were 799 for the JMCFIE and 175 for the mixed formulation, indicating the better stability (and perhaps accuracy) of the mixed formulation. In the case of 0.01, for which the JMCFIE and the mixed formulation were more consistent, the number of iterations was 480 for the JMCFIE and 171 for the mixed formulation.

Figure 9 presents a comparison of the five different lenses (when they had 0.1 relative permittivity and 0.1 relative permeability) in terms of the power-density distributions. Geometry 4 had the weakest focusing ability, leading to a deep shadow in the transmission region. Among the others, Geometry 1 created the strongest power-density values, while the short-distance focus of Geometry 5 was also remarkable.

Finally, Figure 10 depicts the results for the largest lens structure (Geometry 6), the relative permittivity and relative permeability values of which were both 0.1. The electric-field intensity, magnetic-field intensity, and power-density distributions in the vicinity of the lens structure

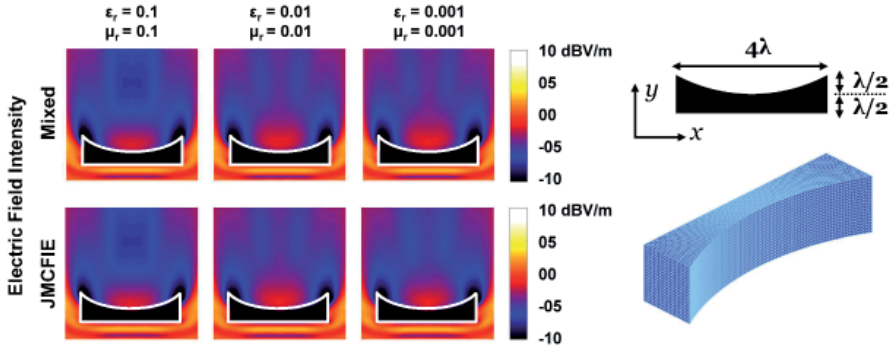

Figure 8. The results (electric-field intensity) for Geometry 5 of SOLBOX-17 when the lens had various relative permittivity and relative permeability values.

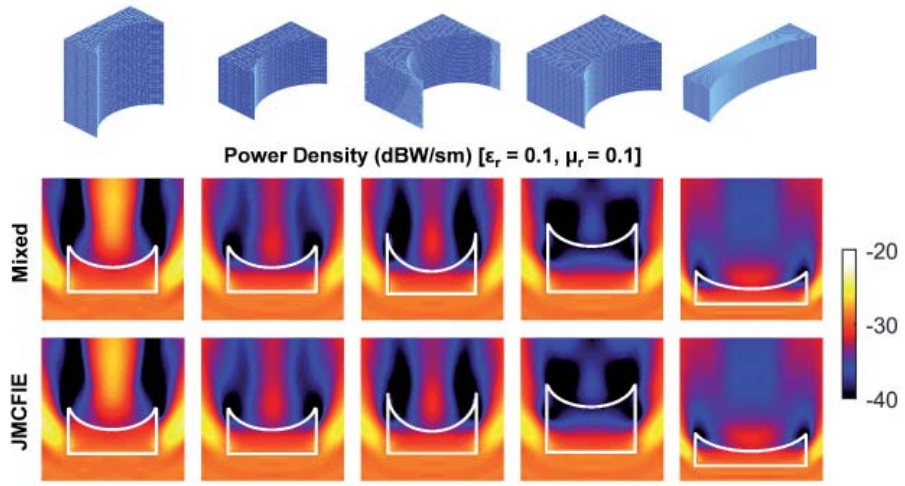

Figure 9. The results (power density) for Geometries 1-5 of SOLBOX-17 when both relative permittivity and relative permeability of the structures were 0.1.

are presented. With the increased size of the lens, the electromagnetic focusing became stronger with large field and power values at the focus point. We noted that this point corresponded to the center of the cylindrical extraction, i.e., since the index of the lens was very small, electromagnetic waves left the structure almost in the normal direction. For this largest problem, consistent results were obtained by using the JMCFIE and the mixed formulation, which required 262 and 186 iterations, respectively.

4. References

1. R. W. Ziolkowski, "Propagation in and Scattering from a Matched Metamaterial Having a Zero Index of Refraction," *Phys. Rev. E*, **70**, 046608, October 2004.

2. M. Silveirinha and N. Engheta, "Tunneling of Electromagnetic Energy Through Subwavelength Channels and Bends Using ε-Near-Zero Materials," *Phys. Rev. B*, **97**, 157403, October 2006.

3. B. Edwards, A. Alu, M. E. Young, M. Silveirinha, and N. Engheta, "Experimental Verification of Epsilon-Near-Zero Metamaterial Coupling and Energy Squeezing Using a Microwave Waveguide," *Phys. Rev. Lett.*, **100**, 033903, January 2008.

4. J. Luo and Y. Lai, "Anisotropic Zero-Index Waveguide with Arbitrary Shapes," *Sci. Rep.*, **4**, 5875, July 2014.

5. I. Liberal and N. Engheta, "Near-Zero Refractive Index Photonics," *Nat. Photon.*, **11**, March 2017, pp. 149-158.

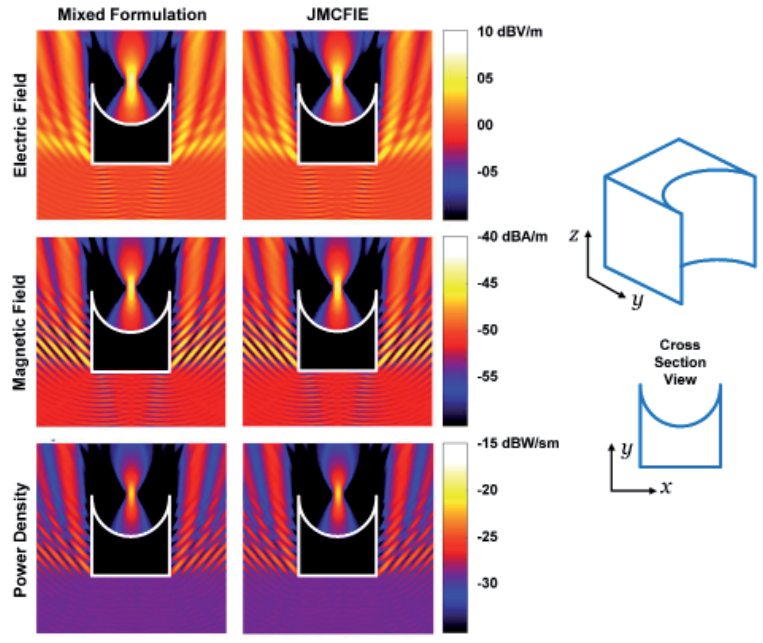

Figure 10. The results (electric-field intensity, magnetic-field intensity, and power density) for Geometry 6 of SOLBOX-17 when both relative permittivity and relative permeability of the lens were 0.1.

6. B. Karaosmanoğlu, U. Özmü, and Ö. Ergül, "Novel SIE Formulations for Accurate and Stable Analysis of Near-Zero-Index Materials," Proceedings of the IEEE International Symposium on Antennas and Propagation, 2019.

7. Ö. Ergül and B. Karaosmanoğlu, "Broadband Multilevel Fast Multipole Algorithm Based on an Approximate Diagonalization of the Green's Function," *IEEE Trans. Antennas Propagat.*, **63**, 7, July 2015, pp. 3035-3041.

8. P. Ylä-Oijala and M. Taskinen, "Application of Combined Field Integral Equation for Electromagnetic Scattering by Dielectric and Composite Objects," *IEEE Trans. Antennas Propagat.*, **53**, 3, March 2005, pp. 1168-1173.

9. Ö. Ergül and L. Gürel, "Comparison of Integral-Equation Formulations for the Fast and Accurate Solution of Scattering Problems Involving Dielectric Objects with the Multilevel Fast Multipole Algorithm," *IEEE Trans. Antennas Propagat.*, **57**, 1, January 2009, pp. 176-187.

10. H. İbili, Y. Koyaz, U. Özmü, B. Karaosmanoğlu, and Ö. Ergül, "Novel SIE Implementations for Efficient and Accurate Electromagnetic Simulations of Zero-Index Materials," Proceedings of Progress in Electromagnetics Research Symposium (PIERS), 2019.

11. Ö. Ergül and L. Gürel, *The Multilevel Fast Multipole Algorithm (MLFMA) for Solving Large-Scale Computational Electromagnetics Problems*, New York, Wiley-IEEE, 2014.

Randy L. Haupt
Colorado School of Mines
Brown Building 249
1510 Illinois Street, Golden, CO 80401 USA
Tel: +1 (303) 273 3721
E-mail: rhaupt@mines.edu

Amy J. Shockley
E-mail: aj4317@gmail.com

Our Bandwidth

A signal's bandwidth determines the amount of information it can carry and how fast the data transfers. Increasing bandwidth increases the amount of data that can be sent in a given period of time. We also have bandwidth, and our bandwidth determines how much we can effectively accomplish in a given period of time.

Our bandwidth is limited and the content perishable, meaning you cannot use the content in last week's bandwidth to accomplish this week's uncompleted tasks. We fill our bandwidth with work, professional activities, home, family, friends, and personal activities. Often, we want to dedicate large amounts of our time to a multitude of these activities, but our bandwidth limits what can actually be accomplished over a defined period of time.

The Planning Fallacy, conceptualized by Daniel Kahneman and Amos Tversky in 1979, describes the phenomenon in which people are overly optimistic about the amount of time required to complete a task (http://freakonomics.com/podcast/project-management-rebroadcast/). The original research on this matter studied honor students' abilities to estimate the amount of time required to complete their thesis. It was found that on average, the actual amount of time required was 164% of their estimate. When extrapolated to additional studies on stock brokers, electrical engineers, doctors, Christmas shopping, and tax submission, Kahneman and Tversky saw similar results of people drastically underestimating the time commitment required to complete the associated task. This tendency to underestimate the amount of time required to complete a task often results in people either failing to meet previously committed obligations or leaving tasks incomplete. The planning fallacy further explains that people are overly biased about their own abilities to complete tasks, and tend to disregard past experience when planning for the future.

People tend to be overly confident in their self-awareness, which leads to the Planning Fallacy. In order to appropriately plan within your bandwidth, it is important to first take an unbiased view on the amount of time required to meet your goals, whether personal or professional. It is also important to understand the number of prior commitments and urgent tasks, and how they will impact your ability to meet these defined goals. True self-awareness requires an honest evaluation of what you can accomplish, and, almost more importantly, what you cannot accomplish. This requires you to evaluate tasks and goals based on true capacity planning, rather than a simple ranking of competing priorities.

We can learn to increase our bandwidth through techniques such as multitasking and leveraging efficiencies. For instance, tomorrow, I will multitask by riding my bike to a medical appointment instead of driving my car. Although biking takes longer, because I have already prioritized exercising, I will be able to go to my medical appointment and exercise in less time than it would take to drive to my appointment and then work out separately. I eliminated the unnecessary component, driving, without much impact. However, this approach is not always effective. For instance, if your spouse wants to have a nice dinner with you, but you try to multitask by constantly checking your e-mail on your smartphone, you will likely be ineffective at both tasks. Dinner probably won't go well, because you will not be mentally present and your spouse will not get the quality time that they were seeking. In addition, you might feel stressed about your phone interactions and make mistakes when drafting e-mails (if you want a good laugh, Google autocorrect mistakes).

In order to effectively prioritize your tasks and goals, you must first honestly evaluate the amount of time required for you to complete these tasks, and so understand your bandwidth.

Historical Corner Column

Giuseppe Pelosi
Department of Information Engineering
University of Florence
Via di S. Marta, 3, 50139 Florence, Italy
E-mail: giuseppe.pelosi@unifi.it

Foreword

HISTELCON (HISTory of ELectrotechnology CONference) is a flagship biennial conference of IEEE Region 8. Its sixth edition just took place, organized by the IEEE UK and Ireland Sections, in Glasgow, Scotland, September 18-19, 2019 (Figure 1).

This was not only the occasion to meet many IEEE members active in historical research (Figure 2), starting from the General Chair, Anthony Davies (emeritus professor, King's College, London), but also to visit two – well, three – of the key places in the life of James Clerk Maxwell. The first was his birthplace in Edinburgh, 14 India Street. The second was his ancestral home of Glenlair, Scotland, a paradisal estate south of Edinburgh. The third was his tomb, in Parton, close to his beloved Glenlair. This paper is a short personal account of our visit to these places.

On such an occasion we also offered to host HISTELCON 2023 in Florence, Italy. Florence is actually the very only city outside Great Britain that Maxwell ever wanted to visit, in his only journey abroad (spring and early summer 1867 [1, pp. 324-325], so the links among Scotland, Italy, and Florence, are strong.

Figure 1. Glasgow City Chambers as seen from George Square.

Figure 2. The HISTELCON2019 group photo on the incredible marble and alabaster spiral stair of Glasgow City Chambers: (front row, l-r) Rod Muttram (IEEE UK&I LMAG committee); Magdalena Salazar-Palma (IEEE R8 Director, Madrid, Spain); Rochelle and Anthony Davies (HISTELCON2019 conference Chair); Dr. Martin Bartos (with gold Chain of Office, Bailie of the City of Glasgow, who welcomed participants); (slightly behind him) Dr. Gene Frantz (invited speaker, ex Texas Instruments, now Rice University, Houston, Texas, USA); (just above Bartos and Frantz) Mike Geselowitz (IEEE History Center Director, New Jersey, USA); (left end, just above Rod Mutram) Peter Nagy (IEEE R8 Conference Committee Chair, Hungary), plus many others, the authors of this paper included, of course.

Reference

1. L. Campbell, W. Garnett, *The Life of James Clerk Maxwell*, Mc Millan, London, 1882.

A Scottish Trail from Edinburgh to Glenlair: James Clerk Maxwell's Houses

Giuseppe Pelosi and Stefano Selleri

Department of Information Engineering
University of Florence
Via di S. Marta, 3, I-30139, Florence, Italy
E-mails: giuseppe.pelosi@unifi.it; stefano.selleri@unifi.it

At the imminent birth of James, his father, lawyer John Clerk Maxwell (1790-1856), and the not-very-young mother, Frances Cay (1792-1839), left the country residence of Glenlair, built by John to live comfortably with his wife, to go to Edinburgh to be in the city and close to any assistance with the birth. In that same 1831, once James was safely born, the family hastily left the severe house on India Street and settled permanently in Glenlair (Figure 1).

The house on India Street is now the seat of the James Clerk Maxwell Foundation, restored and turned into a museum. We were introduced there by Peter Grant, Professor at the University of Edinburgh and Secretary of the Trust. Among the many memorabilia on show at the Foundation, two caught our attention: the Volta Medal (Figure 2a), awarded to J. C. Maxwell in 1878 [1], and Maxwell's handwritten poem, "Scots Academie"

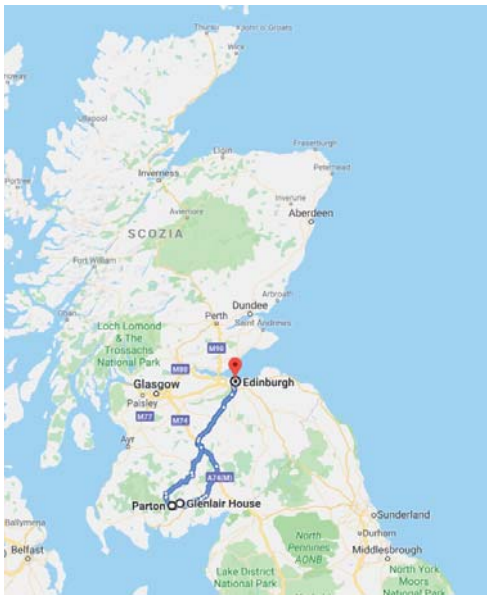

Figure 1. The "Scottish trail" from Edinburgh to Glenlair, Parton, and back to Edinburgh, on modern routes (Google Map).

Figure 2a. One of the many memorabilia preserved at the Foundation on India Street: Volta's medal awarded to Maxwell by the University of Pavia [1] (photo by the authors).

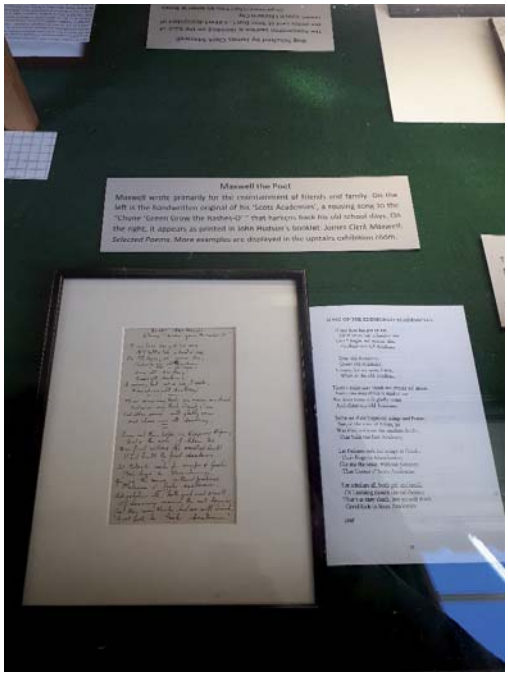

Figure 2b. One of the many memorabilia preserved at the Foundation on India Street: a handwritten poem by Maxwell of "academic" theme [2] (photo by the authors).

Figure 3a. Capt. Duncan Ferguson, owner and keeper of the house, with his dog (photo by the authors).

(Figure 2b). Maxwell's fondness for poetry is not well known [2].

J. C. Maxwell was forced back to Edinburgh to study after the death of his mother, where he lived with his aunt alone at 14 India Street (1842-1849). He later was in Cambridge (1850-1855), Aberdeen (1856-1859), London (King's College, 1860-1864), Glenlair (1865-1870), and again Cambridge (1871-1879). Summing up the youth and mature years, the single place where he yet lived longer was Glenlair.

Figure 3b. Glenlair always had dogs, and J. C. Maxwell was so fond of dogs that his Toby was even reproduced at his feet in the statue dedicated to him in Edinburgh [6] (photo by the authors).

Indeed, in the spring of 1865, Maxwell suddenly resigned from King's College, declaring that he wanted to intensify, avoiding the hindrance of academic commitments, research, and study. In Glenlair, he could finally resume his life, his contact with nature, with his beloved animals, with the open air. The scientific activity continued with important publications. Glenlair holds a record that would be worth placing it in a dominant position in the history of modern thought. Between those walls, respectively in 1871 and 1873, Maxwell's most important works would be born: *Theory of Heat* and *A Treatise of Electricity and Magnetism*.

In those happy years of stay at Glenlair, Maxwell dedicated himself at the same time to making improvements to his estate. With his brother-in-law, he even built a stone bridge over a stream: a bridge that exists today. In addition, restoration and expansion of the paternal home began. In 1867, while the works were in progress on the house, Maxwell made the only journey of his life: a journey that

Figure 4. The restored Glenlair house: the part built by J. C. Maxwell with the large windows in the foreground; on the left, the older part of the house, where he had his studio (photo by the authors).

Figure 5. The tiny, roofless chapel in the graveyard of Parton church where J. C. Maxwell, his wife, and his parents were buried (photo by the authors).

in the spring and summer of that year took him to Italy [3, 4]. He visited Tuscany and Florence, meeting some Italian researchers, most notably Felice Matteucci (1808-1887). Maxwell actually learned Italian mainly to be able to talk with him [4].

Nowadays, driving from Edinburgh to Glenlair takes about two and one-half hours among Scotland's green rolling hills, but it must have been taken two days or more in the mid-19th century. As it is well known, the house caught fire twice (1899 and 1929) [5], and collapsed. It is now owned by Capt. Duncan Ferguson, who created a trust to restore it, and in particular the portion of the building constructed by J. C. Maxwell (Figures 3 and 4).

However, Maxwell's stay in Glenlair was interrupted in 1871. In the context of the renewal of English science, he became the first Professor of Experimental Physics at Cambridge, and the first Director of the Cavendish Laboratory. However, his journey on this Earth soon came to an end. The first symptoms of the disease manifested themselves in June 1877, after which they rapidly proceeded. In June 1879, now prostrate, James left Cambridge and returned definitively to Glenlair, where he died on November 5.

James Clerk Maxwell is not buried among the Great Ones. Anonymously and quietly, as his life had always been, his remains were received in the small cemetery of the small church of Parton, near his beloved Glenlair, among his valleys (Figure 5).

References

1. V. Cantoni and A. P. Morando, "Pavia, April 28-29, 1878: Volta Anniversary and Honorary Degree for Maxwell," *IEEE Antennas and Propagation Magazine*, **53**, 1, February 2011, pp. 205-210.

2. O. M. Bucci, G. Pelosi, and S. Selleri, "James Clerk Maxwell, the Poet," *IEEE Antennas and Propagation Magazine*, **61**, 2, April 2019, pp. 128-133.

3. L. Campbell and W. Garnett, *The Life of James Clerk Maxwell*, London, Mc Millan, 1882, pp. 324-325.

4. G. Pelosi "A Tribute to James Clerk Maxwell on the 150th Anniversary of His Equations (1864–2014)," *IEEE Antennas and Propagation Magazine*, **56**, 6, December 2014, pp. 295-316.

5. J. C. Rautio, "Fire! Fire! Fire! [fire that destroyed the James Clerk Maxwell home]," *IEEE Microwave Magazine*, **14**, 4, June 2013, pp. 140-150.

6. J. C. Rautio, "Toby's Statue," *IEEE Microwave Magazine*, **10**, 4, June 2009, pp. 48-60.

History of Ionospheric Radars

The international open-access journal *History of Geo- and Space Sciences* (*HGSS*) provides, among other contributions, a permanent special issue, "History of Ionospheric Radars." The articles in this special issue may be of interest for readers of the *Radio Science Bulletin*. The articles can be downloaded free of charge from
https://www.hist-geo-space-sci.net/special_issue6.html

Recently published articles (after peer review by two referees) are:

"The Early History of the Jicamarca Radio Observatory and the Incoherent Scatter Technique"
Ronald F. Woodman, Donald T. Farley, Ben B. Balsley, and Marco A. Milla

"Irkutsk Incoherent Scatter Radar: History, Present and Future"
Andrey V. Medvedev and Alexander P. Potekhin

"History of the Juliusruh Ionospheric Observatory on Rügen"
J. Weiß

"The STARE/SABRE Story"
E. Nielsen and W. Schmidt

"A Short History of Geophysical Radar at Arecibo Observatory"
J. D. Mathews

"History of the Development of IS Radars and Founding of the Institute of Ionosphere in Ukraine"
L. Ya. Emelyanov and T. G. Zhivolup

HGSS is free of charge for authors as well, and is indexed by various agencies.

Kristian Schlegel
HGSS Managing Editor
E-mail: kristian.schlegel@copernicus.org

James C. Lin
University of Illinois at Chicago
851 South Morgan Street, M/C 154
Chicago, IL 60607-7053 USA
E-mail: lin@uic.edu

What Must Not Be Neglected Are Overall Cancer Rates in Chronic Effects in NTP's Lifelong RF Exposure Study

Understandably, most accounts of the US National Toxicology Program's (NTP's) final report have focused on the statistically significant finding of "clear evidence" that both GSM- and CDMA-modulated 900 MHz wireless radio-frequency (RF) radiation led to the development of malignant schwannoma, a rare form of tumor in the heart of male rats. Moreover, unusual patterns of cardiomyopathy, or damage to heart tissue, were observed in both RF-exposed male and female Sprague-Dawley rats compared with concurrent control animals, although the findings for female rats were deemed as providing only uncertain or "equivocal" evidence for schwannomas and malignant gliomas, compared to concurrent controls [1, 2].

However, the results also included the pathology findings showing positive indications or "some evidence" of carcinogenic activity in the brain of male rats, specifically glioma. (The designation of "some evidence" for carcinogenicity was based on NTP's classification of the strength of observed evidence in their report). It is significant to note the National Institute of Environmental Health Sciences/National Toxicology Program's (NIEHS/NTP's) statements, "We believe that the link between RF radiation and tumors in male rats is real, and the external experts agreed" [3].

Indeed, the study also concluded that there were positive findings of carcinogenicity in the adrenal gland. The number of pheochromocytomas, a tumor of the adrenal gland, was significantly higher in male rats at 1.5 W/kg and 3 W/kg of specific absorption rates (SAR), compared to the concurrent controls. Furthermore, the increase in malignant tumor-like hyperplasia in the adrenal gland of female rats was significantly higher at 6.0 W/kg, relative to the concurrent controls.

The myriad of carcinogenic observations of the NTP study is prompting questions about the total primary cancer occurrences in these chronically exposed animals.

In all fairness, the primary cancer or overall cancer rates detected in any organ or tissue inside the animal's body do not appear to have been purposefully overlooked or unnoticed. Indeed, the results for total primary cancer or tumor occurrences in NTP study animals can be found in the appendices of their final reports [1]. However, while the data may not have been purposefully disregarded or ignored, the NTP did not include them in any of their publicized report summaries. An independent analysis of the data showed that rats exposed to GSM and CDMA RF radiation had significantly higher overall or total primary tumor rates than the concurrent controls [4]. In particular, the highest overall cancer (or malignant tumors) rates were found in male rats exposed to whole-body SARs of 3 W/kg from 900 MHz mobile-phone RF radiation (42% for GSM; 46% for CDMA), and the lowest rate was found in the concurrent control group (27%). The RF-exposed groups thus had significantly higher overall or total primary cancer rates than the concurrent control rats.

What's more, the highest overall tumor (either a benign or malignant tumor in any organ or tissue) rates were observed in male rats exposed to SARs of 3 W/kg (87% for GSM; 84% for CDMA) mobile-phone RF radiation. Again, the lowest rate was seen in the concurrent control group (63%). The RF-exposed groups had significantly higher overall tumor rates than the concurrent controls. Additionally, male rats in the lowest RF exposure groups (whole-body SARs of 1.5 W/kg) had significantly higher rates of benign primary tumors (76% for GSM; 73% for CDMA) than the concurrent or sham control group (54%).

Many laboratory-rat cancer studies have been conducted and reported during the past quarter century in an attempt to assess the possible health risks of microwave and RF radiation from wireless communication devices and systems [5]. To date, not including the NTP investigation mentioned above, there are six published studies on carcinogenic potentials of two-year or lifelong exposure of Sprague-Dawley rats to RF and microwave radiation.

Some of these investigations involved the use of co-carcinogens to evaluate the potential of mobile-phone RF radiation, especially with regard to induction and promotion of neural and mammary tumors. In one study, rats were injected with a known neural carcinogen, Ethylnitrosourea (ENU), followed by exposure to 860 MHz RF to evaluate any increases in brain-tumor induction. In four papers, the promotion of 900 MHz RF radiation was tested using dimethylbenzanthracene (DMBA)-induced mammary tumors in female Sprague-Dawley rats.

Only one of the six earlier research studies involving Sprague-Dawley rats was designed to study the health effects of lifelong exposure to pulsed microwave radiation. Beginning at eight weeks of age and continuing daily for 21.5 h/day, male Sprague-Dawley rats (100 each for exposure and sham control) were individually irradiated in circularly-polarized waveguide exposure chambers for up to 25 months [6]. Pulsed 2,450 MHz microwave power, modulated at 8 Hz and pulsed at 800 pps and delivered at 0.144 W to the exposure chamber, produced 0.15 W/kg to 0.4 W/kg of whole-body-averaged SARs. A statistically significant increase was observed in primary cancers at death: 18 in exposed rats versus 5 in sham-exposed control, or 18% and 5%, respectively. A near-fourfold increase of primary cancers in the exposed animals is provocative. The biological significance of this difference was questioned at the time; however, these data cannot be considered as an artifact because different statistical analyses led to similar results. The fact remains that the total primary cancer or overall cancer rate was significantly elevated in the RF-exposed group.

Both the most-recent 900-MHz reverberation chamber and the earlier 2,450-MHz circular-waveguide systems provided near-zone whole-body exposure conditions. In fact, these are the only two available RF and microwave exposure studies employing the Sprague-Dawley strain of rats but without the use of any cancer-promotion agents (or co-carcinogens). Despite the methodological differences, both investigations showed consistent results in significantly increased total primary cancer or overall tumor rates for exposure to whole-body SARs of 1.5 W/kg, 3.0 W/kg, and 6.0 W/kg in one case, and 0.15 W/kg and 0.4 W/kg in the other.

What makes these two RF and microwave radiation animal cancer studies so valuable are the good laboratory practice with which the studies were conducted, and the remarkable consistency of the total primary or overall cancer findings.

Some words are in order to place the SARs in proper perspective.

The SARs are accepted metrics or measures that correspond to the relative amount of RF and microwave power deposition or energy absorption rate in a part of or a whole body, such as any part of a user of a wireless device or mobile-phone handset, or the entire body in the radiation domain of a Wi-Fi antenna or base station. In the United States, the RF and microwave exposure rules established by the Federal Communications Commission (FCC) are based on SAR and maximum permissible exposure (MPE) limits [7]. The basic restrictions for human exposure are defined by SAR limits. MPE limits are derived from the SAR limits in terms of free-space field strength and power density.

For exposures from mobile phones, the FCC specifies a quantity of local-tissue SAR of 1.6 W/kg as determined in any one gram (1 g) of body tissue. A value of 0.08 W/kg in any one gram of body tissue was also set for whole-body exposures.

The FCC rules impose basic restrictions on SAR limits for general public and occupational exposures to avoid whole-body heat stress and excessive localized tissue heating, specifically to prevent biological and health effects in response to an induced body temperature rise of 1°C or more for an averaging time of 6 min [7, 8]. This level of temperature increase results from exposure of individuals under moderate environmental conditions to a whole-body SAR of approximately 4 W/kg for about 30 min. A whole-body average SAR of 0.4 W/kg was chosen as the restriction to provide protection for occupational exposure. An additional reduction factor of five was introduced for public exposure, giving an average whole-body SAR limit of 0.08 W/kg. This value was purposefully relaxed by a factor of 20 to permit a maximum local tissue SAR of 1.6 W/kg.

It is noteworthy that the then-recognized protection afforded by the whole-body SAR of 4.0 W/kg is in the midst or within the same range of 1.5 W/kg, 3.0 W/kg, and 6.0 W/kg NTP-study SARs. Furthermore, these SARs did not raise body temperature of exposed rats to more than 1ºC. For the earlier 2,450 MHz study at lower whole-body SARs of 0.15 W/kg and 0.4 W/kg, a body-temperature elevation

was also not reported in the exposed rats. Nevertheless, both experimental studies revealed consistent results in significantly increased total primary cancer or overall tumor rates.

Another point that should be noted with regard to SAR is that the NTP study report indicated that an RF-field uniformity within 10% was achieved throughout the reverberation exposure chamber. This level of field uniformity enabled similar SAR values throughout the rats' bodies. Specifically, the local SARs in the brains and hearts of rats were a mere 1.05 and 2.27 times the whole-body-average SAR, respectively. This also means that tissues and organs inside the rat's body had experienced similar SARs from the RF exposures.

The International Agency for Research on Cancer (IARC) assessed the then-available scientific literature and concluded that epidemiological studies on humans reporting increased risks for malignant gliomas and acoustic neuromas among heavy or long-term users of mobile phones are sufficiently strong to support a classification of 2B: possibly carcinogenic to humans [9]. In classifying RF radiation as a 2B carcinogen, while doing so, IARC had suggested that it also believed the available scientific evidence was incomplete and limited, especially with regard to results from animal experiments.

The time is right for IARC to upgrade its previous epidemiology-based classification of RF exposure to higher levels of classification for the carcinogenicity of RF radiation to humans. Now two relatively well-conducted RF and microwave exposure studies employing the Sprague-Dawley strain of rats, but without the use of any cancer- promotion agents (or co-carcinogens), have shown consistent results in significantly increased total primary cancer or overall tumor rates in animals exposed to RF radiation.

Post Scripts

In August 2018, the Cesare Maltoni Cancer Research Center of the Ramazzini Institute in Italy published its final results from their comprehensive study on carcinogenicity in Sprague-Dawley rats exposed - lifelong or prenatal until death - to 1,800 MHz GSM RF radiation [10]. It involved whole-body exposure of 2,448 male and female rats under plane-wave equivalent or far-zone exposure conditions, with incident electric-field strengths of 5 V/m, 25 V/m, and 50 V/m (the frequency-dependent maximum allowable value was approximately 61 V/m [11]). The author estimated that the whole-body SARs were about 0.001 W/kg, 0.03 W/kg, and 0.1 W/kg during exposures of 19 h/day for about two years. Assuming a differential factor of 20 between the average whole-body SAR and the local-tissue SAR as was done in setting safety guidelines, the corresponding local-tissue SARs could be 0.02 W/kg, 0.6 W/kg, and 2.0 W/kg in this case.

A total primary or overall cancer rate was not reported in this paper (it is not certain if this might be part of the study protocol). However, a statistically significant increase in the rate of schwannomas in the hearts of male rats was detected for the highest RF field strength (50 V/m). Moreover, an increase in the rate of heart Schwann-cell hyperplasia was observed in both exposed male and female rats at the highest RF field strength (50 V/m), although this was not statistically significant. An increase in the rate of gliomas was observed in exposed female rats at the highest field strength (50 V/m), but was not deemed as statistically significant.

It is important to note that the recent NTP and Ramazzini animal RF exposure studies presented similar findings in heart schwannomas and brain gliomas. The increased schwannomas and abnormal heart tissue development or damage to heart tissue are significant findings in RF-exposed animal research studies.

There is more. The incidence of benign pheochromocytomas of the adrenal medulla was found to be higher in the exposed group than in the sham controls for the 2,450 MHz circular waveguide experiment [6]. It is interesting to note that there was "some evidence" for carcinogenicity in the adrenal gland in the recent NTP study. The number of pheochromocytomas was significantly higher ($p < 0.05$) in male rats at 1.5 W/kg and 3 W/kg, compared with the concurrent controls. The increase in malignant tumor-like hyperplasia in the adrenal gland of female rats was also significantly higher at 6.0 W/kg, relative to the concurrent controls ($p < 0.05$).

A perspective to especially keep in mind is that with the induction of cancer by a carcinogen, an agent is typically considered carcinogenic if it induces a significant response in a specific tissue.

References

1. NTP, *Technical Report on the Toxicology and Carcinogenesis Studies in HSD: Sprague Dawley SD Rats Exposed to Whole-Body Radio Frequency Radiation at a Frequency (900 MHz) and Modulations (GSM and CDMA) Used by Cell Phones*, National Toxicology Program, Research Triangle Park, NC 27709, NTP TR 595, National Institutes of Health, Public Health Service, US Department of Health and Human Services, November 2018.

2. J. C. Lin, "Clear Evidence of Cell Phone RF Radiation Cancer Risk," *IEEE Microwave Magazine*, **19**, 6, September 2018, pp. 16-24.

3. NIEHS, "High Exposure to Radio Frequency Radiation Associated with Cancer in Male Rats," https://www.niehs.nih.gov/news/newsroom/releases/2018/november1/index.cfm, accessed on November 1, 2018.

4. J. Moskowitz, "National Toxicology Program Publishes Final Cell Phone Radiation Study Reports," *Electromagnetic Radiation Safety*, November 1, 2018.

5. J. C. Lin, "Cancer Occurrences in Laboratory Rats from Exposure to RF and Microwave Radiation," *IEEE Journal of Electromagnetics, RF and Microwaves in Medicine and Biology (J-ERM)*, **1**, 1, June 2017, pp. 2-13.

6. C. K. Chou, A. W. Guy, L. L. Kunz, R. B. Johnson, J. J. Crowley, and J. H. Krupp, "Long Term, Low-Level Microwave Irradiation of Rats," *Bioelectromagnetics*, **13**, 1992, pp. 469-496.

7. FCC, "Wireless Devices and Health Concerns," https://www.fcc.gov/consumers/guides/wireless-devices-and-health-concerns, accessed on February 21, 2019.

8. FCC, "Evaluating Compliance with FCC Guidelines for Human Exposure to Radio frequency Electromagnetic Fields," https://www.fcc.gov/general/oet-bulletins-line#65, accessed on July 8, 2019.

9. IARC Working Group on the Evaluation of Carcinogenic Risks to Humans, "Non-Ionizing Radiation, Part 2: Radiofrequency Electromagnetic Fields," *IARC Monographs on the Evaluation of Carcinogenic Risks to Humans*, **102**, Pt 2, 2013, pp 1-460.

10. L. Falcioni, L, Bua, E. Tibaldi, M. Lauriola, L. De Angelis, F. Gnudi, D. Mandrioli, M. Manservigi, I. Manzoli, I. Menghetti, R. Montella, S. Panzacchi, S. Sgargi, V. Strollo, A. Vornoli, and F. Belpoggi, "Report of Final Results Regarding Brain and Heart Tumors in Sprague-Dawley Rats Exposed From Prenatal Life Until Natural Death to Mobile Phone Radiofrequency Field Representative of a 1.8 GHz GSM Base Station Environmental Emission," Environ Research, 165, August 2018, pp. 496-503.

11. ICNIRP, "Guidelines for Limiting Exposure to Time-Varying Electric, Magnetic, and Electromagnetic Fields (Up to 300 GHz)," *Health Physics*, **74**, 1998, pp. 494-522.

Women in Radio Science

Asta Pellinen-Wannberg
Umeå University, Department of Physics and
Swedish Institute of Space Physics
S-90187 Umeå, Sweden
Tel: +46 90 786 7492
E-mail: asta.pellinen-wannberg@umu.se

Introducing the Author

In this issue, I present Rowayda Sadek, Professor of Networking Engineering, Security and Signal Processing at the Helwan University in Egypt. It is extremely interesting to get a view of how it is to work as a female scientist in an Arab country. Rowayda was already a brilliant student in school and had a strong family background to act as a pioneer female scientist in her country. She has inspired many young female students to follow her way into science and technology. Here, she describes the challenges for women in the Middle East, which appear quite different from the earlier stories in this column, but there are several similarities, as well.

Rowayda was born in Cairo, Egypt. She grew up in many cities: Aswan, Cairo, Mansoura, Alexandria, all in Egypt. She graduated from the Alexandria University, where she also received her PhD in Electrical Engineering-Communication and Electronics. She has worked for many reputable universities: Fayoum, Helwan, AASTMT, and Beni Suef. She was the initiator and the first head of the Information Technology Department in Helwan University. She is currently the Vice Dean of Student Affairs of the Faculty of Computers and Information at Beni Suef University, Upper Egypt. She teaches undergraduate and postgraduate courses within her faculty, supervises BSc, MSc, and PhD theses, and has acted as a reviewer for several MSc and PhD theses.

Rowayda is the General Secretary of the National URSI Committee of Radio Science in Egypt, and the General Secretary of the annual conference, NRSC, with 36 successful rounds so far. She is a member of the IEEE, and she has been a referee for international conferences and journals. Rowayda's research interests are communication and wireless networks, signal processing, security and artificial intelligence.

Rowayda has published over 70 papers in national and international journals and conferences. She has supervised more than 30 MSc and PhD theses. She has participated in many projects and workshops in several countries: Canada, Sweden, Denmark, France, Greece, etc. She has also been an industrial employee as an engineer, team leader, project manager, and consultant in communication developments in SCADA systems in AEDC Egypt, CAE Montreal Canada, EPS Egypt, and SNC Lavalin, Canada.

Reflections on a Career in Radio Science in Egypt

Rowayda A. Sadek

General Secretary of URSI-NRSC
FCAI, Helwan University and
Beni Suef University, Egypt
E-mail: rowayda_sadek@fcih.helwan.edu.eg, rowayda_sadek@yahoo.com

When I was asked to write this article, I wondered from where I should start. I thought to focus on describing the different disciplines in which I have been working within industry and academia. However, I was also eager to highlight the situation of women scientists in Egypt, in the Arab world, the Middle East, and Africa, since I assume that it is not so well known. I prefer to narrate my story to emphasize the phases of my life, starting with my early childhood, then going to depict the success I gained, the challenges and defiance that I faced during my professional career, which could be specific to my geographical region or global for women scientists all over the world. I hope to shed light on the respected role of women in both industry and academia, and to also explain the family role in every woman's life that isn't given enough attention.

Having a female scientist in a girl's surroundings in her early and teen years inspires her to become a scientist. I am confident to know that my story may leave a legacy for the future generations and serve to encourage other women from diverse backgrounds to believe in themselves, and to pursue their dreams with passion despite any challenges they face. You may literally change the world if you start by yourself and also become a role model, even if for only one person. I'm just a tiny droplet in the notable African, Arab, and Egyptian ocean of women scientists.

I therefore want to enlighten the reader regarding my life's phases, the success I gained and the difficulties I faced, and I want to recognize those who had influence in the different phases. Besides the family responsibilities, marriage and childbirth, I got my MSc, and PhD and worked in industry and academia. Although this caused some delays in my career, I extremely enjoyed those memorable happy years. Receiving more recognition for the extensive effort carried out by Arab female scientists in the Middle-East region is quite recent.

Figure 1. Young scientists in a discussion meeting.

Childhood Development and Engineering Lifestyle

I was happy to be born in a supportive environment, into a family that highly appreciated education and knowledge. "Engineering is a life style" was the main theme of my family life: how to analyze, how to think, how to wonder. I used to ask about the reasons behind each and every thing. My family was always ready to respond, either with answers or with books. My dear father (now deceased), who inspired me, was an extraordinary engineer. My beloved mother, who affected my personality, was a compassionate business teacher. My older brother, who had a real impact on me to be determined in facing any challenge, is a histopathologist. My lovely younger sister, who is more a daughter than a sister for me, is a sociologist, and became a stay-at-home mother, due to a lack of appropriate working opportunities.

In my early years at school, I preferred studying mathematical-related subjects. In our community, an engineering career was the dream for every child who liked mathematics. I have a distinctive school memory of the mathematics. I was in a girls' school in the special class for superior pupils. My mathematics teacher used to give us a challenge quiz. The first girl who finished and submitted a correct answer received a full mark. The quiz had a geometry problem, for which I quickly provided an irregular solution. My teacher was amazed by my submission of a prompt answer, without hesitation. I used to enjoy mathematics, not just studying it. My teacher discussed my proof and announced me to be the winner. However, he told me "you have the ability to use every piece of data you own to solve the problems; you should carry on for engineering or scientific career." He then laughed and added, "you might go to political and diplomatic career for your talent and self-confidence to propose a new irregular solution within a too limited time constraint!"

From my early years, I was always considered remarkable and well-mannered among my peers. Even though high performance and good grades are important, the main principles that should be taught to our children are how to be authentic, respected, and happy people.

Science and Engineering is Challenging for a Female

Engineering and science careers are considered hard, demanding, and especially taxing for girls in our Middle Eastern region, due to the insufficiency in gender equity and the deficiency of support from the surrounding environment. My father knew about these obstacles. He faced many hardships during his career as an engineer in the High Dam construction, rescuing the Abu Simbel Temple, until finally becoming Vice President of the Electricity Distribution Company. He wanted my brother to become an engineer, while he disbelieved what I could gain as a woman in such a male-dominated profession in the Middle Eastern region. However, he democratically left me to choose my own path. I was upset, because I considered that as mistrust in my ability to face and bear the difficulties of making a difference in this career. I chose to face the challenges, and I never regretted my decision of becoming a communication and electronics engineer.

During my BSc studies in electronics and communication engineering, I preferred electronics over communication. This was until my first real exposure to radio science in my graduation project in spread spectrum, which was supervised by Prof. Said El Khamy, and it came to influence my whole career. Later, in parallel with my MSc research, I chose to proceed with an industrial job as a SCADA communication engineer. Completing my MSc and PhD took me a little longer, due to being busy with marriage and having a child in addition to my industrial job. A woman's husband literally is either positively helping or negatively draining her energy. I was fortunate to get married to an amazing husband: Mohamed Hendy. He is also a talented computer engineer. He enjoys engineering as a leisure activity more than as a career. He therefore always encourages me and gives all kinds of physical and moral support to my career. He shares the responsibilities at home, in life, and in raising our daughter. Our exquisite daughter, Salma, was born during my PhD, an exacting but enjoyable period. I'm also blessed and proud to have a super awesome and strong daughter, who just successfully finished her senior year. She is also going to the faculty of engineering electronics and communication department. My story with engineering never ends!

I enjoyed concurrently gaining various experiences, such as research, industry, and family life. Although getting married and having a child is always the toughest period in a women's life with a career, I extremely enjoyed those memorable years that provided me a chance to explore mixed feelings: love, exhaustion, fear, guilt, failure, and meaningful success in every milestone of the child. This is usually reflected in the depth of a women's personality that in turn affects her career. This inspired me to focus more on a wider impact to influence and support young scientists, engineers, researchers, and academic colleagues. In my case, the absence of being in touch with a woman-scientist role model led me to create my own, by borrowing the successful features from exemplar men: my father at the start, later my brother, then my supervisor, and finally my husband.

Many life cycles could be lived in the same time span. Joseph Pettinicchio, an Italian SCADA integration specialist, was the first person who portrayed me as being able to do twice as much as others. Throughout my life, my professors, colleagues, and bosses used to depict me as an energetic and active person. That may be the reason I always appeared younger than my age.

Figure 2. The NRSC committee at the 36th National Radio Science Conference, NRSC2019, Cairo, Egypt.

My Diverse Professional Career

My professional life was very diverse and fantastic. It provided me many chances at a wide range of professions and specialties that extremely elevated my experiences in career aspects as well as personality aspects. My own persistent approach in all professions and private life is "Be yourself, do your job in your own way and do it properly, as if you are in an interview for your dream job!"

As a team leader, then consultant, and finally project manager with a fantastic team of various nationalities, I have worked industrially in AEDC, CAE Electronics, and SNC-LAVALIN Canada, as well as in the EPS consulting firm. This supplied me with many experiences and skills. Here, I would like to emphasize the persuasion of culture on the stereotypical men's jobs.

The Canadian CAE firm was keen on hiring an Egyptian resident engineer to support their local projects. There were many qualified male and female Egyptian engineers. Amongst all, I was selected to be responsible for managing system integration, outstation installation, and testing work. This choice occurred with surprise from the surrounding Egyptian community, as it was considered as a man's tough job! I was the only female engineer in the whole team from Canada and Egypt. As a young female engineer, I succeeded in proving my high performance, leading during hardships with my male colleagues and coworkers. I learned management, and also enjoyed solving problems associated with integration of communication, power protection, software, and hardware in the field work. I also succeeded in influencing the vision of the ability of Arab women to work in tough environments and under pressure in diverse disciplines, as was mentioned by Paul Mariamo, Senior Vice President of SNC LAVALIN. The surrounding society highly appreciated the results. My industrial work also provided a role model of a determined women for young females to be themselves with high self-confidence.

On the other hand, although academic work is less challenging than industrial work, it has much more passion. It has a wider impact in influencing and supporting young scientists and academic colleagues. I discovered strong enthusiasm in teaching, cultivating, and stimulating a new generation to experience the engineering, science, and research atmosphere, and to inculcate students and researchers in the ways of creative thinking. I started in Fayoum University. I later moved to a position at the Helwan University, in my home town. I have also worked four years for AASTMT University. In addition, I have had managerial positions in my academic career. I set up and became the first Head of the Information Technology Department at Helwan University. Recently, I became the Vice Dean for Education and Students Affairs at the Faculty of Computers and Artificial Intelligence (FCAI), Beni Suef University in Upper Egypt. I also lead a promising Hub for Creativity and Scientific Research project in Helwan University that was inspired by and is under the supervision of a great female university Vice President: Prof. Mona Fouad.

Women – Men is an Integrated Formula

Blurring the men-women role causes life imbalance and confusion of duties. I believe that the difference existing between men and women leads to constitute successful complemented equally shared work. They complement each other in talent and creativity as well as in all aspects of life. I like a quote that was written by Prof. Asta Pellinen-Wannberg, "If the intelligence is Gaussian distributed among the whole population, we lose a lot of clever leaders by not letting half of it reach the top." Discrimination should only follow knowledge, ingenuity, and curiosity,

not gender. My dad and mom constructed this faith from my early adolescence, with some existing concerns about the surrounding culture. This belief affects my philosophy in teaching, research, and mentoring, in order to reinforce the impact on personality rather than merely the impact on education. There are unconscious bias and hidden gender-inequity ideologies that were inherited along the past generations. Awareness is highly required. The under-representation of women and their exclusion in science, engineering, and technology might be unintentional, since it sometimes is a result of woman's preservative attitude.

She is always governed with social-context limitations. A woman has to continually prove her superiority to achieve the same recognition, respect, and her deserved rights that a male colleague could obtain with much less effort. A woman as a social gender easily suffers from being not well-liked, well-appreciated, nor well-respected. This causes women to be repulsed from highly male-dominated jobs, such as demanding engineering and science careers. The equality of women and men doesn't only mean giving them equal rights, but also asking them for balanced duties. Continuing these biased cultural norms without resolving them preserves many obstacles for female scientists that results in their under-representation within the C-suite at the upper echelons.

Middle East Milieu Impact on Women

I was very uncertain about how far I can go in my career in radio science and academia, since there were no female role models in my surroundings. I don't remember any female professors during my entire undergraduate studies, but I was fortunate from the early years of my radio science studies to be encouraged by my supervisor, Prof. El-Khamy. Later, I was able to work in several broad fields in communication, electronics, power, and computing from the prospect of academia as well as industry while building my family. This provided me a distinctive vision, experiences, and formula of my own. My formula for interacting with my learners raises their skills with great confidence. I had a great chance to influence young scientists by offering them a woman-scientist model as a researcher and a mother from the same culture. A model or solved example makes the life easier to live, less stressful, and more confident for young female scientists. On the other hand, young male scientists gradually change their opinions on gender discrimination by having a persuasive competent female professor and supervisor. I like to share my experiences with them through academic and social activities. I enjoy being not only a mentor or a colleague but also a mother with them.

Figure 1 shows my students at the end of a discussion day. A bit more encouragement may be all that is needed to keep a promising young female scientist engaged. I am proud to have many male and female young scientists who are interested in research, and ready to influence their surrounding environment. I always wish them the best, and I work to push their achievements beyond my own.

When an Egyptian or Arab woman gets married and becomes a mother, she is usually the only one responsible for child care, house care, and sometimes aged parents. Engineering and science are demanding careers, especially with insufficient pregnancy services and babysitting facilities in the Arab region. Being away from home is therefore a huge problem for new mothers. Balancing between motherhood and a science career is always a tough challenge. Regrettably, I was repeatedly questioned by young female researchers if I would continue my supervision if they became pregnant. A woman suffers from the arbitrariness of supervisors, as they do not depend on a female who marries, becomes pregnant, delivers, and raises a kid. This might have a significant impact on the careers of female scientists, although it could be solved merely by using an innovative mentorship strategy, family, and social support.

As a matter of fact, the women in the Middle East sometimes take a share in some science professions just to fill the gap of the tendency of men to travel and work abroad. The number of women studying radio science is statistically increasing in the Arab world. However, there is a still not a gender balance or equal chances for women. In the Arab world in particular, Egypt has started earlier to provide promising opportunities for ambitious women to reach high positions, C-suites, but this development is still in its kickoff stages, especially in engineering and science.

Women in Radio Science at Egyptian URSI-NRSC

I consider that one of my terrific achievements is being a part of the URSI community through the Egyptian National Committee - URSI committee: National Radio Science Committee (NRSC), which is technically linked with URSI under the umbrella of the Academy of Research and Technology (ASRT). I have a long relationship with its reputable deep-rooted conference, since I used to publish and participate in its rounds. I later was selected as a member, and also as Egyptian representative for Commission A. Starting one year ago, I became the elected General Secretary of the NRSC committee. I have gained a lot from the invaluable colleagues in NRSC. Figure 2 shows the committee and some invited professors during the previous conference. The scientific discussions, events, management meetings, and the social activities that gather together the committee provide a healthy intellectual environment.

Since I knew about URSI women in radio science from two years ago, I was interested in holding an activity to highlight women in science in Egypt and in our Middle Eastern region. During the arrangements for the previous conference round in April 2019, I brought up holding a

Figure 3. A presentation at the NRSC 2019 conference.

new woman in science session. It took quite a long time to convince our committee to hold this session, because they were convinced that the women had already taken enough attention in our country! We are three women with twelve men in the NRSC committee. Finally, I and Prof. Hadia El Hennawy – a wonderful woman scientist role model, whom I recently met in NRSC – with the support of some male colleagues in the NRSC committee, succeeded in convincing those opposed that the aim was not only to inspire and motivate female students to pursue careers in science, technology, engineering, and mathematics (STEM), but to also highlight the area of jurisdiction that was recently gained for women in such Middle East societies. The first WiRSplenary session was remarkably held, and esteemed women from academia and industry were invited. We had great feedback for the session from both men and women colleagues and students. Figure 3 shows my presentation of the awards during the NRSC 2019 closing session.

Conclusion and Conceived Message

Family life affects extensive periods of work, especially in countries without a proper child-care system. As a woman who has accomplished a lot in my academic and industrial career life, I would like to address the issue of achievements usually at the expense of a lot of things compared to male peers. From my early childhood, I dreamed of being an engineer like my father. Later, I was fond of being myself in everything I did. I knocked on every door I encountered in order to gain knowledge and experience. The accomplishments I have really achieved are being a genuine and memorable colleague, an achieving employee, an influential leader, a respectful professor, a supportive supervisor. I was looking at doing my best in whatever career I worked in. My life was full of different experiences in consequence of difficulties, troubles, and struggles. That might be shared with my peers with similar social contexts in the Middle East and maybe for women all over the world. Women have social activities such as maternity breaks, child care, parent care, etc., during the most-fruitful phases of human existence. This in turn impacts a woman's likelihood of gaining tenure positions at the same age as a male, even though she has a longer list of merits.

From my experience, females have more dedicated determination than males, although men have higher confidence levels because of their gender dominance. My advice for a young woman scientist: be confident! In you work, you are a human, the same as a man. You can make mistakes, but you shouldn't repeat them, and you should learn from your own and others' mistakes. Understand and accept colleagues as they are. Stay calm in all tough situations. Choose your husband carefully, be outspoken about challenges in the home, and work and ask for sharing of responsibilities, look for female role models and an older female network to support, be organized, live a happy life even if it costs you some career delay. Balancing work and family with time management is the key for success for all, but it is strongly the real secret behind the success of women due to their diverse responsibilities. Satisfaction is the soul of happiness and success. Spending more happy time with the family is invaluable, and it helps in stress relief. The real woman-scientist role model is the one who developed herself with taking care of her family and other life aspects in a balanced way. Figure 4 shows a journey to Abu Simbel with my beloved family. Give attention for every significant direction and each important person in your life, as it is the only thing you have at a time. "This time slot is completely yours."

Figure 4. My beloved family in Abu Simbel, Aswan, Egypt.

Today, my interdisciplinary research has succeeded in attracting both male and female students, and has resulted in a good research group. Encouraging my students to have teams consisting of both males and females is a way to transfer a clear concrete message of gender nondiscrimination and to emphasize their equal rights and responsibilities. My policy is to honestly share with young scientists all positive and negative traits during their life, and always be open to discussing their problems. I feel responsible to transfer the awareness of gender complementarity for both male and female students in order to boost a healthier science society that respects the diversity and considers it as an added value.

Our life should have long-term moral and respectable goals that live after our death. The death grief of family members affected the meaning of my whole life in a profound philosophy: my father's unexpected death and the later sudden death of my brother's wife with its terrible emotional impact. I deeply perceived that the effective role and beneficial influence of the person on lives of others extends your life in their lives. While time is running out, I always wonder what I have accomplished, was it worth, what should I adapt in my remaining time.

Managerial roles that establish and apply polices could influence a broader range of young scientists to make a real difference. On the other hand, my research group grows with more young female researchers who insist on being under my supervision.

The cultures of the Egyptian and Arab worlds recognize female power in mentoring, leadership, and influencing the new generations in the communication and technology society. Some governmental rules are required to break the ice and to break the male stereotype. Egypt has recently gotten more female members in the parliament, and this for sure is even going to affect other sectors of the society. The same attention to science and technology could empower and inspire young female scientists. Egypt and the Arab region have also recently grown in the knowledge sector. Communication, technology, and the AI fields highly dominated recent research in Egypt, making use of their expertise in the Arab region as well as over the whole African continent. Since these are the interest fields of my research group and the concerns of the NRSC, I look forward to paving significant Arab and Egyptian roads to these developments by myself, with my colleagues, and through my young scientists' research group.

I am grateful to many people for their support during my career, from both males and females: parents, husband, family, daughter, supervisors, and colleagues. Male work-dominance stereotypes exist all over the world. In spite of that, I should express my respect for my lucky personal experience in this aspect: I have received my full chances and all kinds of support from both men and women along the way.

URSI Commission B EMTS 2019 Symposium

In addition to the URSI General Assembly and Scientific Symposium, and the Atlantic and Asia-Pacific Radio Science Conferences, an important meeting within URSI Commission B is the triennial Electromagnetic Theory Symposium (EMTS). The EMTS 2019 symposium was held at the Westin San Diego Hotel, in downtown San Diego, California, USA May 27-31, 2019. The conference provided a forum for researchers to present papers on current topics in fields and waves in radio science.

Radio science covers the study, understanding, and application of electromagnetics and electronics in natural and man-made environments. The impact and importance of radio science for modern technology and society cannot be overstated. Telecommunications, nanotechnology, radio astronomy, and remote sensing for monitoring of the environment and global change are but some of the fields that rest on the foundations of radio science. We believe that the foundations of radio science rest on electromagnetics – the study of fields and waves – which is the domain of Commission B of URSI.

The tradition of the Electromagnetic Theory Symposium (EMTS) is impressive, spanning a rich history of 66 years. The first EMTS was held at McGill University, Montreal, Canada, in 1953. The year 2019 marks the twenty-third time the symposium has been held, this time at Westin San Diego, in San Diego, USA.

The four days of the symposium addressed a wide range of topics in Commission B, consisting of 52 technical sessions and four plenary talks. The technical content of the meeting concentrated on fundamental and theoretical aspects of electromagnetics, from both the analytical and computational points of view. Examples of approaches were scattering and diffraction, high-frequency methods,

Figure 2. The winners of the Young Scientist Best Paper Awards.

novel mathematical methods in electromagnetics, and mathematical modeling of EM problems. However, several application areas were also covered, such as millimeter-wave antennas and 5G communications, and advanced metamaterial concepts in electromagnetics. One of the highlights was a historical session on the International Union of Radio Science: 100 Years of History and Achievements of Commission B, which had 11 interesting papers.

The papers submitted to the conference were evaluated by the review board, which consisted of 44 experts in electromagnetics. The final program included 308 presentations from 31 countries. EMTS 2019 was a perfect platform for scientific interactions after the presentations and during coffee breaks.

Unfortunately, there were 15 no-shows, mostly due to visa problems experienced by the presenters. Participants had the option of submitting extended abstracts or summaries. The two-column, two- to four-page summaries presented

Figure 1. A general lecture.

Figure 3. Prof. Michael Havrilla, course instructor, URSI Commission B School for Young Scientists.

Figure 4. The welcome reception.

by the authors that opted for submission to IEEE Xplore have been submitted to the IEEE and will be published.

In addition to the contributed presentations, each day of the conference included a one-hour general lecture (see Figure 1). The talks covered the scope of Commission B, from theory through computations to applications in 5G communications.

- Prof. Weng Cho Chew (Purdue University, USA), "Progress in Computational Electromagnetics"
- Prof. Akira Ishimaru (University of Washington, USA), "The History and Future of Statistical Electromagnetic Theories and Applications"
- Prof. John Volakis (Florida International University, USA), "Wideband Beaming Arrays for 5G Communications"
- Prof. Ari Sihvola (Aalto University, Finland), "Unimodularity and Magneto-Electric Coupling – Looking for Unconventional Taxonomy of Electromagnetic Materials"

In the best of URSI traditions, a strong emphasis was put on young scientists. 20 Young Scientist Awardees (YSAs) were selected from 42 applicants. These Young Scientist Awardees were given free registration to the conference, free accommodations, and banquet tickets. A poster session of EMTS was dedicated to these Young Scientists, who also gave a poster presentation in addition to their talk in one of the oral sessions.

Based on the submitted summaries and poster presentations, the Young Scientist Program Committee of EMTS 2019, chaired by Kazuya Kobayashi, awarded three Young Scientist best paper prizes. These were given to Viktar S. Asadchy (Aalto University, Espoo, Finland, $1000); Younes Ra'di (Advanced Science Research Center, New York, NY, United States, $750); and Yakir Hadad (School of Electrical Engineering, Tel-Aviv University, Tel-Aviv, Israel, $500). Honorable mention was conferred

Figure 5. The banquet.

on Miguel Camacho (University of Exeter, Exeter, UK) and Mariana Dalarsson (Linnaeus University, Vaxjo, Sweden). The winners are shown in Figure 2.

Commission B also continued the tradition of Young Scientist Schools. On Monday, May 27, before the main conference, the 2019 URSI Commission B School for Young Scientists took place at the Westin San Diego hotel. The topic of this short course was "Field and Potential Based Methods in Anisotropic and Bianisotropic Electromagnetics." The course instructor was Prof. Michael Havrilla, from the Air Force Institute of Technology, Wright-Patterson AFB, OH, USA (Figure 3).

Expanded contributions of selected presentations in the conference will be published in the "Special Issue of the 2019 URSI International Symposium on Electromagnetic Theory" in the journal *Radio Science*. In addition, the "Special Issue of the Papers from the EMTS 2019 Young Scientist Award" will also be published in the *Radio Science Bulletin*, which will contain the full-length versions of the papers by the Young Scientist Awardees.

The welcome reception and the banquet were enjoyed by the attendees, as seen in Figures 4 and 5.

If you missed EMTS 2019, you will have an opportunity to attend the next EMTS. We hope to see you in Moscow, Russia, during EMTS 2022!

Sembiam R. Rengarajan
Chair, Local Organizing Committee, EMTS 2019
Chair, USNC-URSI
E-mail: sembiam.rengarajan@csun.edu

Kazuya Kobayashi
Chair, Technical Program Committee, EMTS 2019
Chair, URSI Commission B
E-mail: kazuya_k@sea.plala.or.jp

The EurAAP Felsen Award

The Felsen Awards were created by the heirs of the late Prof. Leopold B. Felsen (1924-2005). The main purpose was to keep alive Prof. Felsen's memory and scientific legacy, as well as to foster academic excellence in the electromagnetics community. The basic idea was to give recognition to outstanding scientific contributions from early-stage researchers in electrodynamics, with emphasis on wave interactions with complex environments, a subject that was at the core of Prof. Felsen's research.

Originally, several Felsen Awards were created, targeting national communities and disseminated across academic institutions and universities connected with former collaborators and students of Prof. Felsen. In particular, the Leopold B. Felsen Award for Excellence in Electrodynamics was jointly established by the University of Siena (Prof. Stefano Maci) and the University of Sannio (Prof. Vincenzo Galdi). It was funded through a donation from Prof. Felsen's children, Michael and Judy Felsen, in fulfillment of the last wishes of their father. In its sole edition in 2008, this award was given to Dr. Andrea Alù (University of Pennsylvania, USA) and Dr. Guido Valerio (University of Rome "Sapienza," Italy).

However, it was soon noted that the pool of candidates for this award was too small, and the need to enlarge its range and scope quickly arose. Profs. Galdi and Maci found that the European Association of Antennas and Propagation (EurAAP), creator and owner of the annual European Conference on Antennas and Propagation (EuCAP), could provide the perfect framework for a better visibility of the award within the electromagnetics, antenna, and propagation communities. They generously considered the possibility of transforming the Siena and Sannio Felsen Award by upgrading it to a global EurAAP Felsen Award, to be connected with the EuCAP conferences. At the beginning of 2013, they contacted both the Felsen Charitable Fund and the EurAAP Board, informing them about this idea.

Figure 1. The 2019 EurAAP Felsen Award ceremony (l-r): C. Mangenot, EurAAP Chair; Francesco Monticone, award winner; and Michael Felsen.

After internal discussions on both sides of the Atlantic, a formal contact was finally established in October 2013 between Prof. Juan R. Mosig, then Chair of the EurAAP Board, and Michael Felsen, in charge of the Felsen Charitable Fund. Upon this first encounter, everything went on steadily, the process being only slowed down by the unavoidable legal provisions to assign an award financed by a USA trust to a European association. The new EurAAP Felsen Award, endowed with a generous yearly prize of USD $5000, was then created and entrusted to an award jury formed of Profs. Vincenzo Galdi (University of Sannio, Italy); Ehud Heyman (Tel Aviv University, Israel); Raj Mittra, (University of Central Florida); Juan R. Mosig (EPFL, Switzerland); and Werner Wiesbeck (Karlsruhe Institute of Technology, Germany).

The first EurAAP Felsen Award was delivered during the EuCAP 2015 conference in Lisbon, Portugal, and awarded to Prof. Francesco Andriulli (Telecom Bretagne/Institut Mines-Telecom, France). Since then, the Felsen Award has been given every year during the EuCAP conference. The complete list of awardees is:

2015: Francesco Andriulli (Telecom Bretagne/Institut Mines-Telecom, France)

2016: Yakir Hadad (University of Texas, USA)

2017: Juan Sebastian Gomez Diaz (University of California, Davis, USA)

2018: *ex aequo*, Giorgio Carluccio (Delft University of Technology, The Netherlands) and Özgür Ergül (Middle East Technical University, Turkey)

2019: Francesco Monticone (Cornell University, USA)

Figure 2. Michael Felsen's speech during the 2019 EurAAP Felsen Award ceremony.

Figure 3. The EuCAP 2019 conference dinner, the perfect setting for the EurAAP Felsen Award ceremony.

Figure 4. (l-r) Juan Mosig, Tolle Felsen, Cyril Mangenot, Michael Felsen, and Vincenzo Galdi at the EuCAP 2019 conference dinner.

The 2019 Award, presented during the EuCAP 2019 conference in Krakow, Poland, was particularly eventful. For the first time, Michael Felsen was able to attend the ceremony, with his wife, and personally present the award. In his speech, Prof. Felsen's son expressed his pleasure to be in Krakow, and his pride at seeing the Felsen Award fully consolidated as one of the most prestigious prizes in our community. With moving words, he told us of the connections of his family with Poland, where his grandfather, Markus Felsen, was born in 1884 in the town of Przemysl, a few hours southeast of Krakow, on the border with Ukraine.

Prof. Felsen also reminded us of how his father made it alone in June 1939, at age 15, from Germany to England, and then in 1940 to the USA, where "he finally settled, obtained his undergraduate and graduate degrees, had a family, and became the distinguished professor we remember this evening with this award." Prof. Michael Felsen went on, disclosing to the ceremony attendees the last utterances of Prof. Leopold Felsen on his deathbed:

> We were discussing setting up a few awards in his name, like this one. He said they should be for excellence in electromagnetics. Then he closed his eyes, and we thought he had uttered his last words. But no. He opened his eyes one last time and said: "Not electromagnetics. Electrodynamics." Those were his last words. I leave it to you all, the experts in this field, to interpret his meaning.

Michael Felsen also reminded us that his father loved to "play with words." He read us one of his father's last poems, called "Evanescent Professors," composed in 2005, at age 81. Its last lines have now become a well-known saying in our community:

> For those of us who deal with Waves,
> We do not fade, we Evanesce.

He concluded with some words for the awardee, Francesco Monticone, stating that:

> My father, Leo Felsen, has passed the torch to you, Professor Monticone, and to all of you. I know he is with you in spirit, here in the Poland of his ancestors, urging you all to "make waves about waves," as he was pleased to think he had made over the course of his career.

The next 2020 EurAAP Felsen Award will be delivered in Copenhagen, Denmark, during the EuCAP 2020 conference (March 15-20, 2020). Information and application forms for the 2020 edition of the award are available in the link http://www.euraap.org/publications-and-news/EurAAP-Awards/EurAAP-Awards-Description. Potential candidates, nominators, and endorsers are strongly encouraged to apply before the deadline of **January 31, 2020**.

Juan R. Mosig
E-mail: juan.mosig@epfl.ch

Vincenzo Galdi
E-mail: vgaldi@unisannio.it

URSI Conference Calendar

December 2019

ICMO 2019 - International Conference on Meteorological Observations
Chengdu, China 28 - 31 December 2019
Contact: icmo@cuit.edu.cn

February 2020

COSPAR ISWAT Inaugural Working Meeting
Radisson Resort, Port Canaveral, Florida, USA, 10-14 February 2020
Contact: https://www.iswat-cospar.org/

URSI - RCRS 2020
Varanasi, India, 12 - 14 February 2020
Contact: Dr. Somak Bhattacharyya, Convener, RCRS 2020, E-mail: ursi-rcrs2020@itbhu.ac.in

March 2020

EUCAP 2020
Copenhagen, Denmark 19-20 March 2020
Contact: www.eucap2020.org

URSI-France Workshop : Future Networks: 5G and beyond
Palaiseau, France, 11-13 March 2020
Contact: Prof. Alain Sibille, Telecom Paris, E-mail : alain.sibille@telecom-paris.fr

NRSC2020 - 37th National Radio Science Conference
Cairo, Egypt, 17-19 March 2020
Contact: Rowayda A. Sadek, Secretary, URSI- Egypt National Radio Science Committee, Faculty of Computers and Information Technology, Helwan University, Helwan, Egypt, E-mail: Rowayda_sadek@yahoo.com, Rowayda_sadek@fci.helwan.edu.eg

9th VERSIM Workshop - VLF/ELF Remote Sensing of Ionospheres and Magnetospheres
Kyoto, Japan, 23-27 March 2020
Contact : http://pcwave.rish.kyoto-u.ac.jp/versim/

August 2020

ICEAA - IEEE APWC 2020
Honolulu, Hawaii, USA, 10-14 August 2020
Contact: E-mail: iceaa20@iceaa.polito.it

COSPAR 2020 - 43rd Scientific Assembly of the Committee on Space Research (COSPAR) and Associated Events
Sydney, Australia, 15-23 August 2020
Contact : COSPAR Secretariat, 2 place Maurice Quentin, 75039 Paris Cedex 01, France, Tel: +33 1 44 76 75 10, Fax: +33 1 44 76 74 37, E-mail: cospar@cosparhq.cnes.fr http://www.cospar2020.org

URSI GASS 2020
Rome, Italy, 29 August - 5 September 2020
Contact: URSI Secretariat, c/o INTEC, Tech Lane Ghent Science Park - Campus A, Technologiepark-Zwijnaarde 15, B-9052 Gent, Belgium, E-mail gass@ursi.org, http://www.ursi2020.org

September 2020

EuMW 2020
Utrecht, the Netherlands,13 - 18 September 2020
Contact: E-mail: headquarters@eumwa.org

2020 Metamaterials Congress
New York, USA, 28 September - 1 October 2020
Contact: E-mail : contact@metamorphose-vi.org

October 2020

ISAP 2020 - International Symposium on Antennas and Propagation
Osaka, Japan, 26-30 October 2020
Contact : Prof. Hiroyuki Arai, General Chair of ISAP 2020, Yokohama National University, Japan, ap_ac-isap2020@mail.ieice.org, http://www.isap2020.org/

May 2021

AT-RASC 2021
Third URSI Atlantic Radio Science Conference
Gran Canaria, Spain, 23-28 May 2021
Contact: Prof. Peter Van Daele, URSI Secretariat, Ghent University – INTEC, Technologiepark-Zwijnaarde 15, B-9052 Gent, Belgium, Fax: +32 9-264 4288, E-mail: peter.vandaele@ugent.be, http://www.at-rasc.com

August 2022

AP-RASC 2022 - Asia-Pacific Radio Science Conference 2022
Sydney, Australia, 21-25 August 2022
Contact: URSI Secretariat, Ghent University – INTEC, Technologiepark-Zwijnaarde 126, B-9052 Gent, Belgium, E-mail: info@ursi.org

A detailed list of meetings is available on the URSI website at http://www.ursi.org/events.php

Information for Authors

Content

The *Radio Science Bulletin* is published four times per year by the Radio Science Press on behalf of URSI, the International Union of Radio Science. The content of the *Bulletin* falls into three categories: peer-reviewed scientific papers, correspondence items (short technical notes, letters to the editor, reports on meetings, and reviews), and general and administrative information issued by the URSI Secretariat. Scientific papers may be invited (such as papers in the *Reviews of Radio Science* series, from the Commissions of URSI) or contributed. Papers may include original contributions, but should preferably also be of a sufficiently tutorial or review nature to be of interest to a wide range of radio scientists. The *Radio Science Bulletin* is indexed and abstracted by INSPEC.

Scientific papers are subjected to peer review. The content should be original and should not duplicate information or material that has been previously published (if use is made of previously published material, this must be identified to the Editor at the time of submission). Submission of a manuscript constitutes an implicit statement by the author(s) that it has not been submitted, accepted for publication, published, or copyrighted elsewhere, unless stated differently by the author(s) at time of submission. Accepted material will not be returned unless requested by the author(s) at time of submission.

Submissions

Material submitted for publication in the scientific section of the *Bulletin* should be addressed to the Editor, whereas administrative material is handled directly with the Secretariat. Submission in electronic format according to the instructions below is preferred. There are typically no page charges for contributions following the guidelines. No free reprints are provided.

Style and Format

There are no set limits on the length of papers, but they typically range from three to 15 published pages including figures. The official languages of URSI are French and English: contributions in either language are acceptable. No specific style for the manuscript is required as the final layout of the material is done by the URSI Secretariat. Manuscripts should generally be prepared in one column for printing on one side of the paper, with as little use of automatic formatting features of word processors as possible. A complete style guide for the *Reviews of Radio Science* can be downloaded from http://www.ips.gov.au/IPSHosted/NCRS/reviews/. The style instructions in this can be followed for all other *Bulletin* contributions, as well. The name, affiliation, address, telephone and fax numbers, and e-mail address for all authors must be included with

All papers accepted for publication are subject to editing to provide uniformity of style and clarity of language. The publication schedule does not usually permit providing galleys to the author.

Figure captions should be on a separate page in proper style; see the above guide or any issue for examples. All lettering on figures must be of sufficient size to be at least 9 pt in size after reduction to column width. Each illustration should be identified on the back or at the bottom of the sheet with the figure number and name of author(s). If possible, the figures should also be provided in electronic format. TIF is preferred, although other formats are possible as well: please contact the Editor. Electronic versions of figures *must* be of sufficient resolution to permit good quality in print. As a rough guideline, when sized to column width, line art should have a minimum resolution of 300 dpi; color photographs should have a minimum resolution of 150 dpi with a color depth of 24 bits. 72 dpi images intended for the Web are generally *not* acceptable. Contact the Editor for further information.

Electronic Submission

A version of Microsoft *Word* is the preferred format for submissions. Submissions in versions of T_EX can be accepted in some circumstances: please contact the Editor before submitting. *A paper copy of all electronic submissions must be mailed to the Editor, including originals of all figures.* Please do *not* include figures in the same file as the text of a contribution. Electronic files can be send to the Editor in three ways: (1) By sending a floppy diskette or CD-R; (2) By attachment to an e-mail message to the Editor (the maximum size for attachments *after* MIME encoding is about 7 MB); (3) By e-mailing the Editor instructions for downloading the material from an ftp site.

Review Process

The review process usually requires about three months. Authors may be asked to modify the manuscript if it is not accepted in its original form. The elapsed time between receipt of a manuscript and publication is usually less than twelve months.

Copyright

Submission of a contribution to the *Radio Science Bulletin* will be interpreted as assignment and release of copyright and any and all other rights to the Radio Science Press, acting as agent and trustee for URSI. Submission for publication implicitly indicates the author(s) agreement with such assignment, and certification that publication will not violate any other copyrights or other rights associated with the submitted material.

Become An Individual Member of URSI

The URSI Board of Officers is pleased to announce the establishment of Individual Fellowship (FURSI), Individual Membership (MURSI), and Individual Associate Membership (AMURSI). By joining URSI, Individual Associate Members, Individual Members, and Fellows secure recognition with their peers, are better connected to URSI Headquarters, and are better connected to their National Committees. Each can then better provide support to the other. Other benefits include discounted registration fees at URSI conferences (beginning with the 2018 URSI AT RASC) and at some conferences cosponsored by URSI (beginning with some conferences run by IEEE AP-S), a certificate of membership, and e-mail notification of the availability of the electronic edition of the URSI *Radio Science Bulletin*.

Fellowship is by invitation only. Membership and Associate Membership can be applied for through the online forms available at **www.ursi.org/membership.php**, or at **www.ursi.org**